IN THE UNITED STATES PATENT AND TRADEMARK OFFICE

In re Application of: Ashkenazi et al.	Group Art Unit: 1647
Serial No.: 09/903,925	Examiner: Fozia Hamid
Filed: July 11, 2001	**CERTIFICATE OF MAILING** I hereby certify that this correspondence is being deposited with the United States Postal Service with sufficient postage as first class mail in an envelope addressed to: Assistant Commissioner of Patents, Washington, D.C. 20231 on Date
For: SECRETED AND TRANSMEMBRANE POLYPEPTIDES AND NUCLEIC ACIDS	

DECLARATION OF AUDREY D. GODDARD, Ph.D UNDER 37 C.F.R. § 1.132

Assistant Commissioner of Patents
Washington, D.C. 20231

Sir:

I, Audrey D. Goddard, Ph.D. do hereby declare and say as follows:

1.   I am a Senior Clinical Scientist at the Experimental Medicine/BioOncology, Medical Affairs Department of Genentech, Inc., South San Francisco, California 94080.

2.   Between 1993 and 2001, I headed the DNA Sequencing Laboratory at the Molecular Biology Department of Genentech, Inc. During this time, my responsibilities included the identification and characterization of genes contributing to the oncogenic process, and determination of the chromosomal localization of novel genes.

3.   My scientific Curriculum Vitae, including my list of publications, is attached to and forms part of this Declaration (Exhibit A).

4.   I am familiar with a variety of techniques known in the art for detecting and quantifying the amplification of oncogenes in cancer, including the quantitative TaqMan PCR (i.e., "gene amplification") assay described in the above captioned patent application.

5.   The TaqMan PCR assay is described, for example, in the following scientific publications: Higuchi *et al.*, Biotechnology 10:413-417 (1992) (Exhibit B); Livak *et al.*, PCR Methods Appl., 4:357-362 (1995) (Exhibit C) and Heid *et al.*, Genome Res. 6:986-994 (1996) (Exhibit D). Briefly, the assay is based on the principle that successful PCR yields a fluorescent signal due to Taq DNA polymerase-mediated exonuclease digestion of a fluorescently labeled oligonucleotide that is homologous to a sequence between two PCR primers. The extent of digestion depends directly on the amount of PCR, and can be quantified accurately by measuring the increment in fluorescence that results from decreased energy transfer. This is an extremely sensitive technique, which allows detection in the exponential phase of the PCR reaction and, as a result, leads to accurate determination of gene copy number.

6.   The quantitative fluorescent TaqMan PCR assay has been extensively and successfully used to characterize genes involved in cancer development and progression. Amplification of protooncogenes has been studied in a variety of human tumors, and is widely considered as having etiological, diagnostic and prognostic significance. This use of the quantitative TaqMan PCR assay is exemplified by the following scientific publications: Pennica *et al.*, Proc. Natl. Acad. Sci. USA 95(25):14717-14722 (1998) (Exhibit E);   Pitti *et al.*, Nature 396(6712):699-703 (1998) (Exhibit F) and Bieche *et al.*, Int. J. Cancer 78:661-666 (1998) (Exhibit G), the first two of which I am co-author. In particular, Pennica *et al.* have used the quantitative TaqMan PCR assay to study relative gene amplification of WISP and c-myc in various cell lines, colorectal tumors and normal mucosa. Pitti *et al.* studied the genomic amplification of a decoy receptor for Fas ligand in lung and colon cancer, using the quantitative TaqMan PCR assay. Bieche *et al.* used the assay to study gene amplification in breast cancer.

7.   It is my personal experience that the quantitative TaqMan PCR technique is technically sensitive enough to detect at least a 2-fold increase in gene copy number relative to control. It is further my considered scientific opinion that an at least 2-fold increase in gene copy number in a tumor tissue sample relative to a normal (i.e., non-tumor) sample is significant and useful in that the detected increase in gene copy number in the tumor sample relative to the normal sample serves as a basis for using relative gene copy number as quantitated by the TaqMan PCR technique as a diagnostic marker for the presence or absence of tumor in a tissue sample of unknown pathology. Accordingly, a gene identified as being amplified at least 2-fold by the quantitative TaqMan PCR assay in a tumor sample relative to a normal sample is useful as a marker for the diagnosis of cancer, for monitoring cancer development and/or for measuring the efficacy of cancer therapy.

8.   I declare further that all statements made herein of my own knowledge are true and that all statements made on information and belief are believed to be true. I declare that these statements were made with the knowledge that willful false statements and the like so made are punishable by fine or imprisonment, or both, under Section 1001 of Title 18 of the United States Code, and that such willful false statements may jeopardize the validity of the application or any patent issuing thereon.

Jan. 16, 2003

Date

Audrey Goddard

Audrey D. Goddard, Ph.D.

AUDREY D. GODDARD, Ph.D.

Genentech, Inc.
1 DNA Way
South San Francisco, CA, 94080
650.225.6429
goddarda@gene.com

110 Congo St.
San Francisco, CA, 94131
415.841.9154
415.819.2247 (mobile)
agoddard@pacbell.net

PROFESSIONAL EXPERIENCE

Genentech, Inc.   **1993-present**
South San Francisco, CA

2001 - present   Senior Clinical Scientist
Experimental Medicine / BioOncology, Medical Affairs

Responsibilities:
- *Companion diagnostic oncology products*
- *Acquisition of clinical samples from Genentech's clinical trials for translational research*
- *Translational research using clinical specimen and data for drug development and diagnostics*
- *Member of Development Science Review Committee, Diagnostic Oversight Team, 21 CFR Part 11 Subteam*

Interests:
- *Ethical and legal implications of experiments with clinical specimens and data*
- *Application of pharmacogenomics in clinical trials*

1998 - 2001   Senior Scientist
Head of the DNA Sequencing Laboratory, Molecular Biology Department, Research

Responsibilities:
- *Management of a laboratory of up to nineteen –including postdoctoral fellow, associate scientist, senior research associate and research assistants/associate levels*
- *Management of a $750K budget*
- *DNA sequencing core facility supporting a 350+ person research facility.*
- *DNA sequencing for high throughput gene discovery, - ESTs, cDNAs, and constructs*
- *Genomic sequence analysis and gene identification*
- *DNA sequence and primary protein analysis*

Research:
- *Chromosomal localization of novel genes*
- *Identification and characterization of genes contributing to the oncogenic process*
- *Identification and characterization of genes contributing to inflammatory diseases*
- *Design and development of schemes for high throughput genomic DNA sequence analysis*
- *Candidate gene prediction and evaluation*

1993 - 1998   Scientist
Head of the DNA Sequencing Laboratory, Molecular Biology Department, Research

Responsibilities
- *DNA sequencing core facility supporting a 350+ person research facility*
- *Assumed responsibility for a pre-existing team of five technicians and expanded the group into fifteen, introducing a level of middle management and additional areas of research*
- *Participated in the development of the basic plan for high throughput secreted protein discovery program – sequencing strategies, data analysis and tracking, database design*
- *High throughput EST and cDNA sequencing for new gene identification.*
- *Design and implementation of analysis tools required for high throughput gene identification.*
- *Chromosomal localization of genes encoding novel secreted proteins.*

Research:
- *Genomic sequence scanning for new gene discovery.*
- *Development of signal peptide selection methods.*
- *Evaluation of candidate disease genes.*
- *Growth hormone receptor gene SNPs in children with Idiopathic short stature*

Imperial Cancer Research Fund   **1989-1992**
London, UK with Dr. Ellen Solomon

6/89 –12/92 Postdoctoral Fellow
- Cloning and characterization of the genes fused at the acute promyelocytic leukemia translocation breakpoints on chromosomes 17 and 15.
- Prepared a successfully funded European Union multi-center grant application

McMaster University   **1983**
Hamilton, Ontario, Canada with Dr. G. D. Sweeney

5/83 – 8/83: NSERC Summer Student
- *In vitro* metabolism of β-naphthoflavone in C57Bl/6J and DBA mice

EDUCATION

Ph.D.
"Phenotypic and genotypic effects of mutations in the human retinoblastoma gene."
Supervisor: Dr. R. A. Phillips

University of Toronto
Toronto, Ontario, Canada.   1989
Department of Medical
Biophysics.

Honours B.Sc
"The *in vitro* metabolism of the cytochrome P-448 inducer β-naphthoflavone in C57BL/6J mice."
Supervisor: Dr. G. D. Sweeney

McMaster University,
Hamilton, Ontario, Canada.   1983
Department of Biochemistry

ACADEMIC AWARDS

Imperial Cancer Research Fund Postdoctoral Fellowship	1989-1992
Medical Research Council Studentship	1983-1988
NSERC Undergraduate Summer Research Award	1983
Society of Chemical Industry Merit Award (Hons. Biochem.)	1983
Dr. Harry Lyman Hooker Scholarship	1981-1983
J.L.W. Gill Scholarship	1981-1982
Business and Professional Women's Club Scholarship	1980-1981
Wyerhauser Foundation Scholarship	1979-1980

INVITED PRESENTATIONS

Genentech's gene discovery pipeline: High throughput identification, cloning and characterization of novel genes. Functional Genomics: From Genome to Function, Litchfield Park, AZ, USA. October 2000

High throughput identification, cloning and characterization of novel genes. G2K:Back to Science, Advances in Genome Biology and Technology I. Marco Island, FL, USA. February 2000

Quality control in DNA Sequencing: The use of Phred and Phrap. Bay Area Sequencing Users Meeting, Berkeley, CA, USA. April 1999

High throughput secreted protein identification and cloning. Tenth International Genome Sequencing and Analysis Conference, Miami, FL, USA. September 1998

The evolution of DNA sequencing: The Genentech perspective. Bay Area Sequencing Users Meeting, Berkeley, CA, USA. May 1998

Partial Growth Hormone Insensitivity: The role of GH-receptor mutations in Idiopathic Short Stature. Tenth Annual National Cooperative Growth Study Investigators Meeting, San Francisco, CA, USA. October, 1996

Growth hormone (GH) receptor defects are present in selected children with non-GH-deficient short stature: A molecular basis for partial GH-insensitivity. 76th Annual Meeting of The Endocrine Society, Anaheim, CA, USA. June 1994

A previously uncharacterized gene, myl, is fused to the retinoic acid receptor alpha gene in acute promyelocytic leukemia. XV International Association for Comparative Research on Leukemia and Related Disease, Padua, Italy. October 1991

PATENTS

Goddard A, Godowski PJ, Gurney AL. NL2 Tie ligand homologue polypeptide. Patent Number: 6,455,496. Date of Patent: Sept. 24, 2002.

Goddard A, Godowski PJ and Gurney AL. NL3 Tie ligand homologue nucleic acids. Patent Number: 6,426,218. Date of Patent: July 30, 2002.

Godowski P, Gurney A, Hillan KJ, Botstein D, **Goddard A**, Roy M, Ferrara N, Tumas D, Schwall R. NL4 Tie ligand homologue nucleic acid. Patent Number: 6,4137,770. Date of Patent: July 2, 2002.

Ashkenazi A, Fong S, **Goddard A**, Gurney AL, Napier MA, Tumas D, Wood WI. Nucleic acid encoding A-33 related antigen poly peptides. Patent Number: 6,410,708. Date of Patent:: Jun. 25, 2002.

Botstein DA, Cohen RL, **Goddard AD**, Gurney AL, Hillan KJ, Lawrence DA, Levine AJ, Pennica D, Roy MA and Wood WI. WISP polypeptides and nucleic acids encoding same. Patent Number: 6,387,657. Date of Patent: May 14, 2002.

Goddard A, Godowski PJ and Gurney AL. Tie ligands. Patent Number: 6,372,491. Date of Patent: April 16, 2002.

Godowski PJ, Gurney AL, **Goddard A** and Hillan K. TIE ligand homologue antibody. Patent Number: 6,350,450. Date of Patent: Feb. 26, 2002.

Fong S, Ferrara N, **Goddard** A, Godowski PJ, Gurney AL, Hillan K and Williams PM. Tie receptor tyrosine kinase ligand homologues. Patent Number: 6,348,351. Date of Patent: Feb. 19, 2002.

Goddard A, Godowski PJ and Gurney AL. Ligand homologues. Patent Number: 6,348,350. Date of Patent: Feb. 19, 2002.

Attie KM, Carlsson LMS, Gesundheit N and **Goddard A**. Treatment of partial growth hormone insensitivity syndrome. Patent Number: 6,207,640. Date of Patent: March 27, 2001.

Fong S, Ferrara N, **Goddard A**, Godowski PJ, Gurney AL, Hillan K and Williams PM. Nucleic acids encoding NL-3. Patent Number: 6,074,873. Date of Patent: June 13, 2000

Attie K, Carlsson LMS, Gesunheit N and **Goddard A**. Treatment of partial growth hormone insensitivity syndrome. Patent Number: 5,824,642. Date of Patent: October 20, 1998

Attie K, Carlsson LMS, Gesunheit N and **Goddard A**. Treatment of partial growth hormone insensitivity syndrome. Patent Number: 5,646,113. Date of Patent: July 8, 1997

Multiple additional provisional applications filed

PUBLICATIONS

Seshasayee D, Dowd P, Gu Q, Erickson S, **Goddard AD** Comparative sequence analysis of the *HER2* locus in mouse and man. Manuscript in preparation.

Abuzzahab MJ, **Goddard A**, Grigorescu F, Lautier C, Smith RJ and Chernausek SD. Human IGF-1 receptor mutations resulting in pre- and post-natal growth retardation. Manuscript in preparation.

Aggarwal S, Xie, M-H, Foster J, Frantz G, Stinson J, Corpuz RT, Simmons L, Hillan K, Yansura DG, Vandlen RL, **Goddard AD** and Gurney AL. FHFR, a novel receptor for the fibroblast growth factors. Manuscript submitted.

Adams SH, Chui C, Schilbach SL, Yu XX, **Goddard AD**, Grimaldi JC, Lee J, Dowd P, Colman S., Lewin DA. (2001) BFIT, a unique acyl-CoA thioesterase induced in thermogenic brown adipose tissue: Cloning, organization of the human gene, and assessment of a potential link to obesity. *Biochemical Journal* **360**: 135-142.

Lee J. Ho WH. Maruoka M. Corpuz RT. Baldwin DT. Foster JS. **Goddard AD**. Yansura DG. Vandlen RL. Wood WI. Gurney AL. (2001) IL-17E, a novel proinflammatory ligand for the IL-17 receptor homolog IL-17Rh1. *Journal of Biological Chemistry* **276**(2): 1660-1664.

Xie M-H, Aggarwal S, Ho W-H, Foster J, Zhang Z, Stinson J, Wood WI, **Goddard AD** and Gurney AL. (2000) Interleukin (IL)-22, a novel human cytokine that signals through the interferon-receptor related proteins CRF2-4 and IL-22R. *Journal of Biological Chemistry* **275**: 31335-31339.

Weiss GA, Watanabe CK, Zhong A, **Goddard A** and Sidhu SS. (2000) Rapid mapping of protein functional epitopes by combinatorial alanine scanning. *Proc. Natl. Acad. Sci. USA* **97**: 8950-8954.

Guo S, Yamaguchi Y, Schilbach S, Wada T.;Lee J, **Goddard A**, French D , Handa H, Rosenthal A. (2000) A regulator of transcriptional elongation controls vertebrate neuronal development. *Nature* **408**: 366-369.

Yan M, Wang L-C, Hymowitz SG, Schilbach S, Lee J, **Goddard A**, de Vos AM, Gao WQ, Dixit VM. (2000) Two-amino acid molecular switch in an epithelial morphogen that regulates binding to two distinct receptors. *Science* **290**: 523-527.

Sehl PD, Tai JTN, Hillan KJ, Brown LA, **Goddard A**, Yang R, Jin H and Lowe DG. (2000) Application of cDNA microarrays in determining molecular phenotype in cardiac growth, development, and response to injury. *Circulation* **101**: 1990-1999.

Guo S, Brush J, Teraoka H, **Goddard A**, Wilson SW, Mullins MC and Rosenthal A. (1999) Development of noradrenergic neurons in the zebrafish hindbrain requires BMP, FGF8, and the homeodomain protein soulless/Phox2A. *Neuron* **24**: 555-566.

Stone D, Murone, M, Luoh, S, Ye W, Armanini P, Gurney A, Phillips HS, Brush, J, **Goddard A**, de Sauvage FJ and Rosenthal A. (1999) Characterization of the human suppressor of fused; a negative regulator of the zinc-finger transcription factor Gli. *J. Cell Sci.* **112**: 4437-4448.

Xie M-H, Holcomb I, Deuel B, Dowd P, Huang A, Vagts A, Foster J, Liang J, Brush J, Gu Q, Hillan K, **Goddard A** and Gurney, A.L. (1999) FGF-19, a novel fibroblast growth factor with unique specificity for FGFR4. *Cytokine* **11**: 729-735.

Yan M, Lee J, Schilbach S, **Goddard A** and Dixit V. (1999) mE10, a novel caspase recruitment domain-containing proapoptotic molecule. *J. Biol. Chem.* **274**(15): 10287-10292.

Gurney AL, Marsters SA, Huang RM, Pitti RM, Mark DT, Baldwin DT, Gray AM, Dowd P, Brush J, Heldens S, Schow P, **Goddard AD**, Wood WI, Baker KP, Godowski PJ and Ashkenazi A. (1999) Identification of a new member of the tumor necrosis factor family and its receptor, a human ortholog of mouse GITR. *Current Biology* **9**(4): 215-218.

Ridgway JBB, Ng E, Kern JA ,Lee J, Brush J, **Goddard A** and Carter P. (1999) Identification of a human anti-CD55 single-chain Fv by subtractive panning of a phage library using tumor and nontumor cell lines. *Cancer Research* **59**: 2718-2723.

Pitti RM, Marsters SA, Lawrence DA, Roy M, Kischkel FC, Dowd P, Huang A, Donahue CJ, Sherwood SW, Baldwin DT, Godowski PJ, Wood WI, Gurney AL, Hillan KJ, Cohen RL, **Goddard AD**, Botstein D and Ashkenazi A. (1998) Genomic amplification of a decoy receptor for Fas ligand in lung and colon cancer. *Nature* **396**(6712): 699-703.

Pennica D, Swanson TA, Welsh JW, Roy MA, Lawrence DA, Lee J, Brush J, Taneyhill LA, Deuel B, Lew M, Watanabe C, Cohen RL, Melhem MF, Finley GG, Quirke P, **Goddard AD**, Hillan KJ, Gurney AL, Botstein D and Levine AJ. (1998) WISP genes are members of the connective tissue growth factor family that are up-regulated in wnt-1-transformed cells and aberrantly expressed in human colon tumors. *Proc. Natl. Acad. Sci. USA.* **95**(25): 14717-14722.

Yang RB, Mark MR, Gray A, Huang A, Xie MH, Zhang M, **Goddard A**, Wood WI, Gurney AL and Godowski PJ. (1998) Toll-like receptor-2 mediates lipopolysaccharide-induced cellular signalling. *Nature* **395**(6699): 284-288.

Merchant AM, Zhu Z, Yuan JQ, **Goddard A**, Adams CW, Presta LG and Carter P. (1998) An efficient route to human bispecific IgG. *Nature Biotechnology* **16**(7): 677-681.

Marsters SA, Sheridan JP, Pitti RM, Brush J, **Goddard A** and Ashkenazi A. (1998) Identification of a ligand for the death-domain-containing receptor Apo3. *Current Biology* **8**(9): 525-528.

Xie J, Murone M, Luoh SM, Ryan A, Gu Q, Zhang C, Bonifas JM, Lam CW, Hynes M, **Goddard A,** Rosenthal A, Epstein EH Jr. and de Sauvage FJ. (1998) Activating Smoothened mutations in sporadic basal-cell carcinoma. *Nature.* **391**(6662): 90-92.

Marsters SA, Sheridan JP, Pitti RM, Huang A, Skubatch M, Baldwin D, Yuan J, Gumey A, **Goddard AD**, Godowski P and Ashkenazi A. (1997) A novel receptor for Apo2L/TRAIL contains a truncated death domain. *Current Biology.* **7**(12): 1003-1006.

Hynes M, Stone DM, Dowd M, Pitts-Meek S, **Goddard A**, Gurney A and Rosenthal A. (1997) Control of cell pattern in the neural tube by the zinc finger transcription factor *Gli-1*. *Neuron* **19**: 15–26.

Sheridan JP, Marsters SA, Pitti RM, Gurney A., Skubatch M, Baldwin D, Ramakrishnan L, Gray CL, Baker K, Wood WI, **Goddard AD**, Godowski P, and Ashkenazi A. (1997) Control of TRAIL-Induced Apoptosis by a Family of Signaling and Decoy Receptors. *Science* **277** (5327): 818-821.

Goddard AD, Dowd P, Chernausek S, Geffner M, Gertner J, Hintz R, Hopwood N, Kaplan S, Plotnick L, Rogol A, Rosenfield R, Saenger P, Mauras N, Hershkopf R, Angulo M and Attie, K. (1997) Partial growth hormone insensitivity: The role of growth hormone receptor mutations in idiopathic short stature. *J. Pediatr.* **131**: S51-55.

Klein RD, Sherman D, Ho WH, Stone D, Bennett GL, Moffat B, Vandlen R, Simmons L, Gu Q, Hongo JA, Devaux B, Poulsen K, Armanini M, Nozaki C, Asai N, **Goddard A**, Phillips H, Henderson CE, Takahashi M and Rosenthal A. (1997) A GPI-linked protein that interacts with Ret to form a candidate neurturin receptor. *Nature.* **387**(6634): 717-21.

Stone DM, Hynes M, Armanini M, Swanson TA, Gu Q, Johnson RL, Scott MP, Pennica D, **Goddard A**, Phillips H, Noll M, Hooper JE, de Sauvage F and Rosenthal A. (1996) The tumour-suppressor gene patched encodes a candidate receptor for Sonic hedgehog. *Nature* **384**(6605): 129-34.

Marsters SA, Sheridan JP, Donahue CJ, Pitti RM, Gray CL, **Goddard AD**, Bauer KD and Ashkenazi A. (1996) Apo-3, a new member of the tumor necrosis factor receptor family, contains a death domain and activates apoptosis and NF-kappa β. *Current Biology* **6**(12): 1669-76.

Rothe M, Xiong J, Shu HB, Williamson K, **Goddard A** and Goeddel DV. (1996) I-TRAF is a novel TRAF-interacting protein that regulates TRAF-mediated signal transduction. *Proc. Natl. Acad. Sci. USA* **93**: 8241-8246.

Yang M, Luoh SM, **Goddard A**, Reilly D, Henzel W and Bass S. (1996) The bglX gene located at 47.8 min on the Escherichia coli chromosome encodes a periplasmic beta-glucosidase. *Microbiology* **142**: 1659-65.

Goddard AD and Black DM. (1996) Familial Cancer in <u>Molecular Endocrinology of Cancer.</u> Waxman, J. Ed. Cambridge University Press, Cambridge UK, pp.187-215.

Treanor JJS, Goodman L, de Sauvage F, Stone DM, Poulson KT, Beck CD, Gray C, Armanini MP, Pollocks RA, Hefti F, Phillips HS, **Goddard A**, Moore MW, Buj-Bello A, Davis AM, Asai N, Takahashi M, Vandlen R, Henderson CE and Rosenthal A. (1996) Characterization of a receptor for GDNF. *Nature* **382**: 80-83.

Klein RD, Gu Q, **Goddard A** and Rosenthal A. (1996) Selection for genes encoding secreted proteins and receptors. *Proc. Natl. Acad. Sci. USA* **93**: 7108-7113.

Winslow JW, Moran P, Valverde J, Shih A, Yuan JQ, Wong SC, Tsai SP, **Goddard A**, Henzel WJ, Hefti F and Caras I. (1995) Cloning of AL-1, a ligand for an Eph-related tyrosine kinase receptor involved in axon bundle formation. *Neuron* **14**: 973-981.

Bennett BD, Zeigler FC, Gu Q, Fendly B, **Goddard AD**, Gillett N and Matthews W. (1995) Molecular cloning of a ligand for the EPH-related receptor protein-tyrosine kinase Htk. *Proc. Natl. Acad. Sci. USA* **92**: 1866-1870.

Huang X, Yuang J, **Goddard A**, Foulis A, James RF, Lernmark A, Pujol-Borrell R, Rabinovitch A, Somoza N and Stewart TA. (1995) Interferon expression in the pancreases of patients with type I diabetes. *Diabetes* **44**: 658-664.

Goddard AD, Yuan JQ, Fairbairn L, Dexter M, Borrow J, Kozak C and Solomon E. (1995) Cloning of the murine homolog of the leukemia-associated PML gene. *Mammalian Genome* **6**: 732-737.

Goddard AD, Covello R, Luoh SM, Clackson T, Attie KM, Gesundheit N, Rundle AC, Wells JA, Carlsson LMTI and The Growth Hormone Insensitivity Study Group. (1995) Mutations of the growth hormone receptor in children with idiopathic short stature. *N. Engl. J. Med.* **333**: 1093-1098.

Kuo SS, Moran P, Gripp J, Armanini M, Phillips HS, **Goddard A** and Caras IW. (1994) Identification and characterization of Batk, a predominantly brain-specific non-receptor protein tyrosine kinase related to Csk. *J. Neurosci. Res.* **38**: 705-715.

Mark MR, Scadden DT, Wang Z, Gu Q, **Goddard A** and Godowski PJ. (1994) Rse, a novel receptor-type tyrosine kinase with homology to Axl/Ufo, is expressed at high levels in the brain. *Journal of Biological Chemistry* **269**: 10720-10728.

Borrow J, Shipley J, Howe K, Kiely F, **Goddard A**, Sheer D, Srivastava A, Antony AC, Fioretos T, Mitelman F and Solomon E. (1994) Molecular analysis of simple variant translocations in acute promyelocytic leukemia. *Genes Chromosomes Cancer* **9**: 234-243.

Goddard AD and Solomon E. (1993) Genetics of Cancer. *Adv. Hum. Genet.* **21**: 321-376.

Borrow J, **Goddard AD**, Gibbons B, Katz F, Swirsky D, Fioretos T, Dube I, Winfield DA, Kingston J, Hagemeijer A, Rees JKH, Lister AT and Solomon E. (1992) Diagnosis of acute promyelocytic leukemia by RT-PCR: Detection of *PML-RARA* and *RARA-PML* fusion transcripts. *Br. J. Haematol.* **82**: 529-540.

Goddard AD, Borrow J and Solomon E. (1992) A previously uncharacterized gene, PML, is fused to the retinoic acid receptor alpha gene in acute promyelocytic leukemia. *Leukemia* **6 Suppl 3**: 117S–119S.

Zhu X, Dunn JM, **Goddard AD**, Squire JA, Becker A, Phillips RA and Gallie BL. (1992) Mechanisms of loss of heterozygosity in retinoblastoma. *Cytogenet. Cell. Genet.* **59**: 248-252.

Foulkes W, **Goddard A**. and Patel K. (1991) Retinoblastoma linked with Seascale [letter]. *British Med. J.* **302**: 409.

Goddard AD, Borrow J, Freemont PS and Solomon E. (1991) Characterization of a novel zinc finger gene disrupted by the t(15;17) in acute promyelocytic leukemia. *Science* **254**: 1371-1374.

Solomon E, Borrow J and **Goddard AD**. (1991) Chromosomal aberrations in cancer. *Science* **254**: 1153-1160.

Pajunen L, Jones TA, **Goddard A**, Sheer D, Solomon E, Pihlajaniemi T and Kivirikko KI. (1991) Regional assignment of the human gene coding for a multifunctional peptide (P4HB) acting as the β–subunit of prolyl-4-hydroxylase and the enzyme protein disulfide isomerase to 17q25. *Cytogenet. Cell. Genet.* **56**: 165-168.

Borrow J, Black DM, **Goddard AD**, Yagle MK, Frischauf A.-M and Solomon E. (1991) Construction and regional localization of a *Not*I linking library from human chromosome 17q. *Genomics* **10**: 477–480.

Borrow J, **Goddard AD**, Sheer D and Solomon E. (1990) Molecular analysis of acute promyelocytic leukemia breakpoint cluster region on chromosome 17. *Science* **249**: 1577-1580.

Myers JC, Jones TA, Pohjolainen E-R, Kadri AS, **Goddard AD**, Sheer D, Solomon E and Pihlajaniemi T. (1990) Molecular cloning of 5(IV) collagen and assignment of the gene to the region of the region of the X-chromosome containing the Alport Syndrome locus. *Am. J. Hum. Genet.* **46**: 1024-1033.

Gallie BL, Squire JA, **Goddard A**, Dunn JM, Canton M, Hinton D, Zhu X and Phillips RA. (1990) Mechanisms of oncogenesis in retinoblastoma. *Lab. Invest.* **62**: 394-408.

Goddard AD, Phillips RA, Greger V, Passarge E, Hopping W, Gallie BL and Horsthemke B. (1990) Use of the RB1 cDNA as a diagnostic probe in retinoblastoma families. *Clinical Genetics* **37**: 117-126.

Zhu XP, Dunn JM, Phillips RA, **Goddard AD**, Paton KE, Becker A and Gallie BL. (1989) Germline, but not somatic, mutations of the RB1 gene preferentially involve the paternal allele. *Nature* **340**: 312-314.

Gallie BL, Dunn JM, **Goddard A**, Becker A and Phillips RA. (1988) Identification of mutations in the putative retinoblastoma gene. In <u>Molecular Biology of The Eye: Genes, Vision and Ocular Disease</u>. UCLA Symposia on Molecular and Cellular Biology, New Series, Volume 88. J. Piatigorsky, T. Shinohara and P.S. Zelenka, Eds. Alan R. Liss, Inc., New York, 1988, pp. 427-436.

Goddard AD, Balakier H, Canton M, Dunn J, Squire J, Reyes E, Becker A, Phillips RA and Gallie BL. (1988) Infrequent genomic rearrangement and normal expression of the putative RB1 gene in retinoblastoma tumors. *Mol. Cell. Biol.* **8**: 2082-2088.

Squire J, Dunn J, **Goddard A**, Hoffman T, Musarella M, Willard HF, Becker AJ, Gallie BL and Phillips RA. (1986) Cloning of the esterase D gene: A polymorphic gene probe closely linked to the retinoblastoma locus on chromosome 13. *Proc. Natl. Acad. Sci.* USA **83**: 6573-6577.

Squire J, **Goddard AD**, Canton M, Becker A, Phillips RA and Gallie BL (1986) Tumour induction by the retinoblastoma mutation is independent of N-*myc* expression. *Nature* **322**: 555-557.

Goddard AD, Heddle JA, Gallie BL and Phillips RA. (1985) Radiation sensitivity of fibroblasts of bilateral retinoblastoma patients as determined by micronucleus induction *in vitro*. *Mutation Research* **152**: 31-38.

IIIIIResearch

Oligonucleotides with Fluorescent Dyes at Opposite Ends Provide a Quenched Probe System Useful for Detecting PCR Product and Nucleic Acid Hybridization

Kenneth J. Livak, Susan J.A. Flood, Jeffrey Marmaro, William Giusti, and Karin Deetz

Perkin-Elmer, Applied Biosystems Division, Foster City, California 94404

The 5' nuclease PCR assay detects the accumulation of specific PCR product by hybridization and cleavage of a double-labeled fluorogenic probe during the amplification reaction. The probe is an oligonucleotide with both a reporter fluorescent dye and a quencher dye attached. An increase in reporter fluorescence intensity indicates that the probe has hybridized to the target PCR product and has been cleaved by the 5'→3' nucleolytic activity of *Taq* DNA polymerase. In this study, probes with the quencher dye attached to an internal nucleotide were compared with probes with the quencher dye attached to the 3'-end nucleotide. In all cases, the reporter dye was attached to the 5' end. All intact probes showed quenching of the reporter fluorescence. In general, probes with the quencher dye attached to the 3'-end nucleotide exhibited a larger signal in the 5' nuclease PCR assay than the internally labeled probes. It is proposed that the larger signal is caused by increased likelihood of cleavage by *Taq* DNA polymerase when the probe is hybridized to a template strand during PCR. Probes with the quencher dye attached to the 3'-end nucleotide also exhibited an increase in reporter fluorescence intensity when hybridized to a complementary strand. Thus, oligonucleotides with reporter and quencher dyes attached at opposite ends can be used as homogeneous hybridiza-

A homogeneous assay for detecting the accumulation of specific PCR product that uses a double-labeled fluorogenic probe was described by Lee et al.[1] The assay exploits the 5'→3' nucleolytic activity of *Taq* DNA polymerase[7,8] and is diagramed in Figure 1. The fluorogenic probe consists of an oligonucleotide with a reporter fluorescent dye, such as a fluorescein, attached to the 5' end; and a quencher dye, such as a rhodamine, attached internally. When the fluorescein is excited by irradiation, its fluorescent emission will be quenched if the rhodamine is close enough to be excited through the process of fluorescence energy transfer (FET).[4,5] During PCR, if the probe is hybridized to a template strand, *Taq* DNA polymerase will cleave the probe because of its inherent 5'→3' nucleolytic activity. If the cleavage occurs between the fluorescein and rhodamine dyes, it causes an increase in fluorescein fluorescence intensity because the fluorescein is no longer quenched. The increase in fluorescein fluorescence intensity indicates that the probe-specific PCR product has been generated. Thus, FET between a reporter dye and a quencher dye is critical to the performance of the probe in the 5' nuclease PCR assay.

Quenching is completely dependent on the physical proximity of the two dyes.[6] Because of this, it has been assumed that the quencher dye must be attached near the 5' end. Surprisingly, we have found that attaching a rhodamine dye at the 3' end of a probe

PCR assay. Furthermore, cleavage of this type of probe is not required to achieve some reduction in quenching. Oligonucleotides with a reporter dye on the 5' end and a quencher dye on the 3' end exhibit a much higher reporter fluorescence when double-stranded as compared with single-stranded. This should make it possible to use this type of double-labeled probe for homogeneous detection of nucleic acid hybridization.
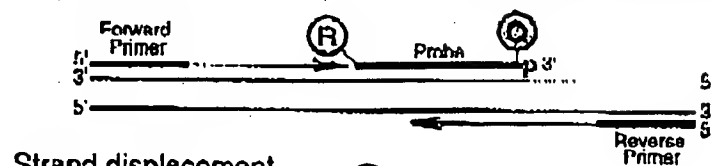
MATERIALS AND METHODS

Oligonucleotides

Table 1 shows the nucleotide sequence of the oligonucleotides used in this study. Linker arm nucleotide (LAN) phosphoramidite was obtained from Glen Research. The standard DNA phosphoramidites, 6-carboxyfluorescein (6-FAM) phosphoramidite, 6-carboxytetramethylrhodamine succinimidyl ester (TAMRA NHS ester), and Phosphalink for attaching a 3'-blocking phosphate, were obtained from Perkin-Elmer, Applied Biosystems Division. Oligonucleotide synthesis was performed using an ABI model 394 DNA synthesizer (Applied Biosystems). Primer and complement oligonucleotides were purified using Oligo Purification Cartridges (Applied Biosystems). Double-labeled probes were synthesized with 6-FAM-labeled phosphoramidite at the 5' end, LAN replacing one of the T's in the sequence, and Phosphalink at the 3' end. Following deprotection and ethanol precipitation,
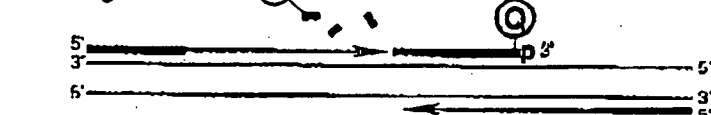
Research

Polymerization

Forward Primer　　　(R)　　Pmbs　　(Q)
5'
3'————————————————————————p 3'
5'————————————————————————
3'
5'
Reverse Primer

Strand displacement

(R)　　　　(Q)
5'
3'————————————————————p 5'
5'
3'
5'

Cleavage

(R)　　　　(Q)
5'
3'————————————————————p 3'
5'
3'
5'

Polymerization completed

(R)　　　(Q)
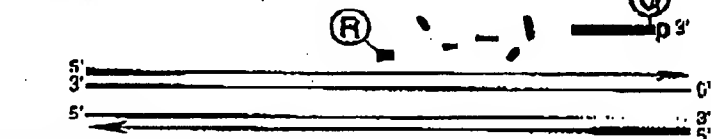5'
3'————————————————————p 3'
5'
3'
5'

FIGURE 1 Diagram of 5' nuclease assay. Stepwise representation of the 5' → 3' nucleolytic activity of *Taq* DNA polymerase acting on a fluorogenic probe during one extension phase of PCR.

mM Na-bicarbonate buffer (pH 9.0) at room temperature. Unreacted dye was removed by passage over a PD-10 Sephadex column. Finally, the double-labeled probe was purified by preparative high-performance liquid chromatography (HPLC) using an Aquapore C_8 221×4.6-mm column with 7-μm particle size. The column was developed with a 24-min linear gradient of 8–20% acetonitrile in 0.1 M TEAA (triethylamine acetate). Probes are named by designating the sequence from Table 1 and the position of the IAN–TAMRA moiety. For example, probe A1-7 has sequence A1 with IAN–TAMRA at nucleotide position 7 from the 5' end.

PCR Systems

All PCR amplifications were performed in the Perkin-Elmer GeneAmp PCR System 9600 using 50-μl reactions that contained 10 mM Tris-HCl (pH 8.3), 50 mM KCl, 200 μM dATP, 200 μM dCTP, 200 μM dGTP, 400 μM dUTP, 0.5 unit of AmpErase uracil N-glycosylase (Perkin-Elmer),

gene (nucleotides 2141–2435 in the sequence of Nakajima-Iijima et al.)[7] was amplified using primers APP and ARP (Table 1), which are modified slightly from those of du Breuil et al.[8] Actin amplification reactions contained 4 mM $MgCl_2$, 20 ng of human genomic DNA, 50 nM A1 or A3 probe, and 300 nM each

primer. The thermal regimen was 50°C (2 min), 95°C (10 min), 40 cycles of 95°C (20 sec), 60°C (1 min), and hold at 72°C. A 515-bp segment was amplified from a plasmid that consists of a segment of λ DNA (nucleotides 32,220–32,747) inserted in the SmaI site of vector pUC119. These reactions contained 3.5 mM $MgCl_2$, 1 ng of plasmid DNA, 50 nM P2 or P5 probe, 200 nM primer F119, and 200 nM primer R119. The thermal regimen was 50°C (2 min), 95°C (10 min), 25 cycles of 95°C (20 sec), 57°C (1 min), and hold at 72°C.

Fluorescence Detection

For each amplification reaction, a 40-μl aliquot of a sample was transferred to an individual well of a white, 96-well microtiter plate (Perkin-Elmer). Fluorescence was measured on the Perkin-Elmer Taq-Man LS-50B System, which consists of a luminescence spectrometer with plate reader assembly, a 485-nm excitation filter, and a 515-nm emission filter. Excitation was at 488 nm using a 5-nm slit width. Emission was measured at 518 nm for 6-FAM (the reporter or R value) and 582 nm for TAMRA (the quencher or Q value) using a 10-nm slit width. To determine the increase in reporter emission that is caused by cleavage of the probe during PCR, three normalizations are applied to the raw emission data. First, emission intensity of a buffer blank is subtracted for each wavelength. Second, emission intensity of the reporter is

TABLE 1 Sequences of Oligonucleotides

Name	Type	Sequence
F119	primer	ACCCACAGGAACTGATCACCACTC
R119	primer	ATGTCGCGTTCCGGCTGACGTTCTGG
P2	probe	TGGCATTACTGATCGTTCCCAACCACTp
P2C	complement	CTACTGGTTGGGAACGATCAGTAATGCCATG
P5	probe	CCGATTTGCTGGTATCTATCACAAGGATp
P5C	complement	TTCATCCTTGTCATAGATACCAGCAAATCCC
APP	primer	TCACCCACACTGTGCCCATCTACGA
ARP	primer	CAGCGTGAACGTGGCTCATTGCCAATGG
A1	probe	ATGCCCTCCCCCCATGCCATCCTGCGTp
A1C	complement	ACAGCGGAGGATGGCGATGGGGGAGGGGCATAC
A3	probe	CGCCCCTGGACTTCCGAGCAAGAGATp
A3C	complement	CCATCTCTTGCTCGGAAGTCCAGGGGCGAC

For each oligonucleotide used in this study, the nucleic acid sequence is given, written in the 5' → 3' direction. There are three types of oligonucleotides: PCR primer, fluorogenic probe used

■Research

A1-2	RAQCCCCTCCCCATCCCATCCTCCGTp	
A1-7	RATGCCCQCCCCATCCCATCCCGCCGTp	
A1-14	RATGCCCCTCCCCCAQCCCATCCTCCCTp	
A1-19	RATGCCCCTCCCCCATCCCAQCCTCCCGTp	
A1-22	RATGCCCCTCCCCCATCCCATCCQCCCGTp	
A1-26	RATCCCCCTCCCCCATCCCATCCTCCCQp	

Probe	518 nm		582 nm		RQ⁻	RQ⁺	ΔRQ
	no temp.	+ temp.	no temp.	+ temp.			
A1-2	26.5 ± 2.1	32.7 ± 1.0	38.2 ± 3.0	38.2 ± 2.0	0.57 ± 0.01	0.80 ± 0.06	0.10 ± 0.06
A1-7	83.8 ± 4.3	306.1 ± 21.4	108.5 ± 6.3	110.3 ± 5.3	0.40 ± 0.03	3.58 ± 0.17	3.09 ± 0.18
A1-14	127.0 ± 4.9	403.5 ± 19.1	109.7 ± 5.3	93.1 ± 6.3	1.16 ± 0.02	4.34 ± 0.15	3.18 ± 0.15
A1-19	187.5 ± 17.9	422.7 ± 7.7	70.3 ± 7.4	73.0 ± 2.0	2.67 ± 0.06	5.80 ± 0.16	3.13 ± 0.16
A1-22	224.6 ± 0.4	480.2 ± 43.6	100.0 ± 4.0	96.2 ± 0.8	2.25 ± 0.03	5.02 ± 0.11	2.77 ± 0.12
A1-26	160.2 ± 6.9	454.1 ± 16.4	93.1 ± 5.4	90.7 ± 3.2	1.72 ± 0.02	5.01 ± 0.08	3.29 ± 0.08

FIGURE 2 Results of 5' nuclease assay comparing β-actin probes with TAMRA at different nucleotide positions. As described in Materials and Methods, PCR amplifications containing the indicated probes were performed, and the fluorescence emission was measured at 518 and 582 nm. Reported values are the average ± 1 s.D. for six reactions run without added template (no temp.) and six reactions run with template (+ temp.). The RQ ratio was calculated for each individual reaction and averaged to give the reported RQ⁻ and RQ⁺ values.

divided by the emission intensity of the quencher to give an RQ ratio for each reaction tube. This normalizes for well-to-well variations in probe concentration and fluorescence measurement. Finally, ΔRQ is calculated by subtracting the RQ value of the no-template control (RQ⁻) from the RQ value for the complete reaction including template (RQ⁺).

RESULTS

A series of probes with increasing distances between the fluorescein reporter and rhodamine quencher were tested to investigate the minimum and maximum spacing that would give an acceptable performance in the 5' nuclease PCR assay. These probes hybridize to a target sequence in the human β-actin gene. Figure 2 shows the results of an experiment in which these probes were included in PCR that amplified a segment of the β-actin gene containing the target sequence. Performance in the 5' nuclease PCR assay is monitored by the magnitude of ΔRQ, which is a measure of the increase in reporter fluorescence caused by PCR amplification of the probe target. Probe A1-2 has a ΔRQ value that is close to zero, indicating that the probe was not cleaved appreciably during the amplification reaction. This suggests that with the quencher dye on the second nucleotide from the 5' end, there is insufficient room for Taq polymerase to cleave efficiently between the reporter and quencher. The other five probes exhibited comparable ΔRQ values that are

clearly different from zero. Thus, all five probes are being cleaved during PCR amplification resulting in a similar increase in reporter fluorescence. It should be noted that complete digestion of a probe produces a much larger increase in reporter fluorescence than that observed in Figure 2 (data not shown). Thus, even in reactions where amplification occurs, the majority of probe molecules remain uncleaved. It is mainly for this reason that the fluorescence intensity of the quencher dye TAMRA changes little with amplification of the target. This is what allows us to use the 582-nm fluorescence reading as a normalization factor.

The magnitude of RQ⁻ depends mainly on the quenching efficiency inherent in the specific structure of the probe and the purity of the oligonucleotide. Thus, the larger RQ⁻ values indicate that probes A1-14, A1-19, A1-22, and A1-26 probably have reduced quenching as compared with A1-7. Still, the degree of quenching is sufficient to detect a highly significant increase in reporter fluorescence when each of these probes is cleaved during PCR.

To further investigate the ability of TAMRA on the 3' end to quench 6-FAM on the 5' end, three additional pairs of probes were tested in the 5' nuclease PCR assay. For each pair, one probe has TAMRA attached to an internal nucleotide and the other has TAMRA attached to the 3' end nucleotide. The results are shown in Table 2. For all three sets, the probe with the 3' quencher exhibits a ΔRQ value that is considerably higher than for the probe with the internal quencher. The RQ⁻ values suggest that differences in quenching are not as great as those observed with some of the A1 probes. These results demonstrate that a quencher dye on the 3' end of an oligonucleotide can quench efficiently the

TABLE 2 Results of 5' Nuclease Assay Comparing Probes with TAMRA Attached to an Internal or 3'-terminal Nucleotide

Probe	518 nm		582 nm		RQ	RQ⁺	ΔRQ
	no temp.	+ temp.	no temp.	+ temp.			
A3-6	54.6 ± 3.2	84.8 ± 3.7	116.2 ± 6.4	115.6 ± 2.5	0.47 ± 0.02	0.73 ± 0.03	0.26 ± 0.04
A3-24	72.1 ± 2.9	236.5 ± 11.1	84.2 ± 4.0	90.2 ± 3.8	0.86 ± 0.02	2.62 ± 0.05	1.76 ± 0.05
P2-7	82.8 ± 4.4	384.0 ± 34.1	105.1 ± 6.4	120.4 ± 10.2	0.79 ± 0.02	3.19 ± 0.16	2.40 ± 0.16
P2-27	113.4 ± 6.6	555.4 ± 14.1	140.7 ± 8.5	118.7 ± 4.8	0.81 ± 0.01	4.68 ± 0.10	3.88 ± 0.10
P5-10	77.5 ± 6.5	244.4 ± 15.9	86.7 ± 4.3	95.8 ± 6.7	0.89 ± 0.05	2.55 ± 0.06	1.66 ± 0.08
P5-28	64.0 ± 5.2	333.6 ± 12.1	100.6 ± 6.1	94.7 ± 6.3	0.63 ± 0.02	3.53 ± 0.12	2.89 ± 0.13

... the indicated probes and calculations were performed as described in Material and Methods and in the legend to Fig. 2.

Research

fluorescence of a reporter dye on the 5' end. The degree of quenching is sufficient for this type of oligonucleotide to be used as a probe in the 5' nuclease PCR assay.

To test the hypothesis that quenching by a 3' TAMRA depends on the flexibility of the oligonucleotide, fluorescence was measured for probes in the single-stranded and double stranded states. Table 3 reports the fluorescence observed at 518 and 582 nm. The relative degree of quenching is assessed by calculating the RQ ratio. For probes with TAMRA 6–10 nucleotides from the 5' end, there is little difference in the RQ values when comparing single-stranded with double-stranded oligonucleotides. The results for probes with TAMRA at the 3' end are much different. For these probes, hybridization to a complementary strand causes a dramatic increase in RQ. We propose that this loss of quenching is caused by the rigid structure of double-stranded DNA, which prevents the 5' and 3' ends from being in proximity.

When TAMRA is placed toward the 3' end, there is a marked Mg^{2+} effect on quenching. Figure 3 shows a plot of observed RQ values for the A1 series of probes as a function of Mg^{2+} concentration. With TAMRA attached near the 5' end (probe A1-2 or A1-7), the RQ value at 0 mM Mg^{2+} is only slightly higher than RQ at 10 mM Mg^{2+}. For probes A1-19, A1-22, and A1-26, the RQ values at 0 mM Mg^{2+} are very high, indicating a much

reduced quenching efficiency. For each of these probes, there is a marked decrease in RQ at 1 mM Mg^{2+} followed by a gradual decline as the Mg^{2+} concentration increases to 10 mM. Probe A1-14 shows an intermediate RQ value at 0 mM Mg^{2+} with a gradual decline at higher Mg^{2+} concentrations. In a low-salt environment with no Mg^{2+} present, a single-stranded oligonucleotide would be expected to adopt an extended conformation because of electrostatic repulsion. The binding of Mg^{2+} ions acts to shield the negative charge of the phosphate backbone so that the oligonucleotide can adopt conformations where the 3' end is close to the 5' end. Therefore, the observed Mg^{2+} effects support the notion that quenching of a 5' reporter dye by TAMRA at or near the 3' end depends on the flexibility of the oligonucleotide.

DISCUSSION

The striking finding of this study is that it seems the rhodamine dye TAMRA, placed at any position in an oligonucleotide, can quench the fluorescent emission of a fluorescein (6-FAM) placed at the 5' end. This implies that a single-stranded, double-labeled oligonucleotide must be able to adopt conformations where the TAMRA is close to the 5' end. It should be noted that the decay of 6-FAM in the excited state requires a certain amount of time. Therefore, what

matters for quenching is not the average distance between 6-FAM and TAMR but, rather, how close TAMRA can get to 6-FAM during the lifetime of the 6-FAM excited state. As long as the decay time of the excited state is relatively long compared with the molecular motions of the oligonucleotide, quenching can occur. Thus, we propose that TAMRA at the 3' end, or any other position, can quench 6-FAM at the 5' end because TAMRA is in proximity to 6-FAM often enough to be able to accept energy transfer from an excited 6-FAM.

Details of the fluorescence measurements remain puzzling. For example, Table 3 shows that hybridization of probes A1-26, A3-24, and P5-28 to their complementary strands not only causes a large increase in 6-FAM fluorescence at 518 nm but also causes a modest increase in TAMRA fluorescence at 582 nm. If TAMRA is being excited by energy transfer from quenched 6-FAM, then loss of quenching attributable to hybridization should cause a decrease in the fluorescence emission of TAMRA. The fact that the fluorescence emission of TAMRA increases indicates that the situation is more complex. For example, we have anecdotal evidence that the bases of the oligonucleotide, especially G, quench the fluorescence of both 6-FAM and TAMRA to some degree. When double stranded, base-pairing may reduce the ability of the bases to quench. The primary factor causing the quenching of 6-FAM in an intact probe is the TAMRA dye. Evidence for the importance of TAMRA is that 6-FAM fluorescence remains relatively unchanged when probes labeled only with 6-FAM are used in the 5' nuclease PCR assay (data not shown). Secondary effectors of fluorescence, both before and after cleavage of the probe, need to be explored further.

Regardless of the physical mechanism, the relative independence of position and quenching greatly simplifies the design of probes for the 5' nuclease PCR assay. There are three main factors that determine the performance of a double-labeled fluorescent probe in the 5' nuclease PCR assay. The first factor is the degree of quenching observed in the intact probe. This is characterized by the value of RQ, which is the ratio of reporter to quencher fluorescent emis-

TABLE 3 Comparison of Fluorescence Emissions of Single-stranded and Double-stranded Fluorogenic Probes

Probe	518 nm		582 nm		RQ	
	ss	ds	ss	ds	ss	ds
A1-7	27.75	68.53	61.08	138.18	0.45	0.50
A1-26	43.31	509.38	53.50	93.86	0.81	5.43
A3-6	16.75	62.88	39.33	165.57	0.43	0.38
A3-24	30.05	578.64	67.72	140.25	0.45	3.21
P2-7	35.02	70.13	54.63	121.09	0.64	0.58
P2-27	39.89	320.47	65.10	61.13	0.61	5.25
P5-10	27.34	144.85	61.95	165.54	0.44	0.87
P5-28	33.65	462.29	72.39	104.61	0.46	4.43

(ss) Single-stranded. The fluorescence emissions at 518 or 582 nm for solutions containing a final concentration of 50 nM indicated probe, 10 mM Tris-HCl (pH 8.3), 50 mM KCl, and 10 mM MgCl₂. (ds) Double-stranded. The solutions contained, in addition, 100 nM A1C for probes A1-7 and A1-26, 100 nM A3C for probes A3-6 and A3-24, 100 nM P2C for probes P2-7 and P2-27, or 100 nM P5C for probes P5-10 and P5-28. Before the addition of MgCl₂, 120 µl of each sample was heated
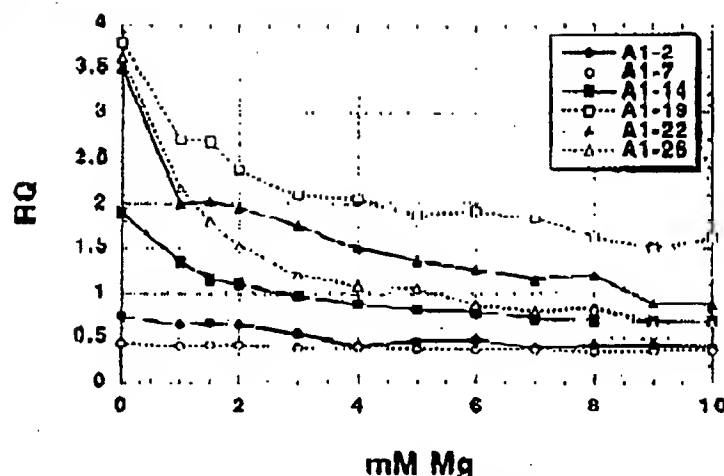
Research

FIGURE 3 Effect of Mg^{++} concentration on RQ ratio for the A1 series of probes. The fluorescence emission intensity at 518 and 582 nm was measured for solutions containing 50 nM probe, 10 mM Tris-HCl (pH 8.3), 50 mM KCl, and varying amounts (0–10 mM) of $MgCl_2$. The calculated RQ ratios (518 nm intensity divided by 582 nm intensity) are plotted vs. $MgCl_2$ concentration (mM Mg). The key (*upper right*) shows the probes examined.

dyes used, spacing between reporter and quencher dyes, nucleotide sequence context effects, presence of structure or other factors that reduce flexibility of the oligonucleotide, and purity of the probe. The second factor is the efficiency of hybridization, which depends on probe T_m, presence of secondary structure in probe or template, annealing temperature, and other reaction conditions. The third factor is the efficiency at which Taq DNA polymerase cleaves the bound probe between the reporter and quencher dyes. This cleavage is dependent on sequence complementarity between probe and template as shown by the observation that mismatches in the segment between reporter and quencher dyes drastically reduce the cleavage of probe.[1]

The rise in RQ values for the A1 series of probes seems to indicate that the degree of quenching is reduced somewhat as the quencher is placed toward the 3' end. The lowest apparent quenching is observed for probe A1-19 (see Fig. 3) rather than for the probe where the TAMRA is at the 3' end (A1-26). This is understandable, as the conformation of the 3' end position would be expected to be less restricted than the conformation of an internal position. In effect, a quencher at the 3' end is freer to adopt conformations close to the 5' reporter dye than is an internally placed

probes, the interpretation of RQ values is less clear-cut. The A3 probes show the same trend as A1, with the 3' TAMRA probe having a larger RQ than the internal TAMRA probe. For the P2 pair, both probes have about the same RQ value. For the P5 probes, the RQ for the 3' probe is less than for the internally labeled probe. Another factor that may explain some of the observed variation is that purity affects the RQ value. Although all probes are HPLC purified, a small amount of contamination with unquenched reporter can have a large effect on RQ.

Although there may be a modest effect on degree of quenching, the position of the quencher apparently can have a large effect on the efficiency of probe cleavage. The most drastic effect is observed with probe A1-2, where placement of the TAMRA on the second nucleotide reduces the efficiency of cleavage to almost zero. For the A3, P2, and P5 probes, ΔRQ is much greater for the 3' TAMRA probes as compared with the internal TAMRA probes. This is explained most easily by assuming that probes with TAMRA at the 3' end are more likely to be cleaved between reporter and quencher than are probes with TAMRA attached internally. For the A1 probes, the cleavage efficiency of probe A1-7 must already be quite high, as ΔRQ does not increase when the quencher is placed closer to the 3' end. This illus-

trates the importance of being able to use probes with a quencher on the 3' end in the 5' nuclease PCR assay. In this assay, an increase in the intensity of reporter fluorescence is observed only when the probe is cleaved between the reporter and quencher dyes. By placing the reporter and quencher dyes on the opposite ends of an oligonucleotide probe, any cleavage that occurs will be detected. When the quencher is attached to an internal nucleotide, sometimes the probe works well (A1-7) and other times not so well (A3-6). The relatively poor performance of probe A3-6 presumably means the probe is being cleaved 3' to the quencher rather than between the reporter and quencher. Therefore, the best chance of having a probe that reliably detects accumulation of PCR product in the 5' nuclease PCR assay is to use a probe with the reporter and quencher dyes on opposite ends.

Placing the quencher dye on the 3' end may also provide a slight benefit in terms of hybridization efficiency. The presence of a quencher attached to an internal nucleotide might be expected to disrupt base-pairing and reduce the T_m of a probe. In fact, a 2°C–3°C reduction in T_m has been observed for two probes with internally attached TAMRAs.[9] This disruptive effect would be minimized by placing the quencher at the 3' end. Thus, probes with 3' quenchers might exhibit slightly higher hybridization efficiencies than probes with internal quenchers.

The combination of increased cleavage and hybridization efficiencies means that probes with 3' quenchers probably will be more tolerant of mismatches between probe and target as compared with internally labeled probes. This tolerance of mismatches can be advantageous, as when trying to use a single probe to detect PCR-amplified products from samples of different species. Also, it means that cleavage of probe during PCR is less sensitive to alterations in annealing temperature or other reaction conditions. The one application where tolerance of mismatches may be a disadvantage is for allelic discrimination. Lee et al.[1] demonstrated that allele-specific probes were cleaved between reporter and quencher only when hybridized to a perfectly complementary target. This allowed them to distinguish the normal human cystic fibrosis allele from the ΔFS08 mutant. Their probes had TAMRA attached to the seventh nucleotide from
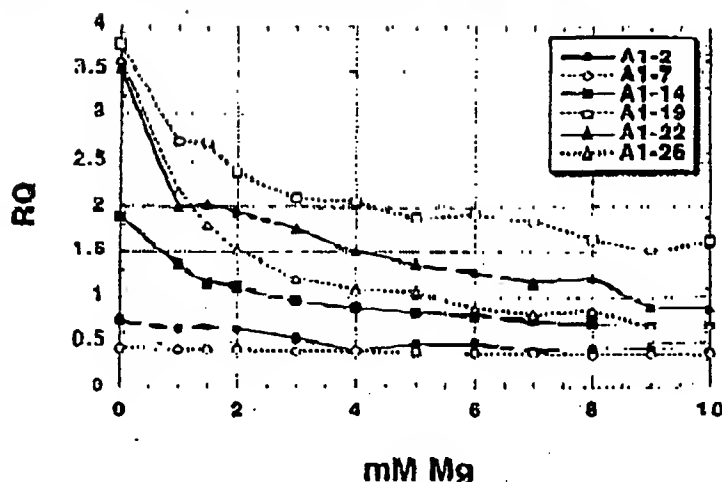
IIIIResearch

FIGURE 3 Effect of Mg^{2+} concentration on RQ ratio for the A1 series of probes. The fluorescence emission intensity at 518 and 582 nm was measured for solutions containing 50 nM probe, 10 mM Tris-HCl (pH 8.3), 50 mM KCl, and varying amounts (0-10 mM) of $MgCl_2$. The calculated RQ ratios (518 nm intensity divided by 582 nm intensity) are plotted vs. $MgCl_2$ concentration (mM Mg). The key (*upper right*) shows the probes examined.

dyes used, spacing between reporter and quencher dyes, nucleotide sequence context effects, presence of structure or other factors that reduce flexibility of the oligonucleotide, and purity of the probe. The second factor is the efficiency of hybridization, which depends on probe T_m, presence of secondary structure in probe or template, annealing temperature, and other reaction conditions. The third factor is the efficiency at which *Taq* DNA polymerase cleaves the bound probe between the reporter and quencher dyes. This cleavage is dependent on sequence complementarity between probe and template as shown by the observation that mismatches in the segment between reporter and quencher dyes drastically reduce the cleavage of probe.[1]

The rise in RQ values for the A1 series of probes seems to indicate that the degree of quenching is reduced somewhat as the quencher is placed toward the 3' end. The lowest apparent quenching is observed for probe A1-19 (see Fig. 3) rather than for the probe where the TAMRA is at the 3' end (A1-26). This is understandable, as the conformation of the 3' end position would be expected to be less restricted than the conformation of an internal position. In effect, a quencher at the 3' end is freer to adopt conformations close to the 5' reporter dye than is an internally placed quencher. For the other three sets of

probes, the interpretation of RQ values is less clear-cut. The A3 probes show the same trend as A1, with the 3' TAMRA probe having a larger RQ than the internal TAMRA probe. For the P2 pair, both probes have about the same RQ value. For the P5 probes, the RQ for the 3' probe is less than for the internally labeled probe. Another factor that may explain some of the observed variation is that purity affects the RQ value. Although all probes are HPLC purified, a small amount of contamination with unquenched reporter can have a large effect on RQ.

Although there may be a modest effect on degree of quenching, the position of the quencher apparently can have a large effect on the efficiency of probe cleavage. The most drastic effect is observed with probe A1-2, where placement of the TAMRA on the second nucleotide reduces the efficiency of cleavage to almost zero. For the A3, P2, and P5 probes, ΔRQ is much greater for the 3' TAMRA probes as compared with the internal TAMRA probes. This is explained most easily by assuming that probes with TAMRA at the 3' end are more likely to be cleaved between reporter and quencher than are probes with TAMRA attached internally. For the A1 probes, the cleavage efficiency of probe A1-7 must already be quite high, as ΔRQ does not increase when the quencher is placed closer to the 3' end. This illus-

trates the importance of being able to use probes with a quencher on the 3' end in the 5' nuclease PCR assay. In this assay, an increase in the intensity of reporter fluorescence is observed only when the probe is cleaved between the reporter and quencher dyes. By placing the reporter and quencher dyes on the opposite ends of an oligonucleotide probe, any cleavage that occurs will be detected. When the quencher is attached to an internal nucleotide, sometimes the probe works well (A1-7) and other times not so well (A3-6). The relatively poor performance of probe A3-6 presumably means the probe is being cleaved 3' to the quencher rather than between the reporter and quencher. Therefore, the best chance of having a probe that reliably detects accumulation of PCR product in the 5' nuclease PCR assay is to use a probe with the reporter and quencher dyes on opposite ends.

Placing the quencher dye on the 3' end may also provide a slight benefit in terms of hybridization efficiency. The presence of a quencher attached to an internal nucleotide might be expected to disrupt base-pairing and reduce the T_m of a probe. In fact, a 2°C–3°C reduction in T_m has been observed for two probes with internally attached TAMRAs.[9] This disruptive effect would be minimized by placing the quencher at the 3' end. Thus, probes with 3' quenchers might exhibit slightly higher hybridization efficiencies than probes with internal quenchers.

The combination of increased cleavage and hybridization efficiencies means that probes with 3' quenchers probably will be more tolerant of mismatches between probe and target as compared with internally labeled probes. This tolerance of mismatches can be advantageous, as when trying to use a single probe to detect PCR-amplified products from samples of different species. Also, it means that cleavage of probe during PCR is less sensitive to alterations in annealing temperature or other reaction conditions. The one application where tolerance of mismatches may be a disadvantage is for allelic discrimination. Lee et al.[6] demonstrated that allele-specific probes were cleaved between reporter and quencher only when hybridized to a perfectly complementary target. This allowed them to distinguish the normal human cystic fibrosis allele from the ΔF508 mutant. Their probes had TAMRA attached to the seventh nucleotide from

Research

the 5' end and were designed so that any mismatches were between the reporter and quencher. Increasing the distance between reporter and quencher would lessen the disruptive effect of mismatches and allow cleavage of the probe on the incorrect target. Thus, probes with a quencher attached to an internal nucleotide may still be useful for allelic discrimination.

In this study loss of quenching upon hybridization was used to show that quenching by a 3' TAMRA is dependent on the flexibility of a single-stranded oligonucleotide. The increase in reporter fluorescence intensity, though, could also be used to determine whether hybridization has occurred or not. Thus, oligonucleotides with reporter and quencher dyes attached at opposite ends should also be useful as hybridization probes. The ability to detect hybridization in real time means that these probes could be used to measure hybridization kinetics. Also, this type of probe could be used to develop homogeneous hybridization assays for diagnostics or other applications. Bagwell et al.[10] describe just this type of homogeneous assay where hybridization of a probe causes an increase in fluorescence caused by a loss of quenching. However, they utilized a complex probe design that requires adding nucleotides to both ends of the probe sequence to form two imperfect hairpins. The results presented here demonstrate that the simple addition of a reporter dye to one end of an oligonucleotide and a quencher dye to the other end generates a fluorogenic probe that can detect hybridization or PCR amplification.

ACKNOWLEDGMENTS

REFERENCES

1. Lee, L.G., C.R. Connell, and W. Bloch. 1993. Allelic discrimination by nick-translation PCR with fluorogenic probes. Nucleic Acids Res. 21: 3761 3766.
2. Holland, P.M., R.D. Abramson, R. Watson et al. by utilizing the 5' to 3' exonuclease activity of Thermus aquaticus DNA polymerase. Proc. Natl. Acad. Sci. 88: 7276 7280.
3. Lyamichev, V., M.A.D. Brow, and J.E. Dahlberg 1993. Structure-specific endonucleolytic cleavage of nucleic acids by eubacterial DNA polymerases. Science 260: 778-783.
4. Förster, V.Th. 1948. Zwischenmolekulare Energiewanderung und Fluoreszenz. Ann. Phys. (Leipzig) 2: 55 75.
5. Lakowicz, J.R 1983 Energy transfer. In Principles of fluorescent spectroscopy, pp. 303 339. Plenum Press, New York, NY.
6. Stryer, L. and R.P. Haugland. 1967. Energy transfer: A spectroscopic ruler. Proc. Natl. Acad. Sci. 58: 719-726.
7. Nakajima-Iijima, S., H. Hamada, P. Reddy, and T. Kakunaga. 1985. Molecular structure of the human cytoplasmic beta-actin gene: Inter-species homology of sequences in the introns. Proc. Natl. Acad. Sci. 82: 6133 6137.
8. du Breuil, R.M., J.M. Patel, and B.V. Mendelow. 1993. Quantitation of β-actin-specific mRNA transcripts using xeno-competitive PCR. PCR Methods Applic. 3: 57–59.
9. Livak, K.J. (unpubl.).
10. Bagwell, C.B., M.E. Munson, R.L. Christensen, and E.J. Lovett. 1994. A new homogeneous assay system for specific nucleic acid sequences. Poly-dA and poly-A detection. Nucleic Acids Res. 22: 2424-2425.

GENOME METHODS

Real Time Quantitative PCR

Christian A. Heid,[1] Junko Stevens,[2] Kenneth J. Livak,[2] and P. Mickey Williams[1,3]

[1]BioAnalytical Technology Department, Genentech, Inc., South San Francisco, California 94080;
[2]Applied BioSystems Division of Perkin Elmer Corp., Foster City, California 94404

We have developed a novel "real time" quantitative PCR method. The method measures PCR product accumulation through a dual-labeled fluorogenic probe (i.e., TaqMan Probe). This method provides very accurate and reproducible quantitation of gene copies. Unlike other quantitative PCR methods, real-time PCR does not require post-PCR sample handling, preventing potential PCR product carry-over contamination and resulting in much faster and higher throughput assays. The real-time PCR method has a very large dynamic range of starting target molecule determination (at least five orders of magnitude). Real-time quantitative PCR is extremely accurate and less labor-intensive than current quantitative PCR methods.

Quantitative nucleic acid sequence analysis has had an important role in many fields of biological research. Measurement of gene expression (RNA) has been used extensively in monitoring biological responses to various stimuli (Tan et al. 1994; Huang et al. 1995a,b; Prud'homme et al. 1995). Quantitative gene analysis (DNA) has been used to determine the genomic quantity of a particular gene, as in the case of the human HER2 gene, which is amplified in ~30% of breast tumors (Slamon et al. 1987). Gene and genome quantitation (DNA and RNA) also have been used for analysis of human immunodeficiency virus (HIV) burden demonstrating changes in the levels of virus throughout the different phases of the disease (Connor et al. 1993; Piatak et al. 1993b; Furtado et al. 1995).

Many methods have been described for the quantitative analysis of nucleic acid sequences (both for RNA and DNA; Southern 1975; Sharp et al. 1980; Thomas 1980). Recently, PCR has proven to be a powerful tool for quantitative nucleic acid analysis. PCR and reverse transcriptase (RT)–PCR have permitted the analysis of minimal starting quantities of nucleic acid (as little as one cell equivalent). This has made possible many experiments that could not have been performed with traditional methods. Although PCR has provided a powerful tool, it is imperative

that it be used properly for quantitation (Raaymaekers 1995). Many early reports of quantitative PCR and RT–PCR described quantitation of the PCR product but did not measure the initial target sequence quantity. It is essential to design proper controls for the quantitation of the initial target sequences (Ferre 1992; Clementi et al. 1993)

Researchers have developed several methods of quantitative PCR and RT–PCR. One approach measures PCR product quantity in the log phase of the reaction before the plateau (Kellogg et al. 1990; Pang et al. 1990). This method requires that each sample has equal input amounts of nucleic acid and that each sample under analysis amplifies with identical efficiency up to the point of quantitative analysis. A gene sequence (contained in all samples at relatively constant quantities, such as β-actin) can be used for sample amplification efficiency normalization. Using conventional methods of PCR detection and quantitation (gel electrophoresis or plate capture hybridization), it is extremely laborious to assure that all samples are analyzed during the log phase of the reaction (for both the target gene and the normalization gene). Another method, quantitative competitive (QC)–PCR, has been developed and is used widely for PCR quantitation. QC–PCR relies on the inclusion of an internal control competitor in each reaction (Becker-Andre 1991; Piatak et al. 1993a,b). The efficiency of each reaction is normalized to the internal competitor. A known amount of internal competitor can be

added to each sample. To obtain relative quantitation, the unknown target PCR product is compared with the known competitor PCR product. Success of a quantitative competitive PCR assay relies on developing an internal control that amplifies with the same efficiency as the target molecule. The design of the competitor and the validation of amplification efficiencies require a dedicated effort. However, because QC–PCR does not require that PCR products be analyzed during the log phase of the amplification, it is the easier of the two methods to use.

Several detection systems are used for quantitative PCR and RT–PCR analysis: (1) agarose gels, (2) fluorescent labeling of PCR products and detection with laser-induced fluorescence using capillary electrophoresis (Fasco et al. 1995; Williams et al. 1996) or acrylamide gels, and (3) plate capture and sandwich probe hybridization (Mulder et al. 1994). Although these methods proved successful, each method requires post-PCR manipulations that add time to the analysis and may lead to laboratory contamination. The sample throughput of these methods is limited (with the exception of the plate capture approach), and, therefore, these methods are not well suited for uses demanding high sample throughput (i.e., screening of large numbers of biomolecules or analyzing samples for diagnostics or clinical trials).

Here we report the development of a novel assay for quantitative DNA analysis. The assay is based on the use of the 5' nuclease assay first described by Holland et al. (1991). The method uses the 5' nuclease activity of *Taq* polymerase to cleave a nonextendible hybridization probe during the extension phase of PCR. The approach uses dual-labeled fluorogenic hybridization probes (Lee et al. 1993; Bassler et al. 1995; Livak et al. 1995a,b). One fluorescent dye serves as a reporter [FAM (i.e., 6-carboxyfluorescein)] and its emission spectra is quenched by the second fluorescent dye, TAMRA (i.e., 6-carboxy-tetramethyl-rhodamine). The nuclease degradation of the hybridization probe releases the quenching of the FAM fluorescent emission, resulting in an increase in peak fluorescent emission at 518 nm. The use of a sequence detector (ABI Prism) allows measurement of fluorescent spectra of all 96 wells of the thermal cycler continuously during the PCR amplification. Therefore, the reactions are monitored in real time. The output data is described and quantitative analysis of input target DNA sequences is discussed below.

RESULTS

PCR Product Detection in Real Time

The goal was to develop a high-throughput, sensitive, and accurate gene quantitation assay for use in monitoring lipid mediated therapeutic gene delivery. A plasmid encoding human factor VIII gene sequence, pF8TM (see Methods), was used as a model therapeutic gene. The assay uses fluorescent Taqman methodology and an instrument capable of measuring fluorescence in real time (ABI Prism 7700 Sequence Detector). The Taqman reaction requires a hybridization probe labeled with two different fluorescent dyes. One dye is a reporter dye (FAM), the other is a quenching dye (TAMRA). When the probe is intact, fluorescent energy transfer occurs and the reporter dye fluorescent emission is absorbed by the quenching dye (TAMRA). During the extension phase of the PCR cycle, the fluorescent hybridization probe is cleaved by the 5'–3' nucleolytic activity of the DNA polymerase. On cleavage of the probe, the reporter dye emission is no longer transferred efficiently to the quenching dye, resulting in an increase of the reporter dye fluorescent emission spectra. PCR primers and probes were designed for the human factor VIII sequence and human β-actin gene (as described in Methods). Optimization reactions were performed to choose the appropriate probe and magnesium concentrations yielding the highest intensity of reporter fluorescent signal without sacrificing specificity. The instrument uses a charge-coupled device (i.e., CCD camera) for measuring the fluorescent emission spectra from 500 to 650 nm. Each PCR tube was monitored sequentially for 25 msec with continuous monitoring throughout the amplification. Each tube was re-examined every 8.5 sec. Computer software was designed to examine the fluorescent intensity of both the reporter dye (FAM) and the quenching dye (TAMRA). The fluorescent intensity of the quenching dye, TAMRA, changes very little over the course of the PCR amplification (data not shown). Therefore, the intensity of TAMRA dye emission serves as an internal standard with which to normalize the reporter dye (FAM) emission variations. The software calculates a value termed ΔRn (or ΔRQ) using the following equation: $\Delta Rn = (Rn^+) (Rn^-)$, where Rn^+ = emission intensity of reporter/emission intensity of quencher at any given time in a reaction tube, and Rn^- = emission intensity of re-

HEID ET AL.

porter/emission intensity of quencher measured prior to PCR amplification in that same reaction tube. For the purpose of quantitation, the last three data points (ΔRns) collected during the extension step for each PCR cycle were analyzed. The nucleolytic degradation of the hybridization probe occurs during the extension phase of PCR, and, therefore, reporter fluorescent emission increases during this time. The three data points were averaged for each PCR cycle and the mean value for each was plotted in an "amplification plot" shown in Figure 1A. The ΔRn mean value is plotted on the y-axis, and time, represented by cycle number, is plotted on the x-axis. During the early cycles of the PCR amplification, the ΔRn

value remains at base line. When sufficient hybridization probe has been cleaved by the *Taq* polymerase nuclease activity, the intensity of reporter fluorescent emission increases. Most PCR amplifications reach a plateau phase of reporter fluorescent emission if the reaction is carried out to high cycle numbers. The amplification plot is examined early in the reaction, at a point that represents the log phase of product accumulation. This is done by assigning an arbitrary threshold that is based on the variability of the base-line data. In Figure 1A, the threshold was set at 10 standard deviations above the mean of base line emission calculated from cycles 1 to 15. Once the threshold is chosen, the point at which
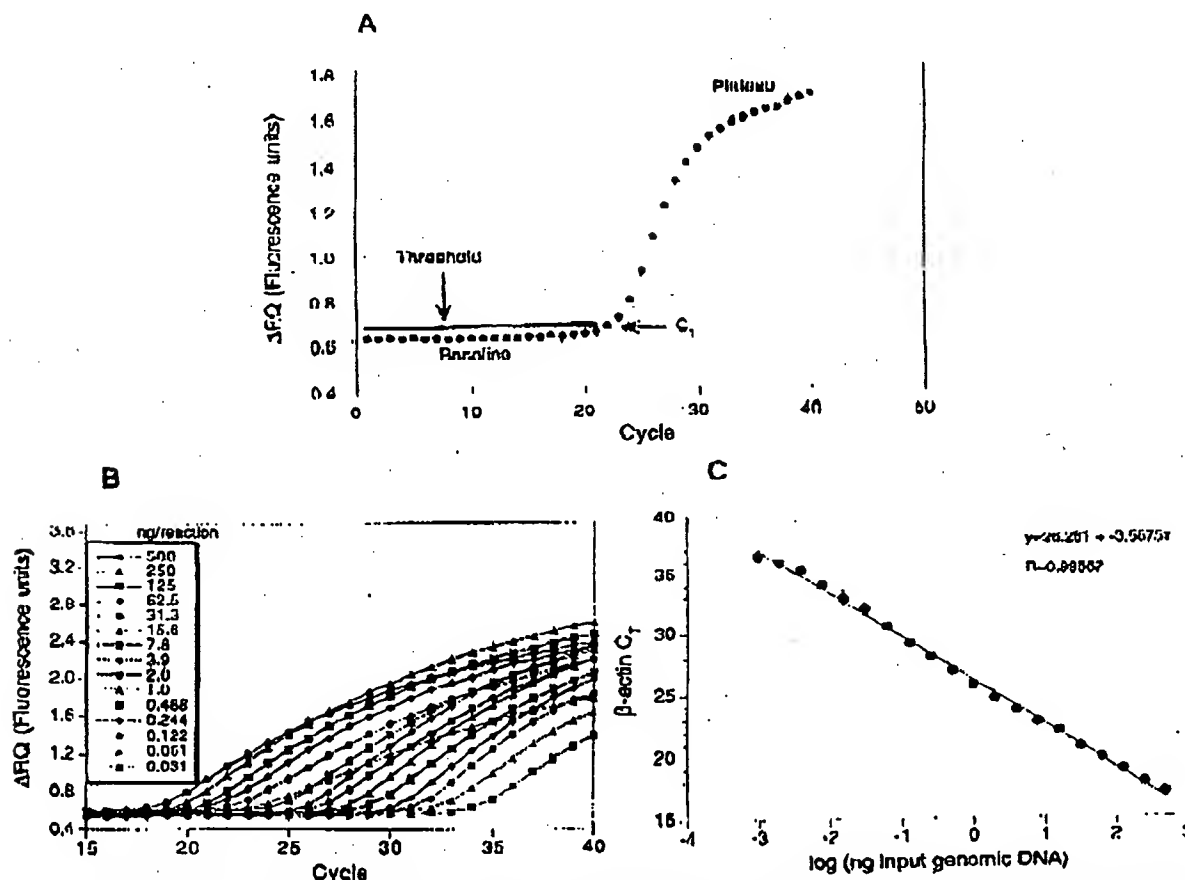

Figure 1 PCR product detection in real time. (*A*) The Model 7700 software will construct amplification plots from the extension phase fluorescent emission data collected during the PCR amplification. The standard deviation is determined from the data points collected from the base line of the amplification plot. C_T values are calculated by determining the point at which the fluorescence exceeds a threshold limit (usually 10 times the standard deviation of the base line). (*B*) Overlay of amplification plots of serially (1:2) diluted human genomic DNA samples amplified with β-actin primers. (*C*) Input DNA concentration of the samples plotted versus C_T. All

the amplification plot crosses the threshold is defined as C_T. C_T is reported as the cycle number at this point. As will be demonstrated, the C_T value is predictive of the quantity of input target.

C_T Values Provide a Quantitative Measurement of Input Target Sequences

Figure 1B shows amplification plots of 15 different PCR amplifications overlaid. The amplifications were performed on a 1:2 serial dilution of human genomic DNA. The amplified target was human β actin. The amplification plots shift to the right (to higher threshold cycles) as the input target quantity is reduced. This is expected because reactions with fewer starting copies of the target molecule require greater amplification to degrade enough probe to attain the threshold fluorescence. An arbitrary threshold of 10 standard deviations above the base line was used to determine the C_T values. Figure 1C represents the C_T values plotted versus the sample dilution value. Each dilution was amplified in triplicate PCR amplifications and plotted as mean values with error bars representing one standard deviation. The C_T values decrease linearly with increasing target quantity. Thus, C_T values can be used as a quantitative measurement of the input target number. It should be noted that the amplification plot for the 15.6-ng sample shown in Figure 1B does not reflect the same fluorescent rate of increase exhibited by most of the other samples. The 15.6-ng sample also achieves endpoint plateau at a lower fluorescent value than would be expected based on the input DNA. This phenomenon has been observed occasionally with other samples (data not shown) and may be attributable to late cycle inhibition; this hypothesis is still under investigation. It is important to note that the flattened slope and early plateau do not impact significantly the calculated C_T value as demonstrated by the fit on the line shown in Figure 1C. All triplicate amplifications resulted in very similar C_T values—the standard deviation did not exceed 0.5 for any dilution. This experiment contains a >100,000-fold range of input target molecules. Using C_T values for quantitation permits a much larger assay range than directly using total fluorescent emission intensity for quantitation. The linear range of fluorescent intensity measurement of the ABI Prism 7700 Sequence

ments over a very large range of relative starting target quantities.

Sample Preparation Validation

Several parameters influence the efficiency of PCR amplification: magnesium and salt concentrations, reaction conditions (i.e., time and temperature), PCR target size and composition, primer sequences, and sample purity. All of the above factors are common to a single PCR assay, except sample to sample purity. In an effort to validate the method of sample preparation for the factor VIII assay, PCR amplification reproducibility and efficiency of 10 replicate sample preparations were examined. After genomic DNA was prepared from the 10 replicate samples, the DNA was quantitated by ultraviolet spectroscopy. Amplifications were performed analyzing β-actin gene content in 100 and 25 ng of total genomic DNA. Each PCR amplification was performed in triplicate. Comparison of C_T values for each triplicate sample show minimal variation based on standard deviation and coefficient of variance (Table 1). Therefore, each of the triplicate PCR amplifications was highly reproducible, demonstrating that real time PCR using this instrumentation introduces minimal variation into the quantitative PCR analysis. Comparison of the mean C_T values of the 10 replicate sample preparations also showed minimal variability, indicating that each sample preparation yielded similar results for β-actin gene quantity. The highest C_T difference between any of the samples was 0.85 and 0.71 for the 100 and 25 ng samples, respectively. Additionally, the amplification of each sample exhibited an equivalent rate of fluorescent emission intensity change per amount of DNA target analyzed as indicated by similar slopes derived from the sample dilutions (Fig. 2). Any sample containing an excess of a PCR inhibitor would exhibit a greater measured β-actin C_T value for a given quantity of DNA. In addition, the inhibitor would be diluted along with the sample in the dilution analysis (Fig. 2), altering the expected C_T value change. Each sample amplification yielded a similar result in the analysis, demonstrating that this method of sample preparation is highly reproducible with regard to sample purity.

Quantitative Analysis of a Plasmid After

HID ET AL

Table 1. Reproducibility of Sample Preparation Method								
Sample no.	100 ng				25 ng			
	C_T	mean	standard deviation	CV	C_T	mean	standard deviation	CV
1	18.24				20.48			
	18.23				20.55			
	18.33	18.27	0.06	0.32	20.5	20.51	0.03	0.17
2	18.33				20.61			
	18.35				20.59			
	18.44	18.37	0.06	0.32	20.41	20.54	0.11	0.54
3	18.3				20.54			
	18.3				20.6			
	18.42	18.34	0.07	0.36	20.49	20.54	0.06	0.28
4	18.15				20.48			
	18.23				20.44			
	18.32	18.23	0.08	0.46	20.38	20.43	0.05	0.26
5	18.4				20.68			
	18.38				20.87			
	18.46	18.42	0.04	0.23	20.63	20.73	0.13	0.61
6	18.54				21.09			
	18.67				21.04			
	19	18.74	0.21	1.26	21.04	21.06	0.03	0.15
7	18.28				20.67			
	18.36				20.73			
	18.52	18.39	0.12	0.66	20.65	20.68	0.04	0.2
8	18.45				20.98			
	18.7				20.84			
	18.73	18.63	0.16	0.83	20.75	20.86	0.12	0.57
9	18.18				20.46			
	18.34				20.54			
	18.36	18.29	0.1	0.55	20.48	20.51	0.07	0.32
10	18.42				20.79			
	18.57				20.78			
	18.66	18.55	0.12	0.65	20.62	20.73	0.1	0.16
Mean	(1 10)	18.42	0.17	0.90		20.66	0.19	0.94

tor containing a partial cDNA for human factor VIII, pF8TM. A series of transfections was set up using a decreasing amount of the plasmid (40, 4, 0.5, and 0.1 µg). Twenty-four hours post-transfection, total DNA was purified from each flask of cells. β-Actin gene quantity was chosen as a value for normalization of genomic DNA concentration from each sample. In this experiment, β-actin gene content should remain constant relative to total genomic DNA. Figure 3 shows the result of the β-actin DNA measurement (100 ng total DNA determined by ultraviolet spectroscopy) of each sample. Each sample was analyzed in triplicate and the mean β-actin C_T values of the triplicates were plotted (error bars represent one standard deviation). The highest difference

between any two sample means was 0.95 C_T. Ten nanograms of total DNA of each sample were also examined for β-actin. The results again showed that very similar amounts of genomic DNA were present; the maximum mean β actin C_T value difference was 1.0. As Figure 3 shows, the rate of β-actin C_T change between the 100 and 10-ng samples was similar (slope values range between 3.56 and 3.45). This verifies again that the method of sample preparation yields samples of identical PCR integrity (i.e., no sample contained an excessive amount of a PCR inhibitor). However, these results indicate that each sample contained slight differences in the actual amount of genomic DNA analyzed. Determination of actual genomic DNA concentration was accomplished
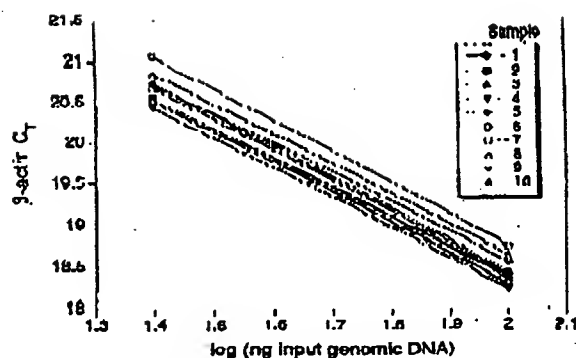
Figure 2 Sample preparation purity. The replicate samples shown in Table 1 were also amplified in triplicate using 25 ng of each DNA sample. The figure shows the input DNA concentration (100 and 25 ng) vs. C_t. In the figure, the 100 and 25 ng points for each sample are connected by a line.

by plotting the mean β-actin C_t value obtained for each 100-ng sample on a β-actin standard curve (shown in Fig. 4C). The actual genomic DNA concentration of each sample, a, was obtained by extrapolation to the x-axis.

Figure 4A shows the measured (i.e., non-normalized) quantities of factor VIII plasmid DNA (pF8TM) from each of the four transient cell transfections. Each reaction contained 100 ng of total sample DNA (as determined by UV spectroscopy). Each sample was analyzed in triplicate
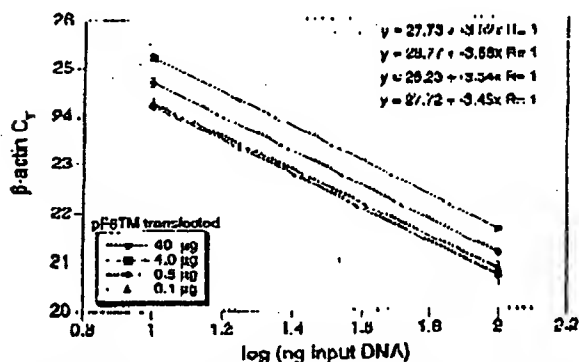

Figure 3 Analysis of transfected cell DNA quantity and purity. The DNA preparations of the four 293 cell transfections (40, 4, 0.5, and 0.1 μg of pF8TM) were analyzed for the β-actin gene. 100 and 10 ng (determined by ultraviolet spectroscopy) of each sample were amplified in triplicate. For each amount of pF8TM that was transfected, the β-actin C_t values are plotted versus the total input DNA concentration

PCR amplifications. As shown, pF8TM purified from the 293 cells decreases (mean C_t values increase) with decreasing amounts of plasmid transfected. The mean C_t values obtained for pF8TM in Figure 4A were plotted on a standard curve comprised of serially diluted pF8TM, shown in Figure 4B. The quantity of pF8TM, b, found in each of the four transfections was determined by extrapolation to the x axis of the standard curve in Figure 4B. These uncorrected values, b, for pF8TM were normalized to determine the actual amount of pF8TM found per 100 ng of genomic DNA by using the equation:

$$\frac{b \times 100\ \text{ng}}{a} = \frac{\text{actual pF8TM copies per}}{100\ \text{ng of genomic DNA}}$$

where a = actual genomic DNA in a sample and b = pF8TM copies from the standard curve. The normalized quantity of pF8TM per 100 ng of genomic DNA for each of the four transfections is shown in Figure 4D. These results show that the quantity of factor VIII plasmid associated with the 293 cells, 24 hr after transfection, decreases with decreasing plasmid concentration used in the transfection. The quantity of pF8TM associated with 293 cells, after transfection with 40 μg of plasmid, was 35 pg per 100 ng genomic DNA. This results in ~520 plasmid copies per cell.

DISCUSSION

We have described a new method for quantitating gene copy numbers using real-time analysis of PCR amplifications. Real-time PCR is compatible with either of the two PCR (RT-PCR) approaches: (1) quantitative competitive where an internal competitor for each target sequence is used for normalization (data not shown) or (2) quantitative comparative PCR using a normalization gene contained within the sample (i.e., β-actin) or a "housekeeping" gene for RT-PCR. If equal amounts of nucleic acid are analyzed for each sample and if the amplification efficiency before quantitative analysis is identical for each sample, the internal control (normalization gene or competitor) should give equal signals for all samples.

The real-time PCR method offers several advantages over the other two methods currently employed (see the introduction). First, the real-time PCR method is performed in a closed-tube system and requires no post-PCR manipulation
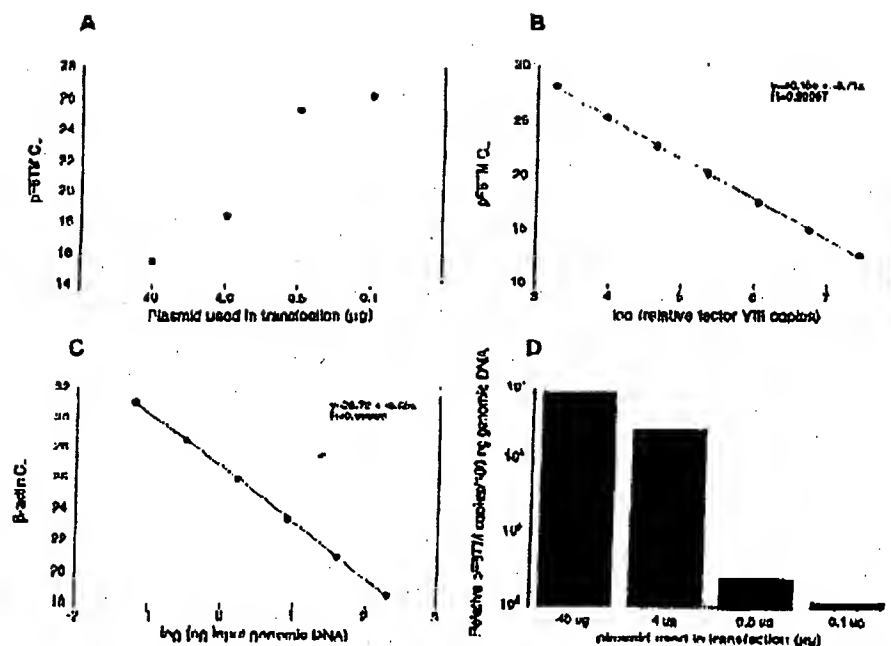
HUD ET AL.

Figure 4 Quantitative analysis of pF8TM in transfected cells. (A) Amount of plasmid DNA used for the transfection plotted against the mean C_t value determined for pF8TM remaining 24 hr after transfection. (B,C) Standard curves of pF8TM and β-actin, respectively. pF8TM DNA (B) and genomic DNA (C) were diluted serially 1:5 before amplification with the appropriate primers. The β-actin standard curve was used to normalize the results of A to 100 ng of genomic DNA. (D) The amount of pF8TM present per 100 ng of genomic DNA.

of sample. Therefore, the potential for PCR contamination in the laboratory is reduced because amplified products can be analyzed and disposed of without opening the reaction tubes. Second, this method supports the use of a normalization gene (i.e., β-actin) for quantitative PCR or housekeeping genes for quantitative RT-PCR controls. Analysis is performed in real time during the log phase of product accumulation. Analysis during log phase permits many different genes (over a wide input target range) to be analyzed simultaneously, without concern of reaching reaction plateau at different cycles. This will make multi-gene analysis assays much easier to develop, because individual internal competitors will not be needed for each gene under analysis. Third, sample throughput will increase dramatically with the new method because there is no post-PCR processing time. Additionally, working in a 96-well format is highly compatible with automation technology.

The real-time PCR method is highly reproducible. Replicate amplifications can be analyzed

for each sample minimizing potential error. The system allows for a very large assay dynamic range (approaching 1,000,000-fold starting target). Using a standard curve for the target of interest, relative copy number values can be determined for any unknown sample. Fluorescent threshold values, C_p, correlate linearly with relative DNA copy numbers. Real time quantitative RT-PCR methodology (Gibson et al., this issue) has also been developed. Finally, real time quantitative PCR methodology can be used to develop high-throughput screening assays for a variety of applications [quantitative gene expression (RT-PCR), gene copy assays (Her2, HIV, etc.), genotyping (knockout mouse analysis), and immuno-PCR].

Real-time PCR may also be performed using intercalating dyes (Higuchi et al. 1992) such as ethidium bromide. The fluorogenic probe method offers a major advantage over intercalating dyes—greater specificity (i.e., primer dimers and nonspecific PCR products are not detected).

METHODS

Generation of a Plasmid Containing a Partial cDNA for Human Factor VIII

Total RNA was harvested (RNAxol B from Tel Test, Inc., Friendswood, TX) from cells transfected with a factor VIII expression vector, pCIS2.8c251) (Eaton et al. 1986; Gorman et al. 1990). A factor VIII partial cDNA sequence was generated by RT PCR [GeneAmp EZ rTth RNA PCR Kit (part N808-0179, PE Applied Biosystems, Foster City, CA)] using the PCR primers F8for and F8rev (primer sequences are shown below). The amplicon was reamplified using modified F8for and F8rev primers (appended with BamH I and HindIII restriction site sequences at the 5' end) and cloned into pGEM-3Z (Promega Corp., Madison, WI). The resulting clone, pF8TM, was used for transient transfection of 293 cells.

Amplification of Target DNA and Detection of Amplicon Factor VIII Plasmid DNA

(pF8TM) was amplified with the primers F8for 5'-CCC-GTCCCAAGAGTGATXHGTC-3' and F8rev 5'-AAACCT-CAGCCTGGATCGTTACG-3'. The reaction produced a 422-bp PCR product. The forward primer was designed to recognize a unique sequence found in the 5' untranslated region of the parent pCIS2.8c251) plasmid and therefore does not recognize and amplify the human factor VIII gene. Primers were chosen with the assistance of the computer program Oligo 4.0 (National Biosciences, Inc., Plymouth, MN). The human β-actin gene was amplified with the primers β-actin forward primer 5'-TCACCCAACACTGT GCCCATCTACGA-3' and β-actin reverse primer 5'-CAG CGGAACCGCTCATTGCCAATGG-3'. The reaction produced a 295-bp PCR product.

Amplification reactions (50 μl) contained a DNA sample, 10X PCR Buffer II (5 μl), 200 μM dATP, dCTP, dGTP, and 400 μM dUTP, 4 mM MgCl₂, 1.25 Units Ampli Taq DNA polymerase, 0.5 unit AmpErase uracil N-glycosylase (UNG), 60 pmole of each factor VIII primer, and 15 pmole of each β-actin primer. The reactions also contained one of the following detection probes (100 nM each): F8probe 5'-(FAM)AGCCTCTCCACCTGCTTCTTTCTCT-GCCTT(TAMRA)p 3' and β-actin probe 5' (FAM)ATGCXXC-X(TAMRA)CCCCCATGCCATCp-3' where p indicates phosphorylation and X indicates a linker arm nucleotide. Reaction tubes were MicroAmp Optical Tubes (part number N801 0933, Perkin Elmer) that were frosted (at Perkin Elmer) to prevent light from reflecting. Tube caps were similar to MicroAmp Caps but specially designed to prevent light scattering. All of the PCR consumables were supplied by PE Applied Biosystems (Foster City, CA) except the factor VIII primers, which were synthesized at Genentech, Inc. (South San Francisco, CA). Probes were designed using the Oligo 4.0 software, following guidelines suggested in the Model 7700 Sequence Detector Instrument manual. Briefly, probe T_m should be at least 5°C higher than the annealing temperature used during thermal cycling; primers should not form stable duplexes with the probe.

The thermal cycling conditions included 2 min at 50°C and 10 min at 95°C. Thermal cycling proceeded with

reactions were performed in the Model 7700 Sequence Detector (PE Applied Biosystems), which contains a Gene-Amp PCR System 9600. Reaction conditions were programmed on a Power Macintosh 7100 (Apple Computer, Santa Clara, CA) linked directly to the Model 7700 Sequence Detector. Analysis of data was also performed on the Macintosh computer. Collection and analysis software was developed at PE Applied Biosystems.

Transfection of Cells with Factor VIII Construct

Four T175 flasks of 293 cells (ATCC CRL 1573), a human fetal kidney suspension cell line, were grown to 80% confluency and transfected pF8TM. Cells were grown in the following media: 50% HAM'S F12 without GHT, 50% low glucose Dulbecco's modified Eagle medium (DMEM) without glycine with sodium bicarbonate, 10% fetal bovine serum, 2 mM L-glutamine, and 1% penicillin–streptomycin. The media was changed 30 min before the transfection. pF8TM DNA amounts of 40, 4, 0.5, and 0.1 μg were added to 1.5 ml of a solution containing 0.125 M CaCl₂ and 1 × HEPES. The four mixtures were left at room temperature for 10 min and then added dropwise to the cells. The flasks were incubated at 37°C and 5% CO₂ for 24 hr, washed with PBS, and resuspended in PBS. The resuspended cells were divided into aliquots and DNA was extracted immediately using the QIAamp Blood Kit (Qiagen, Chatsworth, CA). DNA was eluted into 200 μl of 20 mM Tris-HCl at pH 8.0.

ACKNOWLEDGMENTS

REFERENCES

Bassler, H.A., S.J. Flood, K.J. Livak, J. Marmaro, R. Knorr, and C.A. Batt. 1995. Use of a fluorogenic probe in a PCR-based assay for the detection of Listeria monocytogenes. App. Environ. Microbhil. 61: 3724–3728.

Becker-Andre, M. 1991. Quantitative evaluation of mRNA levels. Meth. Mol. Cell. Biol. 2: 189 201.

Clementi, M., S. Menzo, P. Bagnarelli, A. Manzin, A. Valenza, and P.E. Varaldo. 1993. Quantitative PCR and RT-PCR in virology. [Review]. PCR Methods Applic. 2: 191–196.

Connor, R.I., H. Mohri, Y. Cao, and D.D. Ho. 1993. Increased viral burden and cytopathicity correlate temporally with CD4+ T-lymphocyte decline and clinical progression in human immunodeficiency virus type 1-infected individuals. J. Virol. 67: 1772–1777.

Eaton, D.L., W.I. Wood, D. Eaton, P.E. Hass, P.

HEID ET AL.

Venar, and C. Gorman. 1986. Construction and characterization of an active factor VIII variant lacking the central one third of the molecule. *Biochemistry* 25: 8343–8347.

Fasco, M.J., C.P. Treanor, S. Spivack, H.L. Figge, and L.S. Kaminsky. 1995. Quantitative RNA-polymerase chain reaction-DNA analysis by capillary electrophoresis and laser-induced fluorescence. *Anal. Biochem.* 224: 140–147.

Ferre, F. 1992. Quantitative or semi-quantitative PCR: Reality versus myth. *PCR Methods Applic.* 2: 1–9.

Furtado, M.R., L.A. Kingsley, and S.M. Wolinsky. 1995. Changes in the viral mRNA expression pattern correlate with a rapid rate of CD4+ T-cell number decline in human immunodeficiency virus type 1-infected individuals. *J. Virol.* 69: 2092–2100.

Gibson, U.E.M., C.A. Heid, and P.M. Williams. 1996. A novel method for real time quantitative competitive RT-PCR. *Genome Res.* (this issue).

Gorman, C.M., D.R. Gies, and G. McCray. 1990. Transient production of proteins using an adenovirus transformed cell line. *DNA Prot. Engin. Tech.* 2: 3–10.

Higuchi, R., G. Dollinger, P.S. Walsh, and R. Griffith. 1992. Simultaneous amplification and detection of specific DNA sequences. *Biotechnology* 10: 413–417.

Holland, P.M., R.D. Abramson, R. Watson, and D.H. Gelfand. 1991. Detection of specific polymerase chain reaction product by utilizing the 5'——3' exonuclease activity of Thermus aquaticus DNA polymerase. *Proc. Natl. Acad. Sci.* 88: 7276–7280.

Huang, S.K., H.Q. Xiao, T.J. Kleine, G. Paciotti, D.G. Marsh, L.M. Lichtenstein, and M.C. Liu. 1995a. IL-13 expression at the sites of allergen challenge in patients with asthma. *J. Immun.* 155: 2688–2694.

Huang, S.K., M. Yi, E. Palmer, and D.G. Marsh. 1995b. A dominant T cell receptor beta-chain in response to a short ragweed allergen, Amb a 5. *J. Immun.* 164: 6157–6162.

Kellogg, D.E., J.J. Sninsky, and S. Kwok. 1990. Quantitation of HIV-1 proviral DNA relative to cellular DNA by the polymerase chain reaction. *Anal. Biochem.* 189: 202–208.

Lee, L.G., C.R. Connell, and W. Bloch. 1993. Allelic discrimination by nick-translation PCR with fluorogenic probes. *Nucleic Acids Res.* 21: 3761–3766.

Livak, K.J., S.J. Flood, J. Marmaro, W. Giusti, and K. Deetz. 1995a. Oligonucleotides with fluorescent dyes at opposite ends provide a quenched probe system useful for detecting PCR product and nucleic acid hybridization. *PCR Methods Applic.* 4: 357–362.

Livak, K.J., J. Marmaro, and J.A. Todd. 1995b. Towards

fully automated genome-wide polymorphism screening [Letter] *Nature Genet.* 9: 341–342.

Mulder, J., N. McKinney, C. Christopherson, J. Sninsky, L. Greenfield, and S. Kwok. 1994. Rapid and simple PCR assay for quantitation of human immunodeficiency virus type 1 RNA in plasma: Application to acute retroviral infection. *J. Clin. Microbiol.* 32: 292–300.

Pang, S., Y. Koyanagi, S. Miles, C. Wiley, H.V. Vinters, and I.S. Chen. 1990. High levels of unintegrated HIV-1 DNA in brain tissue of AIDS dementia patients. *Nature* 343: 85–89.

Piatak, M.J., K.C. Luk, B. Williams, and J.D. Lifson. 1993a. Quantitative competitive polymerase chain reaction for accurate quantitation of HIV DNA and RNA species. *BioTechniques* 14: 70–81.

Piatak, M.J., M.S. Saag, L.C. Yang, S.J. Clark, J.C. Kappes, K.C. Luk, B.H. Hahn, G.M. Shaw, and J.D. Lifson. 1993b. High levels of HIV-1 in plasma during all stages of infection determined by competitive PCR [see Comments]. *Science* 259: 1749–1754.

Prud'homme, G.J., D.H. Kono, and A.N. Theofilopoulos. 1995. Quantitative polymerase chain reaction analysis reveals marked overexpression of interleukin-1 beta, interleukin-1 and interferon-gamma mRNA in the lymph nodes of lupus-prone mice. *Mol. Immunol.* 32: 495–503.

Raeymaekers, L. 1995. A commentary on the practical applications of competitive PCR. *Genome Res.* 5: 91–94.

Sharp, P.A., A.J. Berk, and S.M. Berget. 1980. Transcription maps of adenovirus. *Methods Enzymol.* 65: 750–768.

Slamon, D.J., G.M. Clark, S.G. Wong, W.J. Levin, A. Ullrich, and W.L. McGuire. 1987. Human breast cancer: Correlation of relapse and survival with amplification of the HER-2/neu oncogene. *Science* 235: 177–182.

Southern, E.M. 1975. Detection of specific sequences among DNA fragments separated by gel electrophoresis. *J. Mol. Biol.* 98: 503–517.

Tan, X., X. Sun, C.F. Gonzalez, and W. Hsueh. 1994. PAF and TNF increase the precursor of NF-kappa B p50 mRNA in mouse intestine: Quantitative analysis by competitive PCR. *Biochim. Biophys. Acta* 1215: 157–162.

Thomas, P.S. 1980. Hybridization of denatured RNA and small DNA fragments transferred to nitrocellulose. *Proc. Natl. Acad. Sci.* 77: 5201–5205.

Williams, S., C. Schwer, A. Krishnarao, C. Heid, B. Karger, and P.M. Williams. 1996. Quantitative competitive PCR: Analysis of amplified products of the HIV-1 gag gene by capillary electrophoresis with laser induced fluorescence detection. *Anal. Biochem.* (in press).

Received June 3, 1996; accepted in revised form July 29, 1996.

WISP genes are members of the connective tissue growth factor family that are up-regulated in Wnt-1-transformed cells and aberrantly expressed in human colon tumors

DIANE PENNICA*†, TODD A. SWANSON*, JAMES W. WELSH*, MARGARET A. ROY‡, DAVID A. LAWRENCE*, JAMES LEE‡, JENNIFER BRUSH‡, LISA A. TANEYHILL§, BETHANNE DEUEL‡, MICHAEL LEW¶, COLIN WATANABE‖, ROBERT L. COHEN*, MONA F. MELHEM**, GENE G. FINLEY**, PHIL QUIRKE††, AUDREY D. GODDARD‡, KENNETH J. HILLAN¶, AUSTIN L. GURNEY‡, DAVID BOTSTEIN‡,‡‡, AND ARNOLD J. LEVINE§

Departments of *Molecular Oncology, ‡Molecular Biology, ‖Scientific Computing, and ¶Pathology, Genentech Inc., 1 DNA Way, South San Francisco, CA 94080; **University of Pittsburgh School of Medicine, Veterans Administration Medical Center, Pittsburgh, PA 15240; ††University of Leeds, Leeds, LS29JT United Kingdom; ‡‡Department of Genetics, Stanford University, Palo Alto, CA 94305; and §Department of Molecular Biology, Princeton University, Princeton, NJ 08544

Contributed by David Botstein and Arnold J. Levine, October 21, 1998

ABSTRACT   Wnt family members are critical to many developmental processes, and components of the Wnt signaling pathway have been linked to tumorigenesis in familial and sporadic colon carcinomas. Here we report the identification of two genes, WISP-1 and WISP-2, that are up-regulated in the mouse mammary epithelial cell line C57MG transformed by Wnt-1, but not by Wnt-4. Together with a third related gene, WISP-3, these proteins define a subfamily of the connective tissue growth factor family. Two distinct systems demonstrated WISP induction to be associated with the expression of Wnt-1. These included (i) C57MG cells infected with a Wnt-1 retroviral vector or expressing Wnt-1 under the control of a tetracyline repressible promoter, and (ii) Wnt-1 transgenic mice. The WISP-1 gene was localized to human chromosome 8q24.1–8q24.3. WISP-1 genomic DNA was amplified in colon cancer cell lines and in human colon tumors and its RNA overexpressed (2- to >30-fold) in 84% of the tumors examined compared with patient-matched normal mucosa. WISP-3 mapped to chromosome 6q22–6q23 and also was overexpressed (4- to >40-fold) in 63% of the colon tumors analyzed. In contrast, WISP-2 mapped to human chromosome 20q12–20q13 and its DNA was amplified, but RNA expression was reduced (2- to >30-fold) in 79% of the tumors. These results suggest that the WISP genes may be downstream of Wnt-1 signaling and that aberrant levels of WISP expression in colon cancer may play a role in colon tumorigenesis.

Wnt-1 is a member of an expanding family of cysteine-rich, glycosylated signaling proteins that mediate diverse developmental processes such as the control of cell proliferation, adhesion, cell polarity, and the establishment of cell fates (1, 2). Wnt-1 originally was identified as an oncogene activated by the insertion of mouse mammary tumor virus in virus-induced mammary adenocarcinomas (3, 4). Although Wnt-1 is not expressed in the normal mammary gland, expression of Wnt-1 in transgenic mice causes mammary tumors (5).

In mammalian cells, Wnt family members initiate signaling by binding to the seven-transmembrane spanning Frizzled receptors and recruiting the cytoplasmic protein Dishevelled (Dsh) to the cell membrane (1, 2, 6). Dsh then inhibits the kinase activity of the normally constitutively active glycogen synthase kinase-3β (GSK-3β) resulting in an increase in β-catenin levels. Stabilized β-catenin interacts with the transcription factor TCF/Lef1, forming a complex that appears in

the nucleus and binds TCF/Lef1 target DNA elements to activate transcription (7, 8). Other experiments suggest that the adenomatous polyposis coli (APC) tumor suppressor gene also plays an important role in Wnt signaling by regulating β-catenin levels (9). APC is phosphorylated by GSK-3β, binds to β-catenin, and facilitates its degradation. Mutations in either APC or β-catenin have been associated with colon carcinomas and melanomas, suggesting these mutations contribute to the development of these types of cancer, implicating the Wnt pathway in tumorigenesis (1).

Although much has been learned about the Wnt signaling pathway over the past several years, only a few of the transcriptionally activated downstream components activated by Wnt have been characterized. Those that have been described cannot account for all of the diverse functions attributed to Wnt signaling. Among the candidate Wnt target genes are those encoding the nodal-related 3 gene, Xnr3, a member of the transforming growth factor (TGF)-β superfamily, and the homeobox genes, engrailed, goosecoid, twin (Xtwn), and siamois (2). A recent report also identifies c-myc as a target gene of the Wnt signaling pathway (10).

To identify additional downstream genes in the Wnt signaling pathway that are relevant to the transformed cell phenotype, we used a PCR-based cDNA subtraction strategy, suppression subtractive hybridization (SSH) (11), using RNA isolated from C57MG mouse mammary epithelial cells and C57MG cells stably transformed by a Wnt-1 retrovirus. Overexpression of Wnt-1 in this cell line is sufficient to induce a partially transformed phenotype, characterized by elongated and refractile cells that lose contact inhibition and form a multilayered array (12, 13). We reasoned that genes differentially expressed between these two cell lines might contribute to the transformed phenotype.

In this paper, we describe the cloning and characterization of two genes up-regulated in Wnt-1 transformed cells, WISP-1 and WISP-2, and a third related gene, WISP-3. The WISP genes are members of the CCN family of growth factors, which includes connective tissue growth factor (CTGF), Cyr61, and nov, a family not previously linked to Wnt signaling.

MATERIALS AND METHODS

SSH. SSH was performed by using the PCR-Select cDNA Subtraction Kit (CLONTECH). Tester double-stranded

---

Abbreviations: TGF, transforming growth factor; CTGF, connective tissue growth factor; SSH, suppression subtractive hybridization; VWC, von Willebrand factor type C module.
Data deposition: The sequences reported in this paper have been deposited in the Genbank database (accession nos. AF100777, AF100778, AF100779, AF100780, and AF100781).
†To whom reprint requests should be addressed. e-mail: diane@gene.com.

cDNA was synthesized from 2 μg of poly(A)$^+$ RNA isolated from the C57MG/Wnt-1 cell line and driver cDNA from 2 μg of poly(A)$^+$ RNA from the parent C57MG cells. The subtracted cDNA library was subcloned into a pGEM-T vector for further analysis.

cDNA Library Screening. Clones encoding full-length mouse *WISP-1* were isolated by screening a λgt10 mouse embryo cDNA library (CLONTECH) with a 70-bp probe from the original partial clone 568 sequence corresponding to amino acids 128–169. Clones encoding full-length human *WISP-1* were isolated by screening λgt10 lung and fetal kidney cDNA libraries with the same probe at low stringency. Clones encoding full-length mouse and human *WISP-2* were isolated by screening a C57MG/Wnt-1 or human fetal lung cDNA library with a probe corresponding to nucleotides 1463–1512. Full-length cDNAs encoding *WISP-3* were cloned from human bone marrow and fetal kidney libraries.

Expression of Human WISP RNA. PCR amplification of first-strand cDNA was performed with human Multiple Tissue cDNA panels (CLONTECH) and 300 μM of each dNTP at 94°C for 1 sec, 62°C for 30 sec, 72°C for 1 min, for 22–32 cycles. *WISP* and glyceraldehyde-3-phosphate dehydrogenase primer sequences are available on request.

In Situ **Hybridization.** ^{33}P-labeled sense and antisense riboprobes were transcribed from an 897-bp PCR product corresponding to nucleotides 601–1440 of mouse *WISP-1* or a 294-bp PCR product corresponding to nucleotides 82–375 of mouse *WISP-2*. All tissues were processed as described (40).

Radiation Hybrid Mapping. Genomic DNA from each hybrid in the Stanford G3 and Genebridge4 Radiation Hybrid Panels (Research Genetics, Huntsville, AL) and human and hamster control DNAs were PCR-amplified, and the results were submitted to the Stanford or Massachusetts Institute of Technology web servers.

Cell Lines, Tumors, and Mucosa Specimens. Tissue specimens were obtained from the Department of Pathology (University of Pittsburgh) for patients undergoing colon resection and from the University of Leeds, United Kingdom. Genomic DNA was isolated (Qiagen) from the pooled blood of 10 normal human donors, surgical specimens, and the following ATCC human cell lines: SW480, COLO 320DM, HT-29, WiDr, and SW403 (colon adenocarcinomas), SW620 (lymph node metastasis, colon adenocarcinoma), HCT 116 (colon carcinoma), SK-CO-1 (colon adenocarcinoma, ascites), and HM7 (a variant of ATCC colon adenocarcinoma cell line LS 174T). DNA concentration was determined by using Hoechst dye 33258 intercalation fluorimetry. Total RNA was prepared by homogenization in 7 M GuSCN followed by centrifugation over CsCl cushions or prepared by using RNAzol.

Gene Amplification and RNA Expression Analysis. Relative gene amplification and RNA expression of *WISP*s and c-*myc* in the cell lines, colorectal tumors, and normal mucosa were determined by quantitative PCR. Gene-specific primers and fluorogenic probes (sequences available on request) were designed and used to amplify and quantitate the genes. The relative gene copy number was derived by using the formula $2^{(\Delta ct)}$ where ΔCt represents the difference in amplification cycles required to detect the *WISP* genes in peripheral blood lymphocyte DNA compared with colon tumor DNA or colon tumor RNA compared with normal mucosal RNA. The ∂-method was used for calculation of the SE of the gene copy number or RNA expression level. The *WISP*-specific signal was normalized to that of the glyceraldehyde-3-phosphate dehydrogenase housekeeping gene. All TaqMan assay reagents were obtained from Perkin–Elmer Applied Biosystems.

RESULTS

Isolation of *WISP-1* and *WISP-2* by SSH. To identify Wnt-1-inducible genes, we used the technique of SSH using the mouse mammary epithelial cell line C57MG and C57MG cells that stably express Wnt-1 (11). Candidate differentially expressed cDNAs (1,384 total) were sequenced. Thirty-nine percent of the sequences matched known genes or homologues, 32% matched expressed sequence tags, and 29% had no match. To confirm that the transcript was differentially expressed, semiquantitative reverse transcription–PCR and Northern analysis were performed by using mRNA from the C57MG and C57MG/Wnt-1 cells.

Two of the cDNAs, *WISP-1* and *WISP-2*, were differentially expressed, being induced in the C57MG/Wnt-1 cell line, but not in the parent C57MG cells or C57MG cells overexpressing Wnt-4 (Fig. 1 *A* and *B*). Wnt-4, unlike Wnt-1, does not induce the morphological transformation of C57MG cells and has no effect on β-catenin levels (13, 14). Expression of *WISP-1* was up-regulated approximately 3-fold in the C57MG/Wnt-1 cell line and *WISP-2* by approximately 5-fold by both Northern analysis and reverse transcription–PCR.

An independent, but similar, system was used to examine *WISP* expression after Wnt-1 induction. C57MG cells expressing the *Wnt-1* gene under the control of a tetracycline-repressible promoter produce low amounts of Wnt-1 in the repressed state but show a strong induction of *Wnt-1* mRNA and protein within 24 hr after tetracycline removal (8). The levels of Wnt-1 and *WISP* RNA isolated from these cells at various times after tetracycline removal were assessed by quantitative PCR. Strong induction of Wnt-1 mRNA was seen as early as 10 hr after tetracycline removal. Induction of *WISP* mRNA (2- to 6-fold) was seen at 48 and 72 hr (data not shown). These data support our previous observations that show that *WISP* induction is correlated with Wnt-1 expression. Because the induction is slow, occurring after approximately 48 hr, the induction of *WISP*s may be an indirect response to Wnt-1 signaling.

cDNA clones of human *WISP-1* were isolated and the sequence compared with mouse *WISP-1*. The cDNA sequences of mouse and human *WISP-1* were 1,766 and 2,830 bp in length, respectively, and encode proteins of 367 aa, with predicted relative molecular masses of ≈40,000 (M_r 40 K). Both have hydrophobic N-terminal signal sequences, 38 conserved cysteine residues, and four potential N-linked glycosylation sites and are 84% identical (Fig. 2*A*).

Full-length cDNA clones of mouse and human *WISP-2* were 1,734 and 1,293 bp in length, respectively, and encode proteins of 251 and 250 aa, respectively, with predicted relative molecular masses of ≈27,000 (M_r 27 K) (Fig. 2*B*). Mouse and human *WISP-2* are 73% identical. Human *WISP-2* has no potential N-linked glycosylation sites, and mouse *WISP-2* has one at
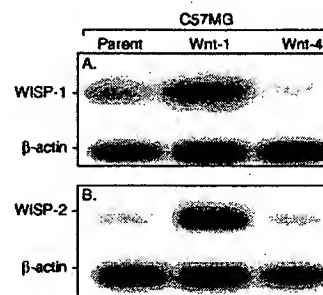

FIG. 1. *WISP-1* and *WISP-2* are induced by Wnt-1, but not Wnt-4, expression in C57MG cells. Northern analysis of *WISP-1* (*A*) and *WISP-2* (*B*) expression in C57MG, C57MG/Wnt-1, and C57MG/Wnt-4 cells. Poly(A)$^+$ RNA (2 μg) was subjected to Northern blot analysis and hybridized with a 70-bp mouse *WISP-1*-specific probe (amino acids 278–300) or a 190-bp *WISP-2*-specific probe (nucleotides 1438–1627) in the 3′ untranslated region. Blots were rehybridized with human β-actin probe.
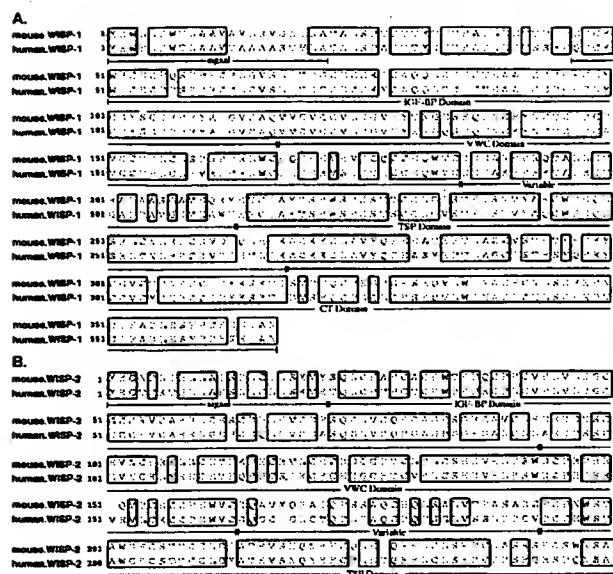
Cell Biology, Medical Sciences: Pennica *et al.*

Proc. Natl. Acad. Sci. USA 95 (1998)   14719

FIG. 2. Encoded amino acid sequence alignment of mouse and human *WISP-1* (*A*) and mouse and human *WISP-2* (*B*). The potential signal sequence, insulin-like growth factor-binding protein (IGF-BP), VWC, thrombospondin (TSP), and C-terminal (CT) domains are underlined.

position 197. WISP-2 has 28 cysteine residues that are conserved among the 38 cysteines found in WISP-1.

Identification of WISP-3. To search for related proteins, we screened expressed sequence tag (EST) databases with the WISP-1 protein sequence and identified several ESTs as potentially related sequences. We identified a homologous protein that we have called WISP-3. A full-length human WISP-3 cDNA of 1,371 bp was isolated corresponding to those ESTs that encode a 354-aa protein with a predicted molecular mass of 39,293. WISP-3 has two potential N-linked glycosylation sites and 36 cysteine residues. An alignment of the three human WISP proteins shows that WISP-1 and WISP-3 are the most similar (42% identity), whereas WISP-2 has 37% identity with WISP-1 and 32% identity with WISP-3 (Fig. 3*A*).

WISPs Are Homologous to the CTGF Family of Proteins. Human *WISP-1*, *WISP-2*, and *WISP-3* are novel sequences; however, mouse *WISP-1* is the same as the recently identified *Elm1* gene. *Elm1* is expressed in low, but not high, metastatic mouse melanoma cells, and suppresses the *in vivo* growth and metastatic potential of K-1735 mouse melanoma cells (15). Human and mouse *WISP-2* are homologous to the recently described rat gene, *rCop-1* (16). Significant homology (36–44%) was seen to the CCN family of growth factors. This family includes three members, CTGF, Cyr61, and the protooncogene *nov*. CTGF is a chemotactic and mitogenic factor for fibroblasts that is implicated in wound healing and fibrotic disorders and is induced by TGF-β (17). Cyr61 is an extracellular matrix signaling molecule that promotes cell adhesion, proliferation, migration, angiogenesis, and tumor growth (18, 19). *nov* (nephroblastoma overexpressed) is an immediate early gene associated with quiescence and found altered in Wilms tumors (20). The proteins of the CCN family share functional, but not sequence, similarity to Wnt-1. All are secreted, cysteine-rich heparin binding glycoproteins that associate with the cell surface and extracellular matrix.

WISP proteins exhibit the modular architecture of the CCN family, characterized by four conserved cysteine-rich domains (Fig. 3*B*) (21). The N-terminal domain, which includes the first 12 cysteine residues, contains a consensus sequence (GCGC-CXXC) conserved in most insulin-like growth factor (IGF)-
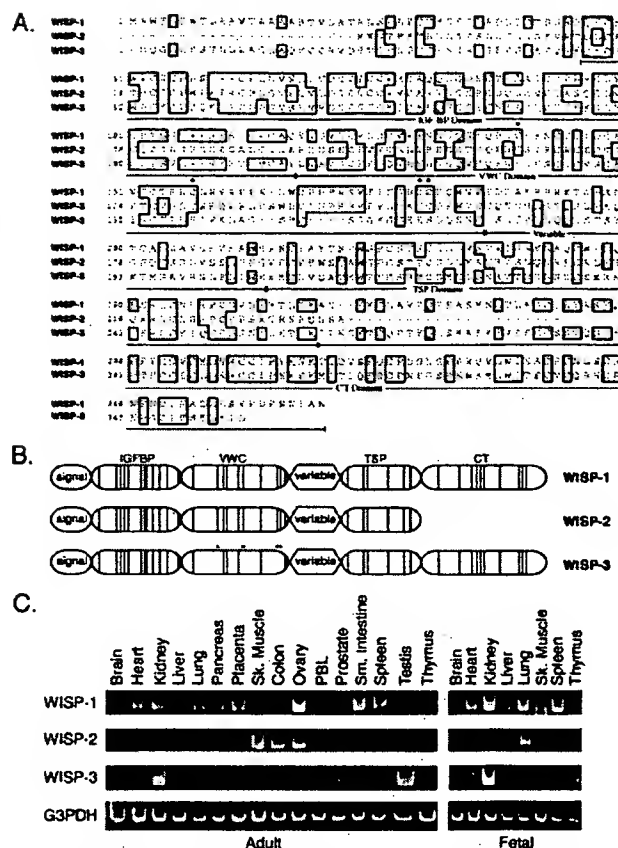
FIG. 3. (*A*) Encoded amino acid sequence alignment of human WISPs. The cysteine residues of WISP-1 and WISP-2 that are not present in WISP-3 are indicated with a dot. (*B*) Schematic representation of the WISP proteins showing the domain structure and cysteine residues (vertical lines). The four cysteine residues in the VWC domain that are absent in WISP-3 are indicated with a dot. (*C*) Expression of *WISP* mRNA in human tissues. PCR was performed on human multiple-tissue cDNA panels (CLONTECH) from the indicated adult and fetal tissues.

binding proteins (BP). This sequence is conserved in WISP-2 and WISP-3, whereas WISP-1 has a glutamine in the third position instead of a glycine. CTGF recently has been shown to specifically bind IGF (22) and a truncated *nov* protein lacking the IGF-BP domain is oncogenic (23). The von Willebrand factor type C module (VWC), also found in certain collagens and mucins, covers the next 10 cysteine residues, and is thought to participate in protein complex formation and oligomerization (24). The VWC domain of WISP-3 differs from all CCN family members described previously, in that it contains only six of the 10 cysteine residues (Fig. 3 *A* and *B*). A short variable region follows the VWC domain. The third module, the thrombospondin (TSP) domain is involved in binding to sulfated glycoconjugates and contains six cysteine residues and a conserved WSxCSxxCG motif first identified in thrombospondin (25). The C-terminal (CT) module containing the remaining 10 cysteines is thought to be involved in dimerization and receptor binding (26). The CT domain is present in all CCN family members described to date but is absent in WISP-2 (Fig. 3 *A* and *B*). The existence of a putative signal sequence and the absence of a transmembrane domain suggest that WISPs are secreted proteins, an observation supported by an analysis of their expression and secretion from mammalian cell and baculovirus cultures (data not shown).

Expression of WISP mRNA in Human Tissues. Tissue-specific expression of human *WISP*s was characterized by PCR

analysis on adult and fetal multiple tissue cDNA panels. *WISP-1* expression was seen in the adult heart, kidney, lung, pancreas, placenta, ovary, small intestine, and spleen (Fig. 3C). Little or no expression was detected in the brain, liver, skeletal muscle, colon, peripheral blood leukocytes, prostate, testis, or thymus. *WISP-2* had a more restricted tissue expression and was detected in adult skeletal muscle, colon, ovary, and fetal lung. Predominant expression of *WISP-3* was seen in adult kidney and testis and fetal kidney. Lower levels of *WISP-3* expression were detected in placenta, ovary, prostate, and small intestine.

In Situ **Localization of *WISP-1* and *WISP-2*.** Expression of *WISP-1* and *WISP-2* was assessed by *in situ* hybridization in mammary tumors from Wnt-1 transgenic mice. Strong expression of *WISP-1* was observed in stromal fibroblasts lying within the fibrovascular tumor stroma (Fig. 4 *A–D*). However, low-level *WISP-1* expression also was observed focally within tumor cells (data not shown). No expression was observed in normal breast. Like *WISP-1*, *WISP-2* expression also was seen in the tumor stroma in breast tumors from Wnt-1 transgenic animals (Fig. 4 *E–H*). However, *WISP-2* expression in the stroma was in spindle-shaped cells adjacent to capillary vessels, whereas

the predominant cell type expressing *WISP-1* was the stromal fibroblasts.

Chromosome Localization of the *WISP* Genes. The chromosomal location of the human *WISP* genes was determined by radiation hybrid mapping panels. *WISP-1* is approximately 3.48 cR from the meiotic marker AFM259xc5 [logarithm of odds (lod) score 16.31] on chromosome 8q24.1 to 8q24.3, in the same region as the human locus of the *novH* family member (27) and roughly 4 Mbs distal to c-*myc* (28). Preliminary fine mapping indicates that *WISP-1* is located near D8S1712 STS. *WISP-2* is linked to the marker SHGC-33922 (lod = 1,000) on chromosome 20q12–20q13.1. Human *WISP-3* mapped to chromosome 6q22–6q23 and is linked to the marker AFM211ze5 (lod = 1,000). *WISP-3* is approximately 18 Mbs proximal to CTGF and 23 Mbs proximal to the human cellular oncogene *MYB* (27, 29).

Amplification and Aberrant Expression of *WISPs* in Human Colon Tumors. Amplification of protooncogenes is seen in many human tumors and has etiological and prognostic significance. For example, in a variety of tumor types, c-*myc* amplification has been associated with malignant progression and poor prognosis (30). Because *WISP-1* resides in the same general chromosomal location (8q24) as c-*myc*, we asked whether it was a target of gene amplification, and, if so, whether this amplification was independent of the c-*myc* locus. Genomic DNA from human colon cancer cell lines was assessed by quantitative PCR and Southern blot analysis. (Fig. 5 *A* and *B*). Both methods detected similar degrees of *WISP-1* amplification. Most cell lines showed significant (2- to 4-fold) amplification, with the HT-29 and WiDr cell lines demonstrating an 8-fold increase. Significantly, the pattern of amplification observed did not correlate with that observed for c-*myc*, indicating that the c-*myc* gene is not part of the amplicon that involves the *WISP-1* locus.

We next examined whether the *WISP* genes were amplified in a panel of 25 primary human colon adenocarcinomas. The relative *WISP* gene copy number in each colon tumor DNA was compared with pooled normal DNA from 10 donors by quantitative PCR (Fig. 6). The copy number of *WISP-1* and *WISP-2* was significantly greater than one, approximately 2-fold for *WISP-1* in about 60% of the tumors and 2- to 4-fold for *WISP-2* in 92% of the tumors (P < 0.001 for each). The copy number for *WISP-3* was indistinguishable from one (P = 0.166). In addition, the copy number of *WISP-2* was significantly higher than that of *WISP-1* (P < 0.001).

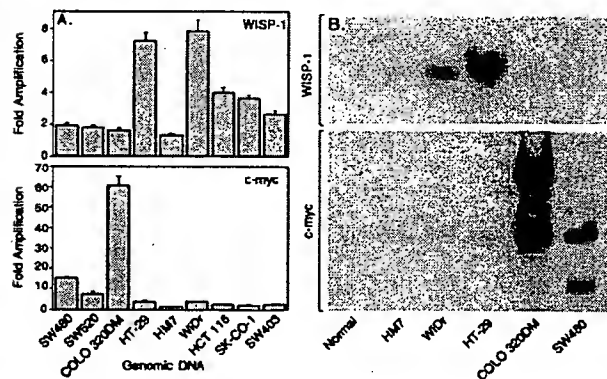The levels of *WISP* transcripts in RNA isolated from 19 adenocarcinomas and their matched normal mucosa were

FIG. 4. (*A, C, E,* and *G*) Representative hematoxylin/eosin-stained images from breast tumors in Wnt-1 transgenic mice. The corresponding dark-field images showing *WISP-1* expression are shown in *B* and *D*. The tumor is a moderately well-differentiated adenocarcinoma showing evidence of adenoid cystic change. At low power (*A* and *B*), expression of *WISP-1* is seen in the delicate branching fibrovascular tumor stroma (arrowhead). At higher magnification, expression is seen in the stromal(s) fibroblasts (*C* and *D*), and tumor cells are negative. Focal expression of *WISP-1*, however, was observed in tumor cells in some areas. Images of *WISP-2* expression are shown in *E–H*. At low power (*E* and *F*), expression of WISP-2 is seen in cells lying within the fibrovascular tumor stroma. At higher magnification, these cells appeared to be adjacent to capillary vessels whereas tumor cells are negative (*G* and *H*).

FIG. 5. Amplification of *WISP-1* genomic DNA in colon cancer cell lines. (*A*) Amplification in cell line DNA was determined by quantitative PCR. (*B*) Southern blots containing genomic DNA (10 μg) digested with *Eco*RI (*WISP-1*) or *Xba*I (c-*myc*) were hybridized with a 100-bp human *WISP-1* probe (amino acids 186–219) or a human c-*myc* probe (located at bp 1901–2000). The *WISP* and *myc* genes are detected in normal human genomic DNA after a longer film exposure.

Cell Biology, Medical Sciences: Pennica *et al.*

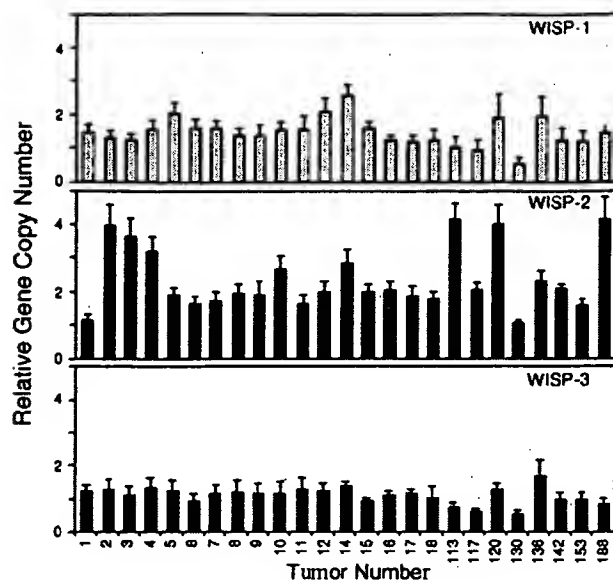*Proc. Natl. Acad. Sci. USA 95 (1998)*   14721

FIG. 6. Genomic amplification of *WISP* genes in human colon tumors. The relative gene copy number of the *WISP* genes in 25 adenocarcinomas was assayed by quantitative PCR, by comparing DNA from primary human tumors with pooled DNA from 10 healthy donors. The data are means ± SEM from one experiment done in triplicate. The experiment was repeated at least three times.

assessed by quantitative PCR (Fig. 7). The level of *WISP-1* RNA present in tumor tissue varied but was significantly increased (2- to >25-fold) in 84% (16/19) of the human colon tumors examined compared with normal adjacent mucosa. Four of 19 tumors showed greater than 10-fold overexpression. In contrast, in 79% (15/19) of the tumors examined, *WISP-2* RNA expression was significantly lower in the tumor than the mucosa. Similar to *WISP-1*, *WISP-3* RNA was overexpressed in 63% (12/19) of the colon tumors compared with the normal
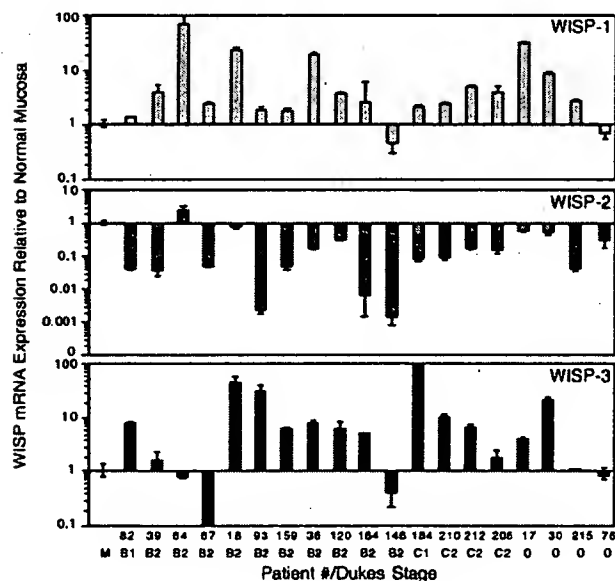
FIG. 7. *WISP* RNA expression in primary human colon tumors relative to expression in normal mucosa from the same patient. Expression of *WISP* mRNA in 19 adenocarcinomas was assayed by quantitative PCR. The Dukes stage of the tumor is listed under the sample number. The data are means ± SEM from one experiment done in triplicate. The experiment was repeated at least twice.

mucosa. The amount of overexpression of *WISP-3* ranged from 4- to >40-fold.

DISCUSSION

One approach to understanding the molecular basis of cancer is to identify differences in gene expression between cancer cells and normal cells. Strategies based on assumptions that steady-state mRNA levels will differ between normal and malignant cells have been used to clone differentially expressed genes (31). We have used a PCR-based selection strategy, SSH, to identify genes selectively expressed in C57MG mouse mammary epithelial cells transformed by Wnt-1.

Three of the genes isolated, *WISP-1*, *WISP-2*, and *WISP-3*, are members of the CCN family of growth factors, which includes CTGF, Cyr61, and *nov*, a family not previously linked to Wnt signaling.

Two independent experimental systems demonstrated that *WISP* induction was associated with the expression of Wnt-1. The first was C57MG cells infected with a Wnt-1 retroviral vector or C57MG cells expressing Wnt-1 under the control of a tetracyline-repressible promoter, and the second was in Wnt-1 transgenic mice, where breast tissue expresses Wnt-1, whereas normal breast tissue does not. No *WISP* RNA expression was detected in mammary tumors induced by polyoma virus middle T antigen (data not shown). These data suggest a link between Wnt-1 and *WISP*s in that in these two situations, *WISP* induction was correlated with Wnt-1 expression.

It is not clear whether the *WISP*s are directly or indirectly induced by the downstream components of the Wnt-1 signaling pathway (i.e., β-catenin-TCF-1/Lef1). The increased levels of *WISP* RNA were measured in Wnt-1-transformed cells, hours or days after Wnt-1 transformation. Thus, *WISP* expression could result from Wnt-1 signaling directly through β-catenin transcription factor regulation or alternatively through Wnt-1 signaling turning on a transcription factor, which in turn regulates *WISP*s.

The *WISP*s define an additional subfamily of the CCN family of growth factors. One striking difference observed in the protein sequence of WISP-2 is the absence of a CT domain, which is present in CTGF, Cyr61, *nov*, WISP-1, and WISP-3. This domain is thought to be involved in receptor binding and dimerization. Growth factors, such as TGF-β, platelet-derived growth factor, and nerve growth factor, which contain a cystine knot motif exist as dimers (32). It is tempting to speculate that WISP-1 and WISP-3 may exist as dimers, whereas WISP-2 exists as a monomer. If the CT domain is also important for receptor binding, WISP-2 may bind its receptor through a different region of the molecule than the other CCN family members. No specific receptors have been identified for CTGF or *nov*. A recent report has shown that integrin $\alpha_v\beta_3$ serves as an adhesion receptor for Cyr61 (33).

The strong expression of *WISP-1* and *WISP-2* in cells lying within the fibrovascular tumor stroma in breast tumors from Wnt-1 transgenic animals is consistent with previous observations that transcripts for the related CTGF gene are primarily expressed in the fibrous stroma of mammary tumors (34). Epithelial cells are thought to control the proliferation of connective tissue stroma in mammary tumors by a cascade of growth factor signals similar to that controlling connective tissue formation during wound repair. It has been proposed that mammary tumor cells or inflammatory cells at the tumor interstitial interface secrete TGF-β1, which is the stimulus for stromal proliferation (34). TGF-β1 is secreted by a large percentage of malignant breast tumors and may be one of the growth factors that stimulates the production of CTGF and WISPs in the stroma.

It was of interest that *WISP-1* and *WISP-2* expression was observed in the stromal cells that surrounded the tumor cells

(epithelial cells) in the Wnt-1 transgenic mouse sections of breast tissue. This finding suggests that paracrine signaling could occur in which the stromal cells could supply WISP-1 and WISP-2 to regulate tumor cell growth on the WISP extracellular matrix. Stromal cell-derived factors in the extracellular matrix have been postulated to play a role in tumor cell migration and proliferation (35). The localization of *WISP-1* and *WISP-2* in the stromal cells of breast tumors supports this paracrine model.

An analysis of *WISP-1* gene amplification and expression in human colon tumors showed a correlation between DNA amplification and overexpression, whereas overexpression of *WISP-3* RNA was seen in the absence of DNA amplification. In contrast, *WISP-2* DNA was amplified in the colon tumors, but its mRNA expression was significantly reduced in the majority of tumors compared with the expression in normal colonic mucosa from the same patient. The gene for human *WISP-2* was localized to chromosome 20q12–20q13, at a region frequently amplified and associated with poor prognosis in node negative breast cancer and many colon cancers, suggesting the existence of one or more oncogenes at this locus (36–38). Because the center of the 20q13 amplicon has not yet been identified, it is possible that the apparent amplification observed for *WISP-2* may be caused by another gene in this amplicon.

A recent manuscript on *rCop-1*, the rat orthologue of *WISP-2*, describes the loss of expression of this gene after cell transformation, suggesting it may be a negative regulator of growth in cell lines (16). Although the mechanism by which *WISP-2* RNA expression is down-regulated during malignant transformation is unknown, the reduced expression of *WISP-2* in colon tumors and cell lines suggests that it may function as a tumor suppressor. These results show that the *WISP* genes are aberrantly expressed in colon cancer and suggest that their altered expression may confer selective growth advantage to the tumor.

Members of the Wnt signaling pathway have been implicated in the pathogenesis of colon cancer, breast cancer, and melanoma, including the tumor suppressor gene adenomatous polyposis coli and β-catenin (39). Mutations in specific regions of either gene can cause the stabilization and accumulation of cytoplasmic β-catenin, which presumably contributes to human carcinogenesis through the activation of target genes such as the *WISP*s. Although the mechanism by which Wnt-1 transforms cells and induces tumorigenesis is unknown, the identification of *WISP*s as genes that may be regulated downstream of Wnt-1 in C57MG cells suggests they could be important mediators of Wnt-1 transformation. The amplification and altered expression patterns of the *WISP*s in human colon tumors may indicate an important role for these genes in tumor development.

1. Cadigan, K. M. & Nusse, R. (1997) *Genes Dev.* 11, 3286–3305.
2. Dale, T. C. (1998) *Biochem. J.* 329, 209–223.
3. Nusse, R. & Varmus, H. E. (1982) *Cell* 31, 99–109.
4. van Ooyen, A. & Nusse, R. (1984) *Cell* 39, 233–240.
5. Tsukamoto, A. S., Grosschedl, R., Guzman, R. C., Parslow, T. & Varmus, H. E. (1988) *Cell* 55, 619–625.
6. Brown, J. D. & Moon, R. T. (1998) *Curr. Opin. Cell. Biol.* 10, 182–187.
7. Molenaar, M., van de Wetering, M., Oosterwegel, M., Peterson-Maduro, J., Godsave, S., Korinek, V., Roose, J., Destree, O. & Clevers, H. (1996) *Cell* 86, 391–399.
8. Korinek, V., Barker, N., Willert, K., Molenaar, M., Roose, J., Wagenaar, G., Markman, M., Lamers, W., Desiree, O. & Clevers, H. (1998) *Mol. Cell. Biol.* 18, 1248–1256.
9. Munemitsu, S., Albert, I., Souza, B., Rubinfeld, B. & Polakis, P. (1995) *Proc. Natl. Acad. Sci. USA* 92, 3046–3050.
10. He, T. C., Sparks, A. B., Rago, C., Hermeking, H., Zawel, L., da Costa, L. T., Morin, P. J., Vogelstein, B. & Kinzler, K. W. (1998) *Science* 281, 1509–1512.
11. Diatchenko, L., Lau, Y. F., Campbell, A. P., Chenchik, A., Moqadam, F., Huang, B., Lukyanov, S., Lukyanov, K., Gurskaya, N., Sverdlov, E. D. & Siebert, P. D. (1996) *Proc. Natl. Acad. Sci. USA* 93, 6025–6030.
12. Brown, A. M., Wildin, R. S., Prendergast, T. J. & Varmus, H. E. (1986) *Cell* 46, 1001–1009.
13. Wong, G. T., Gavin, B. J. & McMahon, A. P. (1994) *Mol. Cell. Biol.* 14, 6278–6286.
14. Shimizu, H., Julius, M. A., Giarre, M., Zheng, Z., Brown, A. M. & Kitajewski, J. (1997) *Cell Growth Differ.* 8, 1349–1358.
15. Hashimoto, Y., Shindo-Okada, N., Tani, M., Nagamachi, Y., Takeuchi, K., Shiroishi, T., Toma, H. & Yokota, J. (1998) *J. Exp. Med.* 187, 289–296.
16. Zhang, R., Averboukh, L., Zhu, W., Zhang, H., Jo, H., Dempsey, P. J., Coffey, R. J., Pardee, A. B. & Liang, P. (1998) *Mol. Cell. Biol.* 18, 6131–6141.
17. Grotendorst, G. R. (1997) *Cytokine Growth Factor Rev.* 8, 171–179.
18. Kireeva, M. L., Mo, F. E., Yang, G. P. & Lau, L. F. (1996) *Mol. Cell. Biol.* 16, 1326–1334.
19. Babic, A. M., Kireeva, M. L., Kolesnikova, T. V. & Lau, L. F. (1998) *Proc. Natl. Acad. Sci. USA* 95, 6355–6360.
20. Martinerie, C., Huff, V., Joubert, I., Badzioch, M., Saunders, G., Strong, L. & Perbal, B. (1994) *Oncogene* 9, 2729–2732.
21. Bork, P. (1993) *FEBS Lett.* 327, 125–130.
22. Kim, H. S., Nagalla, S. R., Oh, Y., Wilson, E., Roberts, C. T., Jr. & Rosenfeld, R. G. (1997) *Proc. Natl. Acad. Sci. USA* 94, 12981–12986.
23. Joliot, V., Martinerie, C., Dambrine, G., Plassiart, G., Brisac, M., Crochet, J. & Perbal, B. (1992) *Mol. Cell. Biol.* 12, 10–21.
24. Mancuso, D. J., Tuley, E. A., Westfield, L. A., Worrall, N. K., Shelton-Inloes, B. B., Sorace, J. M., Alevy, Y. G. & Sadler, J. E. (1989) *J. Biol. Chem.* 264, 19514–19527.
25. Holt, G. D., Pangburn, M. K. & Ginsburg, V. (1990) *J. Biol. Chem.* 265, 2852–2855.
26. Voorberg, J., Fontijn, R., Calafat, J., Janssen, H., van Mourik, J. A. & Pannekoek, H. (1991) *J. Cell. Biol.* 113, 195–205.
27. Martinerie, C., Viegas-Pequignot, E., Guenard, I., Dutrillaux, B., Nguyen, V. C., Bernheim, A. & Perbal, B. (1992) *Oncogene* 7, 2529–2534.
28. Takahashi, E., Hori, T., O'Connell, P., Leppert, M. & White, R. (1991) *Cytogenet. Cell. Genet.* 57, 109–111.
29. Meese, E., Meltzer, P. S., Witkowski, C. M. & Trent, J. M. (1989) *Genes Chromosomes Cancer* 1, 88–94.
30. Garte, S. J. (1993) *Crit. Rev. Oncog.* 4, 435–449.
31. Zhang, L., Zhou, W., Velculescu, V. E., Kern, S. E., Hruban, R. H., Hamilton, S. R., Vogelstein, B. & Kinzler, K. W. (1997) *Science* 276, 1268–1272.
32. Sun, P. D. & Davies, D. R. (1995) *Annu. Rev. Biophys. Biomol. Struct.* 24, 269–291.
33. Kireeva, M. L., Lam, S. C. T. & Lau, L. F. (1998) *J. Biol. Chem.* 273, 3090–3096.
34. Frazier, K. S. & Grotendorst, G. R. (1997) *Int. J. Biochem. Cell. Biol.* 29, 153–161.
35. Wernert, N. (1997) *Virchows Arch.* 430, 433–443.
36. Tanner, M. M., Tirkkonen, M., Kallioniemi, A., Collins, C., Stokke, T., Karhu, R., Kowbel, D., Shadravan, F., Hintz, M., Kuo, W. L., *et al.* (1994) *Cancer Res.* 54, 4257–4260.
37. Brinkmann, U., Gallo, M., Polymeropoulos, M. H. & Pastan, I. (1996) *Genome Res.* 6, 187–194.
38. Bischoff, J. R., Anderson, L., Zhu, Y., Mossie, K., Ng, L., Souza, B., Schryver, B., Flanagan, P., Clairvoyant, F., Ginther, C., *et al.* (1998) *EMBO J.* 17, 3052–3065.
39. Morin, P. J., Sparks, A. B., Korinek, V., Barker, N., Clevers, H., Vogelstein, B. & Kinzler, K. W. (1997) *Science* 275, 1787–1790.
40. Lu, L. H. & Gillett, N. (1994) *Cell Vision* 1, 169–176.

GENOME METHODS

Real Time Quantitative PCR

Christian A. Heid,[1] Junko Stevens,[2] Kenneth J. Livak,[2] and P. Mickey Williams[1,3]

[1]BioAnalytical Technology Department, Genentech, Inc., South San Francisco, California 94080;
[2]Applied BioSystems Division of Perkin Elmer Corp., Foster City, California 94404

We have developed a novel "real time" quantitative PCR method. The method measures PCR product accumulation through a dual-labeled fluorogenic probe (i.e., TaqMan Probe). This method provides very accurate and reproducible quantitation of gene copies. Unlike other quantitative PCR methods, real-time PCR does not require post-PCR sample handling, preventing potential PCR product carry-over contamination and resulting in much faster and higher throughput assays. The real-time PCR method has a very large dynamic range of starting target molecule determination (at least five orders of magnitude). Real-time quantitative PCR is extremely accurate and less labor-intensive than current quantitative PCR methods.

Quantitative nucleic acid sequence analysis has had an important role in many fields of biological research. Measurement of gene expression (RNA) has been used extensively in monitoring biological responses to various stimuli (Tan et al. 1994; Huang et al. 1995a,b; Prud'homme et al. 1995). Quantitative gene analysis (DNA) has been used to determine the genomic quantity of a particular gene, as in the case of the human *HER2* gene, which is amplified in ~30% of breast tumors (Slamon et al. 1987). Gene and genome quantitation (DNA and RNA) also have been used for analysis of human immunodeficiency virus (HIV) burden demonstrating changes in the levels of virus throughout the different phases of the disease (Connor et al. 1993; Piatak et al. 1993b; Furtado et al. 1995).

Many methods have been described for the quantitative analysis of nucleic acid sequences (both for RNA and DNA; Southern 1975; Sharp et al. 1980; Thomas 1980). Recently, PCR has proven to be a powerful tool for quantitative nucleic acid analysis. PCR and reverse transcriptase (RT)-PCR have permitted the analysis of minimal starting quantities of nucleic acid (as little as one cell equivalent). This has made possible many experiments that could not have been performed with traditional methods. Although PCR has provided a powerful tool, it is imperative

that it be used properly for quantitation (Raeymaekers 1995). Many early reports of quantitative PCR and RT-PCR described quantitation of the PCR product but did not measure the initial target sequence quantity. It is essential to design proper controls for the quantitation of the initial target sequences (Ferre 1992; Clementi et al. 1993).

Researchers have developed several methods of quantitative PCR and RT-PCR. One approach measures PCR product quantity in the log phase of the reaction before the plateau (Kellogg et al. 1990; Pang et al. 1990). This method requires that each sample has equal input amounts of nucleic acid and that each sample under analysis amplifies with identical efficiency up to the point of quantitative analysis. A gene sequence (contained in all samples at relatively constant quantities, such as β-actin) can be used for sample amplification efficiency normalization. Using conventional methods of PCR detection and quantitation (gel electrophoresis or plate capture hybridization), it is extremely laborious to assure that all samples are analyzed during the log phase of the reaction (for both the target gene and the normalization gene). Another method, quantitative competitive (QC)-PCR, has been developed and is used widely for PCR quantitation. QC-PCR relies on the inclusion of an internal control competitor in each reaction (Becker-Andre 1991; Piatak et al. 1993a,b). The efficiency of each reaction is normalized to the internal competitor. A known amount of internal competitor can be

[3]Corresponding author.

added to each sample. To obtain relative quantitation, the unknown target PCR product is compared with the known competitor PCR product. Success of a quantitative competitive PCR assay relies on developing an internal control that amplifies with the same efficiency as the target molecule. The design of the competitor and the validation of amplification efficiencies require a dedicated effort. However, because QC–PCR does not require that PCR products be analyzed during the log phase of the amplification, it is the easier of the two methods to use.

Several detection systems are used for quantitative PCR and RT–PCR analysis: (1) agarose gels, (2) fluorescent labeling of PCR products and detection with laser-induced fluorescence using capillary electrophoresis (Fasco et al. 1995; Williams et al. 1996) or acrylamide gels, and (3) plate capture and sandwich probe hybridization (Mulder et al. 1994). Although these methods proved successful, each method requires post-PCR manipulations that add time to the analysis and may lead to laboratory contamination. The sample throughput of these methods is limited (with the exception of the plate capture approach), and, therefore, these methods are not well suited for uses demanding high sample throughput (i.e., screening of large numbers of biomolecules or analyzing samples for diagnostics or clinical trials).

Here we report the development of a novel assay for quantitative DNA analysis. The assay is based on the use of the 5' nuclease assay first described by Holland et al. (1991). The method uses the 5' nuclease activity of Taq polymerase to cleave a nonextendible hybridization probe during the extension phase of PCR. The approach uses dual-labeled fluorogenic hybridization probes (Lee et al. 1993; Bassler et al. 1995; Livak et al. 1995a,b). One fluorescent dye serves as a reporter [FAM (i.e., 6-carboxyfluorescein)] and its emission spectra is quenched by the second fluorescent dye, TAMRA (i.e., 6-carboxy-tetramethyl-rhodamine). The nuclease degradation of the hybridization probe releases the quenching of the FAM fluorescent emission, resulting in an increase in peak fluorescent emission at 518 nm. The use of a sequence detector (ABI Prism) allows measurement of fluorescent spectra of all 96 wells of the thermal cycler continuously during the PCR amplification. Therefore, the reactions are monitored in real time. The output data is described and quantitative analysis of input target DNA sequences is discussed below.

RESULTS

PCR Product Detection in Real Time

The goal was to develop a high-throughput, sensitive, and accurate gene quantitation assay for use in monitoring lipid mediated therapeutic gene delivery. A plasmid encoding human factor VIII gene sequence, pF8TM (see Methods), was used as a model therapeutic gene. The assay uses fluorescent Taqman methodology and an instrument capable of measuring fluorescence in real time (ABI Prism 7700 Sequence Detector). The Taqman reaction requires a hybridization probe labeled with two different fluorescent dyes. One dye is a reporter dye (FAM), the other is a quenching dye (TAMRA). When the probe is intact, fluorescent energy transfer occurs and the reporter dye fluorescent emission is absorbed by the quenching dye (TAMRA). During the extension phase of the PCR cycle, the fluorescent hybridization probe is cleaved by the 5'–3' nucleolytic activity of the DNA polymerase. On cleavage of the probe, the reporter dye emission is no longer transferred efficiently to the quenching dye, resulting in an increase of the reporter dye fluorescent emission spectra. PCR primers and probes were designed for the human factor VIII sequence and human β-actin gene (as described in Methods). Optimization reactions were performed to choose the appropriate probe and magnesium concentrations yielding the highest intensity of reporter fluorescent signal without sacrificing specificity. The instrument uses a charge-coupled device (i.e., CCD camera) for measuring the fluorescent emission spectra from 500 to 650 nm. Each PCR tube was monitored sequentially for 25 msec with continuous monitoring throughout the amplification. Each tube was re-examined every 8.5 sec. Computer software was designed to examine the fluorescent intensity of both the reporter dye (FAM) and the quenching dye (TAMRA). The fluorescent intensity of the quenching dye, TAMRA, changes very little over the course of the PCR amplification (data not shown). Therefore, the intensity of TAMRA dye emission serves as an internal standard with which to normalize the reporter dye (FAM) emission variations. The software calculates a value termed ΔRn (or ΔRQ) using the following equation: $\Delta Rn = (Rn^+)(Rn^-)$, where Rn^+ = emission intensity of reporter/emission intensity of quencher at any given time in a reaction tube, and Rn = emission intensity of re-

HUD ET AL.

porter/emission intensity of quencher measured prior to PCR amplification in that same reaction tube. For the purpose of quantitation, the last three data points (ΔRns) collected during the extension step for each PCR cycle were analyzed. The nucleolytic degradation of the hybridization probe occurs during the extension phase of PCR, and, therefore, reporter fluorescent emission increases during this time. The three data points were averaged for each PCR cycle and the mean value for each was plotted in an "amplification plot" shown in Figure 1A. The ΔRn mean value is plotted on the y-axis, and time, represented by cycle number, is plotted on the x-axis. During the early cycles of the PCR amplification, the ΔRn

value remains at base line. When sufficient hybridization probe has been cleaved by the Taq polymerase nuclease activity, the intensity of reporter fluorescent emission increases. Most PCR amplifications reach a plateau phase of reporter fluorescent emission if the reaction is carried on to high cycle numbers. The amplification plot is examined early in the reaction, at a point that represents the log phase of product accumulation. This is done by assigning an arbitrary threshold that is based on the variability of the base-line data. In Figure 1A, the threshold was set at 10 standard deviations above the mean of base line emission calculated from cycles 1 to 15. Once the threshold is chosen, the point at which

Figure 1   PCR product detection in real time. (*A*) The Model 7700 software will construct amplification plots from the extension phase fluorescent emission data collected during the PCR amplification. The standard deviation is determined from the data points collected from the base line of the amplification plot. C_T values are calculated by determining the point at which the fluorescence exceeds a threshold limit (usually 10 times the standard deviation of the base line). (*B*) Overlay of amplification plots of serially (1:2) diluted human genomic DNA samples amplified with β-actin primers. (*C*) Input DNA concentration of the samples plotted versus C_T. All

the amplification plot crosses the threshold is defined as C_T. C_T is reported as the cycle number at this point. As will be demonstrated, the C_T value is predictive of the quantity of input target.

C_T Values Provide a Quantitative Measurement of Input Target Sequences

Figure 1B shows amplification plots of 15 different PCR amplifications overlaid. The amplifications were performed on a 1:2 serial dilution of human genomic DNA. The amplified target was human β actin. The amplification plots shift to the right (to higher threshold cycles) as the input target quantity is reduced. This is expected because reactions with fewer starting copies of the target molecule require greater amplification to degrade enough probe to attain the threshold fluorescence. An arbitrary threshold of 10 standard deviations above the base line was used to determine the C_T values. Figure 1C represents the C_T values plotted versus the sample dilution value. Each dilution was amplified in triplicate PCR amplifications and plotted as mean values with error bars representing one standard deviation. The C_T values decrease linearly with increasing target quantity. Thus, C_T values can be used as a quantitative measurement of the input target number. It should be noted that the amplification plot for the 15.6-ng sample shown in Figure 1B does not reflect the same fluorescent rate of increase exhibited by most of the other samples. The 15.6-ng sample also achieves endpoint plateau at a lower fluorescent value than would be expected based on the input DNA. This phenomenon has been observed occasionally with other samples (data not shown) and may be attributable to late cycle inhibition; this hypothesis is still under investigation. It is important to note that the flattened slope and early plateau do not impact significantly the calculated C_T value as demonstrated by the fit on the line shown in Figure 1C. All triplicate amplifications resulted in very similar C_T values—the standard deviation did not exceed 0.5 for any dilution. This experiment contains a >100,000-fold range of input target molecules. Using C_T values for quantitation permits a much larger assay range than directly using total fluorescent emission intensity for quantitation. The linear range of fluorescent intensity measurement of the ABI Prism 7700 Se-

ments over a very large range of relative starting target quantities.

Sample Preparation Validation

Several parameters influence the efficiency of PCR amplification: magnesium and salt concentrations, reaction conditions (i.e., time and temperature), PCR target size and composition, primer sequences, and sample purity. All of the above factors are common to a single PCR assay, except sample to sample purity. In an effort to validate the method of sample preparation for the factor VIII assay, PCR amplification reproducibility and efficiency of 10 replicate sample preparations were examined. After genomic DNA was prepared from the 10 replicate samples, the DNA was quantitated by ultraviolet spectroscopy. Amplifications were performed analyzing β-actin gene content in 100 and 25 ng of total genomic DNA. Each PCR amplification was performed in triplicate. Comparison of C_T values for each triplicate sample show minimal variation based on standard deviation and coefficient of variance (Table 1). Therefore, each of the triplicate PCR amplifications was highly reproducible, demonstrating that real time PCR using this instrumentation introduces minimal variation into the quantitative PCR analysis. Comparison of the mean C_T values of the 10 replicate sample preparations also showed minimal variability, indicating that each sample preparation yielded similar results for β-actin gene quantity. The highest C_T difference between any of the samples was 0.85 and 0.71 for the 100 and 25 ng samples, respectively. Additionally, the amplification of each sample exhibited an equivalent rate of fluorescent emission intensity change per amount of DNA target analyzed as indicated by similar slopes derived from the sample dilutions (Fig. 2). Any sample containing an excess of a PCR inhibitor would exhibit a greater measured β-actin C_T value for a given quantity of DNA. In addition, the inhibitor would be diluted along with the sample in the dilution analysis (Fig. 2), altering the expected C_T value change. Each sample amplification yielded a similar result in the analysis, demonstrating that this method of sample preparation is highly reproducible with regard to sample purity.

Quantitative Analysis of a Plasmid After

HED HI AL

Table 1. Reproducibility of Sample Preparation Method

Sample no.	100 ng				25 ng			
	C_T	mean	standard deviation	CV	C_T	mean	standard deviation	CV
1	18.24				20.48			
	18.23				20.55			
	18.33	18.27	0.06	0.32	20.5	20.51	0.03	0.17
2	18.33				20.61			
	18.35				20.59			
	18.44	18.37	0.06	0.32	20.41	20.54	0.11	0.54
3	18.3				20.54			
	18.3				20.6			
	18.42	18.34	0.07	0.36	20.49	20.54	0.06	0.28
4	18.15				20.48			
	18.23				20.44			
	18.32	18.23	0.08	0.46	20.38	20.43	0.05	0.26
5	18.4				20.68			
	18.38				20.87			
	18.46	18.42	0.04	0.23	20.63	20.73	0.13	0.61
6	18.54				21.09			
	18.67				21.04			
	19	18.74	0.24	1.26	21.04	21.06	0.03	0.15
7	18.28				20.67			
	18.36				20.73			
	18.52	18.39	0.12	0.66	20.65	20.68	0.04	0.2
8	18.45				20.98			
	18.7				20.84			
	18.73	18.63	0.16	0.83	20.75	20.86	0.12	0.57
9	18.18				20.46			
	18.34				20.54			
	18.36	18.29	0.1	0.55	20.48	20.51	0.07	0.32
10	18.42				20.79			
	18.57				20.78			
	18.66	18.55	0.12	0.65	20.62	20.73	0.1	0.46
Mean	(1 10)	18.42	0.17	0.90		20.66	0.19	0.94

tor containing a partial cDNA for human factor VIII, pF8TM. A series of transfections was set up using a decreasing amount of the plasmid (40, 4, 0.5, and 0.1 µg). Twenty-four hours post-transfection, total DNA was purified from each flask of cells. β-Actin gene quantity was chosen as a value for normalization of genomic DNA concentration from each sample. In this experiment, β-actin gene content should remain constant relative to total genomic DNA. Figure 3 shows the result of the β-actin DNA measurement (100 ng total DNA determined by ultraviolet spectroscopy) of each sample. Each sample was analyzed in triplicate and the mean β-actin C_T values of the triplicates were plotted (error bars represent one standard deviation). The highest difference

between any two sample means was 0.95 C_T. Ten nanograms of total DNA of each sample were also examined for β-actin. The results again showed that very similar amounts of genomic DNA were present: the maximum mean β actin C_T value difference was 1.0. As Figure 3 shows, the rate of β-actin C_T change between the 100 and 10-ng samples was similar (slope values range between 3.56 and -3.45). This verifies again that the method of sample preparation yields samples of identical PCR integrity (i.e., no sample contained an excessive amount of a PCR inhibitor). However, these results indicate that each sample contained slight differences in the actual amount of genomic DNA analyzed. Determination of actual genomic DNA concentration was accomplished

Figure 2 Sample preparation purity. The replicate samples shown in Table 1 were also amplified in triplicate using 25 ng of each DNA sample. The figure shows the input DNA concentration (100 and 25 ng) vs. C_i. In the figure, the 100 and 25 ng points for each sample are connected by a line.

by plotting the mean β-actin C_i value obtained for each 100-ng sample on a β-actin standard curve (shown in Fig. 4C). The actual genomic DNA concentration of each sample, a, was obtained by extrapolation to the x-axis.

Figure 4A shows the measured (i.e., non-normalized) quantities of factor VIII plasmid DNA (pF8TM) from each of the four transient cell transfections. Each reaction contained 100 ng of total sample DNA (as determined by UV spectroscopy). Each sample was analyzed in triplicate

Figure 3 Analysis of transfected cell DNA quantity and purity. The DNA preparations of the four 293 cell transfections (40, 4, 0.5, and 0.1 µg of pF8TM) were analyzed for the β-actin gene. 100 and 10 ng (determined by ultraviolet spectroscopy) of each sample were amplified in triplicate. For each amount of pF8TM that was transfected, the β-actin C_T values are plotted versus the total input DNA concentration

PCR amplifications. As shown, pF8TM purified from the 293 cells decreases (mean C_i values increase) with decreasing amounts of plasmid transfected. The mean C_i values obtained for pF8TM in Figure 4A were plotted on a standard curve comprised of serially diluted pF8TM, shown in Figure 4B. The quantity of pF8TM, b, found in each of the four transfections was determined by extrapolation to the x axis of the standard curve in Figure 4B. These uncorrected values, b, for pF8TM were normalized to determine the actual amount of pF8TM found per 100 ng of genomic DNA by using the equation:

$$\frac{b \times 100 \text{ ng}}{a} = \text{actual pF8TM copies per } 100 \text{ ng of genomic DNA}$$

where a = actual genomic DNA in a sample and b = pF8TM copies from the standard curve. The normalized quantity of pF8TM per 100 ng of genomic DNA for each of the four transfections is shown in Figure 4D. These results show that the quantity of factor VIII plasmid associated with the 293 cells, 24 hr after transfection, decreases with decreasing plasmid concentration used in the transfection. The quantity of pF8TM associated with 293 cells, after transfection with 40 µg of plasmid, was 35 pg per 100 ng genomic DNA. This results in ~520 plasmid copies per cell.

DISCUSSION

We have described a new method for quantitating gene copy numbers using real-time analysis of PCR amplifications. Real-time PCR is compatible with either of the two PCR (RT–PCR) approaches: (1) quantitative competitive where an internal competitor for each target sequence is used for normalization (data not shown) or (2) quantitative comparative PCR using a normalization gene contained within the sample (i.e., β-actin) or a "housekeeping" gene for RT-PCR. If equal amounts of nucleic acid are analyzed for each sample and if the amplification efficiency before quantitative analysis is identical for each sample, the internal control (normalization gene or competitor) should give equal signals for all samples.

The real-time PCR method offers several advantages over the other two methods currently employed (see the Introduction). First, the real-time PCR method is performed in a closed-tube system and requires no post-PCR manipulation
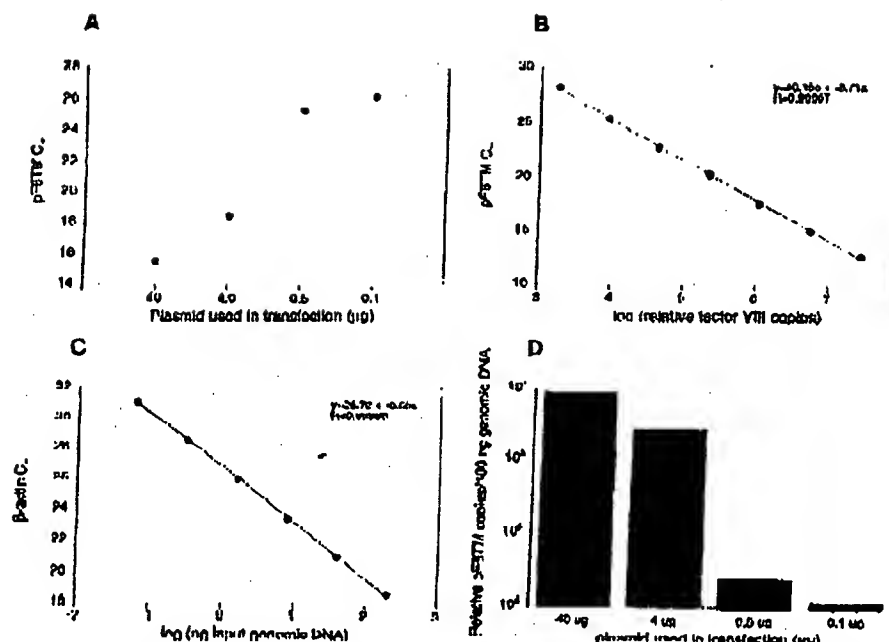
HUD ET AL.

Figure 4 Quantitative analysis of pF8TM in transfected cells. (A) Amount of plasmid DNA used for the transfection plotted against the mean C_t value determined for pF8TM remaining 24 hr after transfection. (B,C) Standard curves of pF8TM and β-actin, respectively. pF8TM DNA (B) and genomic DNA (C) were diluted serially 1:5 before amplification with the appropriate primers. The β-actin standard curve was used to normalize the results of A to 100 ng of genomic DNA. (D) The amount of pF8TM present per 100 ng of genomic DNA.

of sample. Therefore, the potential for PCR contamination in the laboratory is reduced because amplified products can be analyzed and disposed of without opening the reaction tubes. Second, this method supports the use of a normalization gene (i.e., β-actin) for quantitative PCR or housekeeping genes for quantitative RT-PCR controls. Analysis is performed in real time during the log phase of product accumulation. Analysis during log phase permits many different genes (over a wide input target range) to be analyzed simultaneously, without concern of reaching reaction plateau at different cycles. This will make multigene analysis assays much easier to develop, because individual internal competitors will not be needed for each gene under analysis. Third, sample throughput will increase dramatically with the new method because there is no post-PCR processing time. Additionally, working in a 96-well format is highly compatible with automation technology.

The real-time PCR method is highly reproducible. Replicate amplifications can be analyzed

for each sample minimizing potential error. The system allows for a very large assay dynamic range (approaching 1,000,000-fold starting target). Using a standard curve for the target of interest, relative copy number values can be determined for any unknown sample. Fluorescent threshold values, C_t, correlate linearly with relative DNA copy numbers. Real time quantitative RT-PCR methodology (Gibson et al., this issue) has also been developed. Finally, real time quantitative PCR methodology can be used to develop high-throughput screening assays for a variety of applications [quantitative gene expression (RT-PCR), gene copy assays (Her2, HIV, etc.), genotyping (knockout mouse analysis), and Immuno-PCR].

Real-time PCR may also be performed using intercalating dyes (Higuchi et al. 1992) such as ethidium bromide. The fluorogenic probe method offers a major advantage over intercalating dyes—greater specificity (i.e., primer dimers and nonspecific PCR products are not detected).

METHODS

Generation of a Plasmid Containing a Partial cDNA for Human Factor VIII

Total RNA was harvested (RNAsol B from Tel Test, Inc., Friendswood, TX) from cells transfected with a factor VIII expression vector, pCIS2.8c251) (Eaton et al. 1986; Gorman et al. 1990). A factor VIII partial cDNA sequence was generated by RT-PCR [GeneAmp EZ rTth RNA PCR Kit (part N808-0179, PE Applied Biosystems, Foster City, CA)] using the PCR primers F8for and F8rev (primer sequences are shown below). The amplicon was reamplified using modified F8for and F8rev primers (appended with BamHI and HindIII restriction site sequences at the 5' end) and cloned into pGEM-3Z (Promega Corp., Madison, WI). The resulting clone, pF8TM, was used for transient transfection of 293 cells.

Amplification of Target DNA and Detection of Amplicon Factor VIII Plasmid DNA

(pF8TM) was amplified with the primers F8for 5'-CCCGTCCCAAGAGTGA(X)GTC-3' and F8rev 5'-AAACGTCACGCCTGGATCGGTACG-3'. The reaction produced a 422-bp PCR product. The forward primer was designed to recognize a unique sequence found in the 5' untranslated region of the parent pCIS2.8c251) plasmid and therefore does not recognize and amplify the human factor VIII gene. Primers were chosen with the assistance of the computer program Oligo 4.0 (National Biosciences, Inc., Plymouth, MN). The human β-actin gene was amplified with the primers β-actin forward primer 5'-TCACCCAACACTGTGCCCATCTACGA-3' and β-actin reverse primer 5'-CAGCGGAACCGCTCATTGCCAATGG-3'. The reaction produced a 295-bp PCR product.

Amplification reactions (50 μl) contained a DNA sample, 10X PCR Buffer II (5 μl), 200 μM dATP, dCTP, dGTP, and 400 μM dUTP, 4 mM MgCl₂, 1.25 Units AmpliTaq DNA polymerase, 0.5 unit AmpErase uracil N-glycosylase (UNG), 60 pmole of each factor VIII primer, and 15 pmole of each β-actin primer. The reactions also contained one of the following detection probes (100 nM each): F8probe 5'-(FAM)AGCCTCTCCACCTGCTTCTTTCTGT-GCCTT(TAMRA)p 3' and β-actin probe 5'-(FAM)ATGCCCX(TAMRA)CCCCCATGCCATCp-3' where p indicates phosphorylation and X indicates a linker arm nucleotide. Reaction tubes were MicroAmp Optical Tubes (part number N801-0933, Perkin Elmer) that were frosted (at Perkin Elmer) to prevent light from reflecting. Tube caps were similar to MicroAmp Caps but specially designed to prevent light scattering. All of the PCR consumables were supplied by PE Applied Biosystems (Foster City, CA) except the factor VIII primers, which were synthesized at Genentech, Inc. (South San Francisco, CA). Probes were designed using the Oligo 4.0 software, following guidelines suggested in the Model 7700 Sequence Detector instrument manual. Briefly, probe Tₘ should be at least 5°C higher than the annealing temperature used during thermal cycling; primers should not form stable duplexes with the probe.

The thermal cycling conditions included 2 min at 50°C and 10 min at 95°C. Thermal cycling proceeded with

reactions were performed in the Model 7700 Sequence Detector (PE Applied Biosystems), which contains a GeneAmp PCR System 9600. Reaction conditions were programmed on a Power Macintosh 7100 (Apple Computer, Santa Clara, CA) linked directly to the Model 7700 Sequence Detector. Analysis of data was also performed on the Macintosh computer. Collection and analysis software was developed at PE Applied Biosystems.

Transfection of Cells with Factor VIII Construct

Four T175 flasks of 293 cells (ATCC CRL 1573), a human fetal kidney suspension cell line, were grown to 80% confluency and transfected pF8TM. Cells were grown in the following media: 50% HAM'S F12 without GHT, 50% low glucose Dulbecco's modified Eagle medium (DMEM) without glycine with sodium bicarbonate, 10% fetal bovine serum, 2 mM L-glutamine, and 1% penicillin–streptomycin. The media was changed 30 min before the transfection. pF8TM DNA amounts of 40, 4, 0.5, and 0.1 μg were added to 1.5 ml of a solution containing 0.125 M CaCl₂ and 1× HEPES. The four mixtures were left at room temperature for 10 min and then added dropwise to the cells. The flasks were incubated at 37°C and 5% CO₂ for 24 hr, washed with PBS, and resuspended in PBS. The resuspended cells were divided into aliquots and DNA was extracted immediately using the QIAamp Blood Kit (Qiagen, Chatsworth, CA). DNA was eluted into 200 μl of 20 mM Tris-HCl at pH 8.0.

REFERENCES

Bassler, H.A., S.J. Flood, K.J. Livak, J. Marmaro, R. Knorr, and C.A. Batt. 1995. Use of a fluorogenic probe in a PCR-based assay for the detection of Listeria monocytogenes. App. Environ. Microbiol. 61: 3724–3728.

Becker-Andre, M. 1991. Quantitative evaluation of mRNA levels. Meth. Mol. Cell. Biol. 2: 189-201.

Clementi, M., S. Menzo, P. Bagnarelli, A. Manzin, A. Valenza, and P.E. Varaldo. 1993. Quantitative PCR and RT-PCR in virology. [Review]. PCR Methods Applic. 2: 191–196.

Connor, R.I., H. Mohri, Y. Cao, and D.D. Ho. 1993. Increased viral burden and cytopathicity correlate temporally with CD4+ T-lymphocyte decline and clinical progression in human immunodeficiency virus type 1-infected individuals. J. Virol. 67: 1772–1777.

Eaton, D.L., W.I. Wood, D. Eaton, P.E. Hass, P.

HEID ET AL.

Venar, and C. Gorman. 1986. Construction and characterization of an active factor VIII variant lacking the central one third of the molecule. *Biochemistry* 25: 8343-8347.

Fasco, M.J., C.P. Treanor, S. Spivack, H.L. Figge, and L.S. Kaminsky. 1995. Quantitative RNA-polymerase chain reaction-DNA analysis by capillary electrophoresis and laser-induced fluorescence. *Anal. Biochem.* 224: 140-147.

Ferre, F. 1992. Quantitative or semi-quantitative PCR: Reality versus myth. *PCR Methods Applic.* 2: 1-9.

Furtado, M.R., L.A. Kingsley, and S.M. Wolinsky. 1995. Changes in the viral mRNA expression pattern correlate with a rapid rate of CD4+ T-cell number decline in human immunodeficiency virus type 1-infected individuals. *J. Virol.* 69: 2092-2100.

Gibson, U.E.M., C.A. Heid, and P.M. Williams. 1996. A novel method for real time quantitative competitive RT-PCR. *Genome Res.* (this issue).

Gorman, C.M., D.R. Gies, and G. McCray. 1990. Transient production of proteins using an adenovirus transformed cell line. *DNA Prot. Engin. Tech.* 2: 3-10.

Higuchi, R., G. Dollinger, P.S. Walsh, and R. Griffith. 1992. Simultaneous amplification and detection of specific DNA sequences. *Biotechnology* 10: 413-417.

Holland, P.M., R.D. Abramson, R. Watson, and D.H. Gelfand. 1991. Detection of specific polymerase chain reaction product by utilizing the 5'—3' exonuclease activity of Thermus aquaticus DNA polymerase. *Proc. Natl. Acad. Sci.* 88: 7276-7280.

Huang, S.K., H.Q. Xiao, T.J. Kleine, G. Paciotti, H.G. Marsh, L.M. Lichtenstein, and M.C. Liu. 1995a. IL-13 expression at the sites of allergen challenge in patients with asthma. *J. Immun.* 155: 2688-2694.

Huang, S.K., M. Yi, E. Palmer, and D.G. Marsh. 1995b. A dominant T cell receptor beta-chain in response to a short ragweed allergen, Amb a 5. *J. Immun.* 154: 6157-6162.

Kellogg, D.E., J.J. Sninsky, and S. Kowk. 1990. Quantitation of HIV-1 proviral DNA relative to cellular DNA by the polymerase chain reaction. *Anal. Biochem.* 189: 202-208.

Lee, L.G., C.R. Connell, and W. Bloch. 1993. Allelic discrimination by nick-translation PCR with fluorogenic probes. *Nucleic Acids Res.* 21: 3761-3766.

Livak, K.J., S.J. Flood, J. Marmaro, W. Giusti, and K. Deetz. 1995a. Oligonucleotides with fluorescent dyes at opposite ends provide a quenched probe system useful for detecting PCR product and nucleic acid hybridization. *PCR Methods Applic.* 4: 357-362.

Livak, K.J., J. Marmaro, and J.A. Todd. 1995b. Towards

fully automated genome-wide polymorphism screening. [Letter] *Nature Genet.* 9: 341-342.

Mulder, J., N. McKinney, C. Christopherson, J. Sninsky, L. Greenfield, and S. Kwok. 1994. Rapid and simple PCR assay for quantitation of human immunodeficiency virus type 1 RNA in plasma: Application to acute retroviral infection. *J. Clin. Microbiol.* 32: 292-300.

Pang, S., Y. Koyanagi, S. Miles, C. Wiley, H.V. Vinters, and I.S. Chen. 1990. High levels of unintegrated HIV-1 DNA in brain tissue of AIDS dementia patients. *Nature* 343: 85-89.

Piatak, M.J., K.C. Luk, B. Williams, and J.D. Lifson. 1993a. Quantitative competitive polymerase chain reaction for accurate quantitation of HIV DNA and RNA species. *BioTechniques* 14: 70-81.

Piatak, M.J., M.S. Saag, L.C. Yang, S.J. Clark, J.C. Kappes, K.C. Luk, B.H. Hahn, G.M. Shaw, and J.D. Lifson. 1993b. High levels of HIV-1 in plasma during all stages of infection determined by competitive PCR [see Comments]. *Science* 259: 1749-1754.

Prud'homme, G.J., D.H. Kono, and A.N. Theofilopoulos. 1995. Quantitative polymerase chain reaction analysis reveals marked overexpression of interleukin-1 beta, interleukin-1 and interferon-gamma mRNA in the lymph nodes of lupus-prone mice. *Mol. Immunol.* 32: 495-503.

Raeymaekers, L. 1995. A commentary on the practical applications of competitive PCR. *Genome Res.* 5: 91-94.

Sharp, P.A., A.J. Berk, and S.M. Berget. 1980. Transcription maps of adenovirus. *Methods Enzymol.* 65: 750-768.

Slamon, D.J., G.M. Clark, S.G. Wong, W.J. Levin, A. Ullrich, and W.L. McGuire. 1987. Human breast cancer: Correlation of relapse and survival with amplification of the HER-2/neu oncogene. *Science* 235: 177-182.

Southern, E.M. 1975. Detection of specific sequences among DNA fragments separated by gel electrophoresis. *J. Mol. Biol.* 98: 503-517.

Tan, X., X. Sun, C.F. Gonzalez, and W. Hsueh. 1994. PAF and TNF increase the precursor of NF-kappa B p50 mRNA in mouse intestine: Quantitative analysis by competitive PCR. *Biochim. Biophys. Acta* 1215: 157-162.

Thomas, P.S. 1980. Hybridization of denatured RNA and small DNA fragments transferred to nitrocellulose. *Proc. Natl. Acad. Sci.* 77: 5201-5205.

Williams, S., C. Schwer, A. Krishnarao, C. Heid, B. Karger, and P.M. Williams. 1996. Quantitative competitive PCR: Analysis of amplified products of the HIV-1 gag gene by capillary electrophoresis with laser induced fluorescence detection. *Anal. Biochem.* (in press).

methods. Peptides AENK or AEQK were dissolved in water, made isotonic with NaCl and diluted into RPMI growth medium. T-cell-proliferation assays were done essentially as described[20,21]. Briefly, after antigen pulsing (30 μg ml^{-1} TTCF) with tetrapeptides (1–2 mg ml^{-1}), PBMCs or EBV-B cells were washed in PBS and fixed for 45 s in 0.05% glutaraldehyde. Glycine was added to a final concentration of 0.1M and the cells were washed five times in RPMI 1640 medium containing 1% FCS before co-culture with T-cell clones in round-bottom 96-well microtitre plates. After 48 h, the cultures were pulsed with 1 μCi of ^{3}H-thymidine and harvested for scintillation counting 16 h later. Predigestion of native TTCF was done by incubating 200 μg TTCF with 0.25 μg pig kidney legumain in 500 μl 50 mM citrate buffer, pH 5.5, for 1 h at 37 °C.

Glycopeptide digestions. The peptides HIDNEEDI, HIDN(N-glucosamine)EEDI and HIDNESDI, which are based on the TTCF sequence, and QQQHLFGSNVTDCSGNFCLFR(KKK), which is based on human transferrin, were obtained by custom synthesis. The three C-terminal lysine residues were added to the natural sequence to aid solubility. The transferrin glycopeptide QQQHLFGSNVTDCSGNFCLFR was prepared by tryptic (Promega) digestion of 5 mg reduced, carboxy-methylated human transferrin followed by concanavalin A chromatography[11]. Glycopeptides corresponding to residues 622–642 and 421–452 were isolated by reverse-phase HPLC and identified by mass spectrometry and N-terminal sequencing. The lyophilized transferrin-derived peptides were redissolved in 50 mM sodium acetate, pH 5.5, 10 mM dithiothreitol, 20% methanol. Digestions were performed for 3 h at 30 °C with 5–50 mU ml^{-1} pig kidney legumain or B-cell AEP. Products were analysed by HPLC or MALDI-TOF mass spectrometry using a matrix of 10 mg ml^{-1} α-cyanocinnamic acid in 50% acetonitrile/0.1% TFA and a PerSeptive Biosystems Elite STR mass spectrometer set to linear or reflector mode. Internal standardization was obtained with a matrix ion of 568.13 mass units.

1. Chen, J. M. et al. Cloning, isolation, and characterisation of mammalian legumain, an asparaginyl endopeptidase. J. Biol. Chem. 272, 8090–8098 (1997).
2. Kembhavi, A. A., Buttle, D. J., Knight, C. G. & Barrett, A. J. The two cysteine endopeptidases of legume seeds: purification and characterization by use of specific fluorometric assays. Arch. Biochem. Biophys. 303, 208–213 (1993).
3. Dalton, J. P., Hola Jamriska, L. & Bridley, P. J. Asparaginyl endopeptidase activity in adult Schistosoma mansoni. Parasitology 111, 575–580 (1995).
4. Bennett, K. et al. Antigen processing for presentation by class II major histocompatibility complex requires cleavage by cathepsin E. Eur. J. Immunol. 22, 1519–1524 (1992).
5. Riese, R. J. et al. Essential role for cathepsin S in MHC class II-associated invariant chain processing and peptide loading. Immunity 4, 357–366 (1996).
6. Rodriguez, G. M. & Diment, S. Role of cathepsin D in antigen presentation of ovalbumin. J. Immunol. 149, 2894–2898 (1992).
7. Hewitt, E. W. et al. Natural processing sites for human cathepsin E and cathepsin D in tetanus toxin: implications for T cell epitope generation. J. Immunol. 159, 4693–4699 (1997).
8. Watts, C. Capture and processing of exogenous antigens for presentation on MHC molecules. Annu. Rev. Immunol. 15, 821–850 (1997).
9. Chapman, H. A. Endosomal proteases and MHC class II function. Curr. Opin. Immunol. 10, 93–102 (1998).
10. Fineschi, B. & Miller, J. Endosomal proteases and antigen processing. Trends Biochem. Sci. 22, 377–382 (1997).
11. Lu, J. & van Halbeek, H. Complete ^{1}H and ^{13}C resonance assignments of a 21-amino acid glycopeptide prepared from human serum transferrin. Carbohydr. Res. 296, 1–21 (1996).
12. Fearon, D. T. & Locksley, R. M. The instructive role of innate immunity in the acquired immune response. Science 272, 50–54 (1996).
13. Medzhitov, R. & Janeway, C. A. J. Innate immunity: the virtues of a nonclonal system of recognition. Cell 91, 295–298 (1997).
14. Wyatt, R. et al. The antigenic structure of the HIV gp120 envelope glycoprotein. Nature 393, 705–711 (1998).
15. Botarelli, P. et al. N-glycosylation of HIV gp120 may constrain recognition by T lymphocytes. J. Immunol. 147, 3128–3132 (1991).
16. Davidson, H. W., West, M. A. & Watts, C. Endocytosis, intracellular trafficking, and processing of membrane IgG and monovalent antigen/membrane IgG complexes in B lymphocytes. J. Immunol. 144, 4101–4109 (1990).
17. Barrett, A. J. & Kirschke, H. Cathepsin B, cathepsin H and cathepsin L. Methods Enzymol. 80, 535–559 (1981).
18. Makoff, A. J., Ballantine, S. P., Smallwood, A. E. & Fairweather, N. F. Expression of tetanus toxin fragment C in E. coli: its purification and potential use as a vaccine. Biotechnology 7, 1043–1046 (1989).
19. Lane, D. P. & Harlow, E. Antibodies: A Laboratory Manual (Cold Spring Harbor Laboratory Press, 1988).
20. Lanzavecchia, A. Antigen-specific interaction between T and B cells. Nature 314, 537–539 (1985).
21. Pond, L. & Watts, C. Characterization of transport of newly assembled, T cell-stimulatory MHC class II-peptide complexes from MHC class II compartments to the cell surface. J. Immunol. 159, 543–553 (1997).

Genomic amplification of a decoy receptor for Fas ligand in lung and colon cancer

Robert M. Pitti*†, Scot A. Marsters*†, David A. Lawrence*†, Margaret Roy*, Frank C. Kischkel*, Patrick Dowd*, Arthur Huang*, Christopher J. Donahue*, Steven W. Sherwood*, Daryl T. Baldwin*, Paul J. Godowski*, William I. Wood*, Austin L. Gurney*, Kenneth J. Hillan*, Robert L. Cohen*, Audrey D. Goddard*, David Botstein‡ & Avi Ashkenazi*

* Departments of Molecular Oncology, Molecular Biology, and Immunology, Genentech Inc., 1 DNA Way, South San Francisco, California 94080, USA
‡ Department of Genetics, Stanford University, Stanford, California 94305, USA
† These authors contributed equally to this work

Fas ligand (FasL) is produced by activated T cells and natural killer cells and it induces apoptosis (programmed cell death) in target cells through the death receptor Fas/Apo1/CD95 (ref. 1). One important role of FasL and Fas is to mediate immune-cytotoxic killing of cells that are potentially harmful to the organism, such as virus-infected or tumour cells[1]. Here we report the discovery of a soluble decoy receptor, termed decoy receptor 3 (DcR3), that binds to FasL and inhibits FasL-induced apoptosis. The DcR3 gene was amplified in about half of 35 primary lung and colon tumours studied, and DcR3 messenger RNA was expressed in malignant tissue. Thus, certain tumours may escape FasL-dependent immune-cytotoxic attack by expressing a decoy receptor that blocks FasL.

By searching expressed sequence tag (EST) databases, we identified a set of related ESTs that showed homology to the tumour necrosis factor (TNF) receptor (TNFR) gene superfamily[2]. Using the overlapping sequence, we isolated a previously unknown full-length complementary DNA from human fetal lung. We named the protein encoded by this cDNA decoy receptor 3 (DcR3). The cDNA encodes a 300-amino-acid polypeptide that resembles members of the TNFR family (Fig. 1a): the amino terminus contains a leader sequence, which is followed by four tandem cysteine-rich domains (CRDs). Like one other TNFR homologue, osteoprotegerin (OPG)[3], DcR3 lacks an apparent transmembrane sequence, which indicates that it may be a secreted, rather than a membrane-asscociated, molecule. We expressed a recombinant, histidine-tagged form of DcR3 in mammalian cells; DcR3 was secreted into the cell culture medium, and migrated on polyacrylamide gels as a protein of relative molecular mass 35,000 (data not shown). DcR3 shares sequence identity in particular with OPG (31%) and TNFR2 (29%), and has relatively less homology with Fas (17%). All of the cysteines in the four CRDs of DcR3 and OPG are conserved; however, the carboxy-terminal portion of DcR3 is 101 residues shorter.

We analysed expression of DcR3 mRNA in human tissues by northern blotting (Fig. 1b). We detected a predominant 1.2-kilobase transcript in fetal lung, brain, and liver, and in adult spleen, colon and lung. In addition, we observed relatively high DcR3 mRNA expression in the human colon carcinoma cell line SW480.

To investigate potential ligand interactions of DcR3, we generated a recombinant, Fc-tagged DcR3 protein. We tested binding of DcR3–Fc to human 293 cells transfected with individual TNF-family ligands, which are expressed as type 2 transmembrane proteins (these transmembrane proteins have their N termini in the cytosol). DcR3–Fc showed a significant increase in binding to cells transfected with FasL[4] (Fig. 2a), but not to cells transfected with TNF[5], Apo2L/TRAIL[6,7], Apo3L/TWEAK[8,9], or OPGL/TRANCE/

RANKL[10-12] (data not shown). DcR3–Fc immunoprecipitated shed FasL from FasL-transfected 293 cells (Fig. 2b) and purified soluble FasL (Fig. 2c), as did the Fc-tagged ectodomain of Fas but not TNFR1. Gel-filtration chromatography showed that DcR3–Fc and soluble FasL formed a stable complex (Fig. 2d). Equilibrium analysis indicated that DcR3–Fc and Fas–Fc bound to soluble FasL with a comparable affinity ($K_d = 0.8 \pm 0.2$ and 1.1 ± 0.1 nM, respectively; Fig. 2e), and that DcR3–Fc could block nearly all of the binding of soluble FasL to Fas–Fc (Fig. 2e, inset). Thus, DcR3 competes with Fas for binding to FasL.

To determine whether binding of DcR3 inhibits FasL activity, we tested the effect of DcR3–Fc on apoptosis induction by soluble FasL in Jurkat T leukaemia cells, which express Fas (Fig. 3a). DcR3–Fc and Fas–Fc blocked soluble-FasL-induced apoptosis in a similar dose-dependent manner, with half-maximal inhibition at ~ 0.1 μg ml^{-1}. Time-course analysis showed that the inhibition did not merely delay cell death, but rather persisted for at least 24 hours (Fig. 3b). We also tested the effect of DcR3–Fc on activation-induced cell death (AICD) of mature T lymphocytes, a FasL-dependent process[1]. Consistent with previous results[13], activation of interleukin-2-stimulated CD4-positive T cells with anti-CD3 antibody increased the level of apoptosis twofold, and Fas–Fc blocked this effect substantially (Fig. 3c); DcR3–Fc blocked the

induction of apoptosis to a similar extent. Thus, DcR3 binding blocks apoptosis induction by FasL.

FasL-induced apoptosis is important in elimination of virus-infected cells and cancer cells by natural killer cells and cytotoxic T lymphocytes; an alternative mechanism involves perforin and granzymes[1,14-16]. Peripheral blood natural killer cells triggered marked cell death in Jurkat T leukaemia cells (Fig. 3d); DcR3–Fc and Fas–Fc each reduced killing of target cells from $\sim 65\%$ to $\sim 30\%$, with half-maximal inhibition at ~ 1 μg ml^{-1}; the residual killing was probably mediated by the perforin/granzyme pathway. Thus, DcR3 binding blocks FasL-dependent natural killer cell activity. Higher DcR3–Fc and Fas–Fc concentrations were required to block natural killer cell activity compared with those required to block soluble FasL activity, which is consistent with the greater potency of membrane-associated FasL compared with soluble FasL[17].

Given the role of immune-cytotoxic cells in elimination of tumour cells and the fact that DcR3 can act as an inhibitor of FasL, we proposed that DcR3 expression might contribute to the ability of some tumours to escape immune-cytotoxic attack. As genomic amplification frequently contributes to tumorigenesis, we investigated whether the DcR3 gene is amplified in cancer. We analysed DcR3 gene-copy number by quantitative polymerase chain
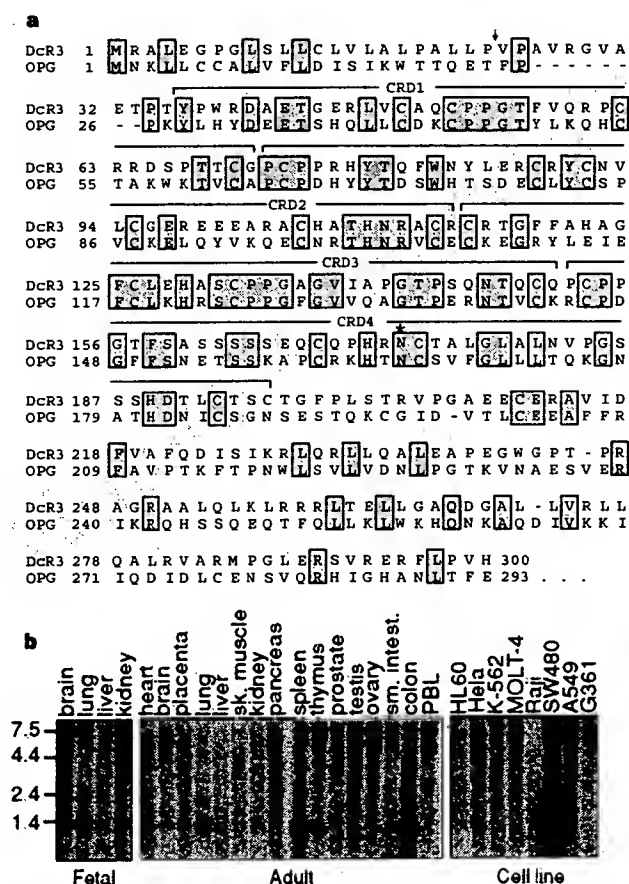

Figure 1 Primary structure and expression of human DcR3. **a**, Alignment of the amino-acid sequences of DcR3 and of osteoprotegerin (OPG); the C-terminal 101 residues of OPG are not shown. The putative signal cleavage site (arrow), the cysteine-rich domains (CRD 1-4), and the N-linked glycosylation site (asterisk) are shown. **b**, Expression of DcR3 mRNA. Northern hybridization analysis was done using the DcR3 cDNA as a probe and blots of poly(A)* RNA (Clontech) from human fetal and adult tissues or cancer cell lines. PBL, peripheral blood lymphocyte.
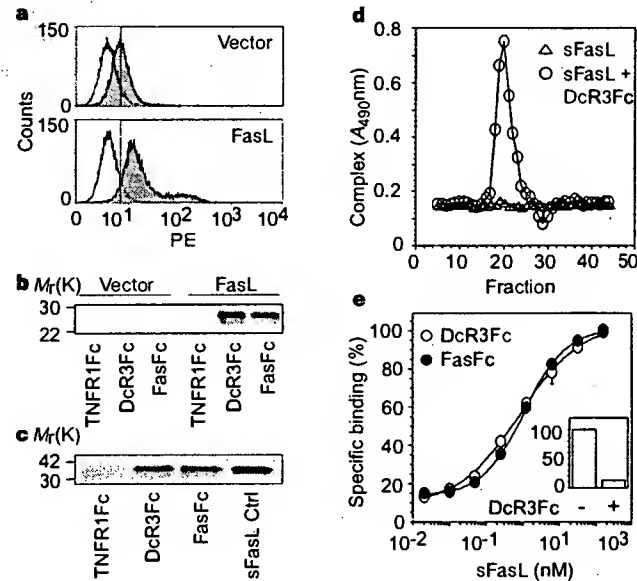

Figure 2 Interaction of DcR3 with FasL. **a**, 293 cells were transfected with pRK5 vector (top) or with pRK5 encoding full-length FasL (bottom), incubated with DcR3-Fc (solid line, shaded area), TNFR1-Fc (dotted line) or buffer control (dashed line) (the dashed and dotted lines overlap), and analysed for binding by FACS. Statistical analysis showed a significant difference ($P < 0.001$) between the binding of DcR3-Fc to cells transfected with FasL or pRK5. PE, phycoerythrin-labelled cells. **b**, 293 cells were transfected as in **a** and metabolically labelled, and cell supernatants were immunoprecipitated with Fc-tagged TNFR1, DcR3 or Fas. **c**, Purified soluble FasL (sFasL) was immunoprecipitated with TNFR1-Fc, DcR3-Fc or Fas-Fc and visualized by immunoblot with anti-FasL antibody. sFasL was loaded directly for comparison in the right-hand lane. **d**, Flag-tagged sFasL was incubated with DcR3-Fc or with buffer and resolved by gel filtration; column fractions were analysed in an assay that detects complexes containing DcR3-Fc and sFasL-Flag. **e**, Equilibrium binding of DcR3-Fc or Fas-Fc to sFasL-Flag. Inset, competition of DcR3-Fc with Fas-Fc for binding to sFasL-Flag.

reaction (PCR)[18] in genomic DNA from 35 primary lung and colon tumours, relative to pooled genomic DNA from peripheral blood leukocytes (PBLs) of 10 healthy donors. Eight of 18 lung tumours and 9 of 17 colon tumours showed DcR3 gene amplification, ranging from 2- to 18-fold (Fig. 4a, b). To confirm this result, we analysed the colon tumour DNAs with three more, independent sets of DcR3-based PCR primers and probes; we observed nearly the same amplification (data not shown).

We then analysed DcR3 mRNA expression in primary tumour tissue sections by in situ hybridization. We detected DcR3 expression in 6 out of 15 lung tumours, 2 out of 2 colon tumours, 2 out of 5 breast tumours, and 1 out of 1 gastric tumour (data not shown). A section through a squamous-cell carcinoma of the lung is shown in Fig. 4c. DcR3 mRNA was localized to infiltrating malignant epithelium, but was essentially absent from adjacent stroma, indicating tumour-specific expression. Although the individual tumour specimens that we analysed for mRNA expression and gene amplification were different, the in situ hybridization results are consistent with the finding that the DcR3 gene is amplified frequently in tumours. SW480 colon carcinoma cells, which showed abundant DcR3 mRNA expression (Fig. 1b), also had marked DcR3 gene amplification, as shown by quantitative PCR (fourfold) and by Southern blot hybridization (fivefold) (data not shown).

If DcR3 amplification in cancer is functionally relevant, then DcR3 should be amplified more than neighbouring genomic regions that are not important for tumour survival. To test this,

we mapped the human DcR3 gene by radiation-hybrid analysis; DcR3 showed linkage to marker AFM218xe7 (T160), which maps to chromosome position 20q13. Next, we isolated from a bacterial artificial chromosome (BAC) library a human genomic clone that carries DcR3, and sequenced the ends of the clone's insert. We then determined, from the nine colon tumours that showed twofold or greater amplification of DcR3, the copy number of the DcR3-flanking sequences (reverse and forward) from the BAC, and of seven genomic markers that span chromosome 20 (Fig. 4d). The DcR3-linked reverse marker showed an average amplification of roughly threefold, slightly less than the approximately fourfold amplification of DcR3; the other markers showed little or no amplification. These data indicate that DcR3 may be at the 'epicentre' of a distal chromosome 20 region that is amplified in colon cancer, consistent with the possibility that DcR3 amplification promotes tumour survival.

Our results show that DcR3 binds specifically to FasL and inhibits FasL activity. We did not detect DcR3 binding to several other TNF-ligand-family members; however, this does not rule out the possibility that DcR3 interacts with other ligands, as do some other TNFR family members, including OPG[2,19].

FasL is important in regulating the immune response; however, little is known about how FasL function is controlled. One mechanism involves the molecule cFLIP, which modulates apoptosis signalling downstream of Fas[20]. A second mechanism involves proteolytic shedding of FasL from the cell surface[17]. DcR3 competes with Fas for
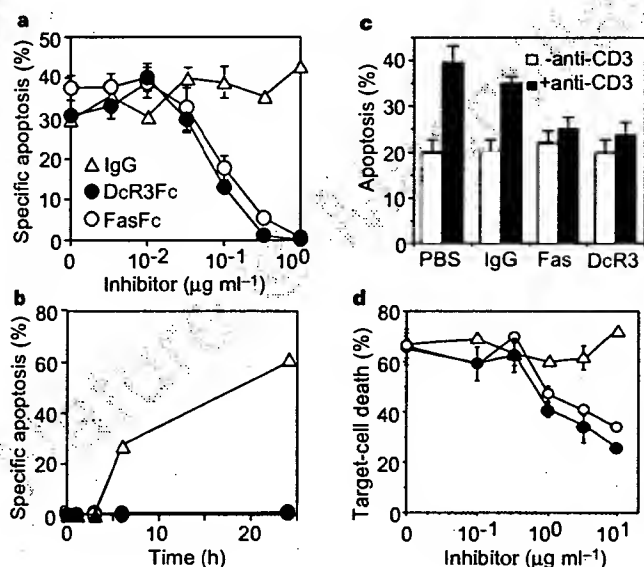

Figure 3 Inhibition of FasL activity by DcR3. a, Human Jurkat T leukaemia cells were incubated with Flag-tagged soluble FasL (sFasL; 5 ng ml^{-1}) oligomerized with anti-Flag antibody (0.1 μg ml^{-1}) in the presence of the proposed inhibitors DcR3-Fc, Fas-Fc or human IgG1 and assayed for apoptosis (mean ± s.e.m. of triplicates). b, Jurkat cells were incubated with sFasL–Flag plus anti-Flag antibody as in a, in presence of 1 μg ml^{-1} DcR3-Fc (filled circles), Fas-Fc (open circles) or human IgG1 (triangles), and apoptosis was determined at the indicated time points. c, Peripheral blood T cells were stimulated with PHA and interleukin-2, followed by control (white bars) or anti-CD3 antibody (filled bars), together with phosphate-buffered saline (PBS), human IgG1, Fas-Fc, or DcR3-Fc (10 μg ml^{-1}). After 16 h, apoptosis of CD4^{+} cells was determined (mean ± s.e.m. of results from five donors). d, Peripheral blood natural killer cells were incubated with ^{51}Cr-labelled Jurkat cells in the presence of DcR3-Fc (filled circles), Fas-Fc (open circles) or human IgG1 (triangles), and target-cell death was determined by release of [51]Cr (mean ± s.d. for two donors, each in triplicate).

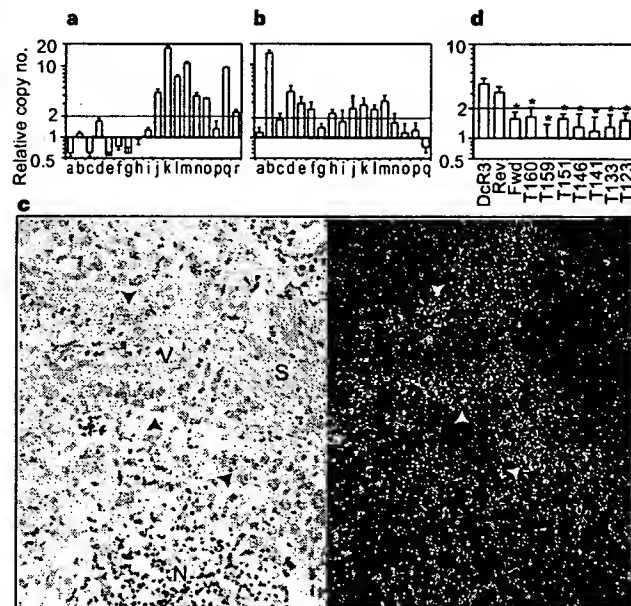**Figure 4** Genomic amplification of DcR3 in tumours. a, Lung cancers, comprising eight adenocarcinomas (c, d, f, g, h, j, k, r), seven squamous-cell carcinomas (a, e, m, n, o, p, q), one non-small-cell carcinoma (b), one small-cell carcinoma (i), and one bronchial adenocarcinoma (l). The data are means ± s.d. of 2 experiments done in duplicate. b, Colon tumours, comprising 17 adenocarcinomas. Data are means ± s.e.m. of five experiments done in duplicate. c, In situ hybridization analysis of DcR3 mRNA expression in a squamous-cell carcinoma of the lung. A representative bright-field image (left) and the corresponding dark-field image (right) show DcR3 mRNA over infiltrating malignant epithelium (arrowheads). Adjacent non-malignant stroma (S), blood vessel (V) and necrotic tumour tissue (N) are also shown. d, Average amplification of DcR3 compared with amplification of neighbouring genomic regions (reverse and forward, Rev and Fwd), the DcR3-linked marker T160, and other chromosome-20 markers, in the nine colon tumours showing DcR3 amplification of twofold or more (b). Data are from two experiments done in duplicate. Asterisk indicates P < 0.01 for a Student's t-test comparing each marker with DcR3.

FasL binding; hence, it may represent a third mechanism of extracellular regulation of FasL activity. A decoy receptor that modulates the function of the cytokine interleukin-1 has been described[21]. In addition, two decoy receptors that belong to the TNFR family, DcR1 and DcR2, regulate the FasL-related apoptosis-inducing molecule Apo2L[22]. Unlike DcR1 and DcR2, which are membrane-associated proteins, DcR3 is directly secreted into the extracellular space. One other secreted TNFR-family member is OPG[3], which shares greater sequence homology with DcR3 (31%) than do DcR1 (17%) or DcR2 (19%); OPG functions as a third decoy for Apo2L[19]. Thus, DcR3 and OPG define a new subset of TNFR-family members that function as secreted decoys to modulate ligands that induce apoptosis. Pox viruses produce soluble TNFR homologues that neutralize specific TNF-family ligands, thereby modulating the antiviral immune response[2]. Our results indicate that a similar mechanism, namely, production of a soluble decoy receptor for FasL, may contribute to immune evasion by certain tumours. ☐

Methods

Isolation of DcR3 cDNA. Several overlapping ESTs in GenBank (accession numbers AA025672, AA025673 and W67560) and in Lifeseq™ (Incyte Pharmaceuticals; accession numbers 1339238, 1533571, 1533650, 1542861, 1789372 and 2207027) showed similarity to members of the TNFR family. We screened human cDNA libraries by PCR with primers based on the region of EST consensus; fetal lung was positive for a product of the expected size. By hybridization to a PCR-generated probe based on the ESTs, one positive clone (DNA30942) was identified. When searching for potential alternatively spliced forms of DcR3 that might encode a transmembrane protein, we isolated 50 more clones; the coding regions of these clones were identical in size to that of the initial clone (data not shown).

Fc-fusion proteins (immunoadhesins). The entire DcR3 sequence, or the ectodomain of Fas or TNFRI, was fused to the hinge and Fc region of human IgG1, expressed in insect SF9 cells or in human 293 cells, and purified as described[23].

Fluorescence-activated cell sorting (FACS) analysis. We transfected 293 cells using calcium phosphate or Effectene (Qiagen) with pRK5 vector or pRK5 encoding full-length human FasL[4] (2 μg), together with pRK5 encoding CrmA (2 μg) to prevent cell death. After 16 h, the cells were incubated with biotinylated DcR3–Fc or TNFRI–Fc and then with phycoerythrin-conjugated streptavidin (GibcoBRL), and were assayed by FACS. The data were analysed by Kolmogorov–Smirnov statistical analysis. There was some detectable staining of vector-transfected cells by DcR3–Fc; as these cells express little FasL (data not shown), it is possible that DcR3 recognized some other factor that is expressed constitutively on 293 cells.

Immunoprecipitation. Human 293 cells were transfected as above, and metabolically labelled with [35S]cysteine and [35S]methionine (0.5 mCi; Amersham). After 16 h of culture in the presence of z-VAD-fmk (10 μM), the medium was immunoprecipitated with DcR3–Fc, Fas–Fc or TNFRI–Fc (5 μg), followed by protein A–Sepharose (Repligen). The precipitates were resolved by SDS–PAGE and visualized on a phosphorimager (Fuji BAS2000). Alternatively, purified, Flag-tagged soluble FasL (1 μg) (Alexis) was incubated with each Fc-fusion protein (1 μg), precipitated with protein A–Sepharose, resolved by SDS–PAGE and visualized by immunoblotting with rabbit anti-FasL antibody (Oncogene Research).

Analysis of complex formation. Flag-tagged soluble FasL (25 μg) was incubated with buffer or with DcR3–Fc (40 μg) for 1.5 h at 24 °C. The reaction was loaded onto a Superdex 200 HR 10/30 column (Pharmacia) and developed with PBS; 0.6-ml fractions were collected. The presence of DcR3–Fc–FasL complex in each fraction was analysed by placing 100 μl aliquots into microtitre wells precoated with anti-human IgG (Boehringer) to capture DcR3–Fc, followed by detection with biotinylated anti-Flag antibody Bio M2 (Kodak) and streptavidin–horseradish peroxidase (Amersham). Calibration of the column indicated an apparent relative molecular mass of the complex of 420K (data not shown), which is consistent with a stoichiometry of two DcR3–Fc homodimers to two soluble FasL homotrimers.

Equilibrium binding analysis. Microtitre wells were coated with anti-human

IgG, blocked with 2% BSA in PBS. DcR3–Fc or Fas–Fc was added, followed by serially diluted Flag-tagged soluble FasL. Bound ligand was detected with anti-Flag antibody as above. In the competition assay, Fas–Fc was immobilized as above, and the wells were blocked with excess IgG1 before addition of Flag-tagged soluble FasL plus DcR3–Fc.

T-cell AICD. CD3+ lymphocytes were isolated from peripheral blood of individual donors using anti-CD3 magnetic beads (Miltenyi Biotech), stimulated with phytohaemagglutinin (PHA; 2 μg ml⁻¹) for 24 h, and cultured in the presence of interleukin-2 (100 U ml⁻¹) for 5 days. The cells were plated in wells coated with anti-CD3 antibody (Pharmingen) and analysed for apoptosis 16 h later by FACS analysis of annexin-V-binding of CD4+ cells[24].

Natural killer cell activity. Natural killer cells were isolated from peripheral blood of individual donors using anti-CD56 magnetic beads (Miltenyi Biotech), and incubated for 16 h with 51Cr-loaded Jurkat cells at an effector-to-target ratio of 1:1 in the presence of DcR3–Fc, Fas–Fc or human IgG1. Target-cell death was determined by release of 51Cr in effector–target co-cultures relative to release of 51Cr by detergent lysis of equal numbers of Jurkat cells.

Gene-amplification analysis. Surgical specimens were provided by J. Kern (lung tumours) and P. Quirke (colon tumours). Genomic DNA was extracted (Qiagen) and the concentration was determined using Hoechst dye 33258 intercalation fluorometry. Amplification was determined by quantitative PCR[18] using a TaqMan instrument (ABI). The method was validated by comparison of PCR and Southern hybridization data for the Myc and HER-2 oncogenes (data not shown). Gene-specific primers and fluorogenic probes were designed on the basis of the sequence of DcR3 or of nearby regions identified on a BAC carrying the human DcR3 gene; alternatively, primers and probes were based on Stanford Human Genome Center marker AFM218xe7 (T160), which is linked to DcR3 (likelihood score = 5.4), SHGC-36268 (T159), the nearest available marker which maps to ~500 kilobases from T160, and five extra markers that span chromosome 20. The DcR3-specific primer sequences were 5'-CTTCTTCGCGCACGCTG-3' and 5'-ATCACGCCGGCACCAG-3' and the fluorogenic probe sequence was 5'-(FAM-ACACGATGCGTGCTCCAAGCAG AAp-(TAMARA), where FAM is 5'-fluorescein phosphoramidite. Relative gene-copy numbers were derived using the formula $2^{(\Delta CT)}$, where ΔCT is the difference in amplification cycles required to detect DcR3 in peripheral blood lymphocyte DNA compared to test DNA.

1. Nagata, S. Apoptosis by death factor. Cell 88, 355–365 (1997).
2. Smith, C. A., Farrah, T. & Goodwin, R. G. The TNF receptor superfamily of cellular and viral proteins: activation, costimulation, and death. Cell 76, 959–962 (1994).
3. Simonet, W. S. et al. Osteoprotegerin: a novel secreted protein involved in the regulation of bone density. Cell 89, 309–319 (1997).
4. Suda, T., Takahashi, T., Golstein, P. & Nagata, S. Molecular cloning and expression of Fas ligand, a novel member of the TNF family. Cell 75, 1169–1178 (1993).
5. Pennica, D. et al. Human tumour necrosis factor: precursor structure, expression and homology to lymphotoxin. Nature 312, 724–729 (1984).
6. Pitti, R. M. et al. Induction of apoptosis by Apo-2 ligand, a new member of the tumor necrosis factor receptor family. J. Biol. Chem. 271, 12687–12690 (1996).
7. Wiley, S. R. et al. Identification and characterization of a new member of the TNF family that induces apoptosis. Immunity 3, 673–682 (1995).
8. Marsters, S. A. et al. Identification of a ligand for the death-domain-containing receptor Apo3. Curr. Biol. 8, 525–528 (1998).
9. Chicheportiche, Y. et al. TWEAK, a new secreted ligand in the TNF family that weakly induces apoptosis. J. Biol. Chem. 272, 32401–32410 (1997).
10. Wong, B. R. et al. TRANCE is a novel ligand of the TNFR family that activates c-Jun-N-terminal kinase in T cells. J. Biol. Chem. 272, 25190–25194 (1997).
11. Anderson, D. M. et al. A homolog of the TNF receptor and its ligand enhance T-cell growth and dendritic-cell function. Nature 390, 175–179 (1997).
12. Lacey, D. L. et al. Osteoprotegerin ligand is a cytokine that regulates osteoclast differentiation and activation. Cell 93, 165–176 (1998).
13. Dhein, J., Walczak, H., Baumler, C., Debatin, K. M. & Krammer, P. H. Autocrine T-cell suicide mediated by Apo1/(Fas/CD95). Nature 373, 438–441 (1995).
14. Arase, H., Arase, N. & Saito, T. Fas-mediated cytotoxicity by freshly isolated natural killer cells. J. Exp. Med. 181, 1235–1238 (1995).
15. Medvedev, A. E. et al. Regulation of Fas and Fas ligand expression in NK cells by cytokines and the involvement of Fas ligand in NK/LAK cell-mediated cytotoxicity. Cytokine 9, 394–404 (1997).
16. Moretta, A. Mechanisms in cell-mediated cytotoxicity. Cell 90, 13–18 (1997).
17. Tanaka, M., Itai, T., Adachi, M. & Nagata, S. Downregualtion of Fas ligand by shedding. Nature Med. 4, 31–36 (1998).
18. Gelmini, S. et al. Quantitative PCR-based homogeneous assay with fluorogenic probes to measure c-erbB-2 oncogene amplification. Clin. Chem. 43, 752–758 (1997).
19. Emery, J. G. et al. Osteoprotegerin is a receptor for the cytotoxic ligand TRAIL. J. Biol. Chem. 273, 14363–14367 (1998).
20. Wallach, D. Placing death under control. Nature 388, 123–125 (1997).
21. Collota, F. et al. Interleukin-1 type II receptor: a decoy target for IL-1 that is regulated by IL-4. Science 261, 472–475 (1993).

22. Ashkenazi, A. & Dixit, V. M. Death receptors: signaling and modulation. *Science* **281**, 1305–1308 (1998).
23. Ashkenazi, A. & Chamow, S. M. Immunoadhesins as research tools and therapeutic agents. *Curr. Opin. Immunol.* **9**, 195–200 (1997).
24. Marsters, S. *et al.* Activation of apoptosis by Apo-2 ligand is independent of FADD but blocked by CrmA. *Curr. Biol.* **6**, 750–752 (1996).

Crystal structure of the ATP-binding subunit of an ABC transporter

Li-Wei Hung*, Iris Xiaoyan Wang†, Kishiko Nikaido†, Pei-Qi Liu†, Giovanna Ferro-Luzzi Ames† & Sung-Hou Kim*‡

* E. O. Lawrence Berkeley National Laboratory, † Department of Molecular and Cell Biology, and ‡ Department of Chemistry, University of California at Berkeley, Berkeley, California 94720, USA

ABC transporters (also known as traffic ATPases) form a large family of proteins responsible for the translocation of a variety of compounds across membranes of both prokaryotes and eukaryotes[1]. The recently completed *Escherichia coli* genome sequence revealed that the largest family of paralogous *E. coli* proteins is composed of ABC transporters[2]. Many eukaryotic proteins of medical significance belong to this family, such as the cystic fibrosis transmembrane conductance regulator (CFTR), the P-glycoprotein (or multidrug-resistance protein) and the heterodimeric transporter associated with antigen processing (Tap1–Tap2). Here we report the crystal structure at 1.5 Å resolution of HisP, the ATP-binding subunit of the histidine permease, which is an ABC transporter from *Salmonella typhimurium*. We correlate the details of this structure with the biochemical, genetic and biophysical properties of the wild-type and several mutant HisP proteins. The structure provides a basis for understanding properties of ABC transporters and of defective CFTR proteins.

ABC transporters contain four structural domains: two nucleotide-binding domains (NBDs), which are highly conserved throughout the family, and two transmembrane domains[1]. In prokaryotes these domains are often separate subunits which are assembled into a membrane-bound complex; in eukaryotes the domains are generally fused into a single polypeptide chain. The periplasmic histidine permease of *S. typhimurium* and *E. coli*[1,3–8] is a well-characterized ABC transporter that is a good model for this superfamily. It consists of a membrane-bound complex, HisQMP$_2$, which comprises integral membrane subunits, HisQ and HisM, and two copies of HisP, the ATP-binding subunit. HisP, which has properties intermediate between those of integral and peripheral membrane proteins[9], is accessible from both sides of the membrane, presumably by its interaction with HisQ and HisM[6]. The two HisP subunits form a dimer, as shown by their cooperativity in ATP hydrolysis[5], the requirement for both subunits to be present for activity[8], and the formation of a HisP dimer upon chemical cross-linking. Soluble HisP also forms a dimer[3]. HisP has been purified and characterized in an active soluble form[3] which can be reconstituted into a fully active membrane-bound complex[8].

The overall shape of the crystal structure of the HisP monomer is that of an 'L' with two thick arms (arm I and arm II); the ATP-binding pocket is near the end of arm I (Fig. 1). A six-stranded β-sheet (β3 and β8–β12) spans both arms of the L, with a domain of a α- plus β-type structure (β1, β2, β4–β7, α1 and α2) on one side (within arm I) and a domain of mostly α-helices (α3–α9) on the
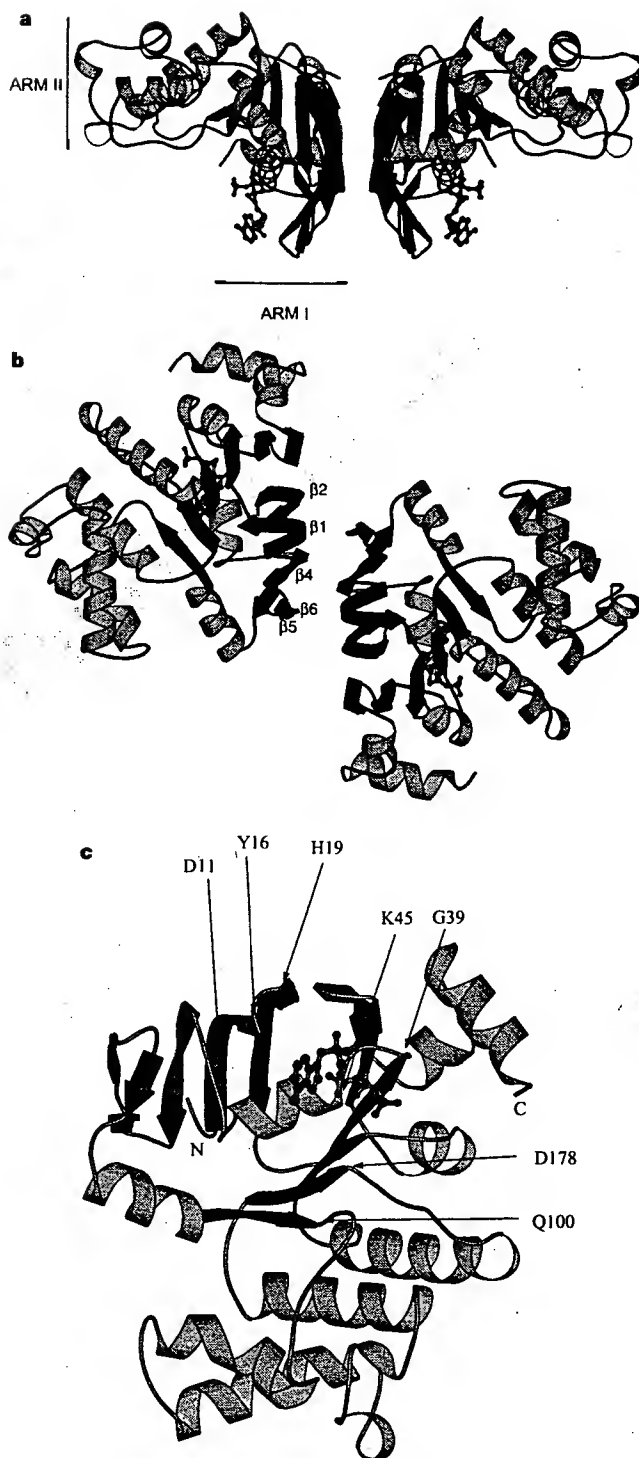

Figure 1 Crystal structure of HisP. **a**, View of the dimer along an axis perpendicular to its two-fold axis. The top and bottom of the dimer are suggested to face towards the periplasmic and cytoplasmic sides, respectively (see text). The thickness of arm II is about 25 Å, comparable to that of membrane. α-Helices are shown in orange and β-sheets in green. **b**, View along the two-fold axis of the HisP dimer, showing the relative displacement of the monomers not apparent in **a**. The β-strands at the dimer interface are labelled. **c**, View of one monomer from the bottom of arm I, as shown in **a**, towards arm II, showing the ATP-binding pocket. **a**-**c**, The protein and the bound ATP are in 'ribbon' and 'ball-and-stick' representations, respectively. Key residues discussed in the text are indicated in **c**. These figures were prepared with MOLSCRIPT[29]. N, amino terminus; C, C terminus.

NOVEL APPROACH TO QUANTITATIVE POLYMERASE CHAIN REACTION USING REAL-TIME DETECTION: APPLICATION TO THE DETECTION OF GENE AMPLIFICATION IN BREAST CANCER

Ivan Bièche[1,2], Martine Olivi[1], Marie-Hélène Champème[2], Dominique Vidaud[1], Rosette Lidereau[2] and Michel Vidaud[1]*

[1]*Laboratoire de Génétique Moléculaire, Faculté des Sciences Pharmaceutiques et Biologiques de Paris, Paris, France*
[2]*Laboratoire d'Oncogénétique, Centre René Huguenin, St-Cloud, France*

Gene amplification is a common event in the progression of human cancers, and amplified oncogenes have been shown to have diagnostic, prognostic and therapeutic relevance. A kinetic quantitative polymerase-chain-reaction (PCR) method, based on fluorescent TaqMan methodology and a new instrument (ABI Prism 7700 Sequence Detection System) capable of measuring fluorescence in real-time, was used to quantify gene amplification in tumor DNA. Reactions are characterized by the point during cycling when PCR amplification is still in the exponential phase, rather than the amount of PCR product accumulated after a fixed number of cycles. None of the reaction components is limited during the exponential phase, meaning that values are highly reproducible in reactions starting with the same copy number. This greatly improves the precision of DNA quantification. Moreover, real-time PCR does not require post-PCR sample handling, thereby preventing potential PCR-product carry-over contamination; it possesses a wide dynamic range of quantification and results in much faster and higher sample throughput. The real-time PCR method, was used to develop and validate a simple and rapid assay for the detection and quantification of the 3 most frequently amplified genes (*myc, ccnd1* and *erb*B2) in breast tumors. Extra copies of *myc, ccnd1* and *erb*B2 were observed in 10, 23 and 15%, respectively, of 108 breast-tumor DNA; the largest observed numbers of gene copies were 4.6, 18.6 and 15.1, respectively. These results correlated well with those of Southern blotting. The use of this new semi-automated technique will make molecular analysis of human cancers simpler and more reliable, and should find broad applications in clinical and research settings. *Int. J. Cancer* 78:661–666, 1998.
© *1998 Wiley-Liss, Inc.*

Gene amplification plays an important role in the pathogenesis of various solid tumors, including breast cancer, probably because over-expression of the amplified target genes confers a selective advantage. The first technique used to detect genomic amplification was cytogenetic analysis. Amplification of several chromosome regions, visualized either as extrachromosomal double minutes (dmins) or as integrated homogeneously staining regions (HSRs), are among the main visible cytogenetic abnormalities in breast tumors. Other techniques such as comparative genomic hybridization (CGH) (Kallioniemi *et al.*, 1994) have also been used in broad searches for regions of increased DNA copy numbers in tumor cells, and have revealed some 20 amplified chromosome regions in breast tumors. Positional cloning efforts are underway to identify the critical gene(s) in each amplified region. To date, genes known to be amplified frequently in breast cancers include *myc* (8q24), *ccnd*1 (11q13), and *erb*B2 (17q12-q21) (for review, see Bièche and Lidereau, 1995).

Amplification of the *myc, ccnd1,* and *erb*B2 proto-oncogenes should have clinical relevance in breast cancer, since independent studies have shown that these alterations can be used to identify sub-populations with a worse prognosis (Berns *et al.,* 1992; Schuuring *et al.,* 1992; Slamon *et al.,* 1987). Muss *et al.* (1994) suggested that these gene alterations may also be useful for the prediction and assessment of the efficacy of adjuvant chemotherapy and hormone therapy.

However, published results diverge both in terms of the frequency of these alterations and their clinical value. For instance, over 500 studies in 10 years have failed to resolve the controversy surrounding the link suggested by Slamon *et al.* (1987) between *erb*B2 amplification and disease progression. These discrepancies are partly due to the clinical, histological and ethnic heterogeneity of breast cancer, but technical considerations are also probably involved.

Specific genes (DNA) were initially quantified in tumor cells by means of blotting procedures such as Southern and slot blotting. These batch techniques require large amounts of DNA (5–10 µg/reaction) to yield reliable quantitative results. Furthermore, meticulous care is required at all stages of the procedures to generate blots of sufficient quality for reliable dosage analysis. Recently, PCR has proven to be a powerful tool for quantitative DNA analysis, especially with minimal starting quantities of tumor samples (small, early-stage tumors and formalin-fixed, paraffin-embedded tissues).

Quantitative PCR can be performed by evaluating the amount of product either after a given number of cycles (end-point quantitative PCR) or after a varying number of cycles during the exponential phase (kinetic quantitative PCR). In the first case, an internal standard distinct from the target molecule is required to ascertain PCR efficiency. The method is relatively easy but implies generating, quantifying and storing an internal standard for each gene studied. Nevertheless, it is the most frequently applied method to date.

One of the major advantages of the kinetic method is its rapidity in quantifying a new gene, since no internal standard is required (an external standard curve is sufficient). Moreover, the kinetic method has a wide dynamic range (at least 5 orders of magnitude), giving an accurate value for samples differing in their copy number. Unfortunately, the method is cumbersome and has therefore been rarely used. It involves aliquot sampling of each assay mix at regular intervals and quantifying, for each aliquot, the amplification product. Interest in the kinetic method has been stimulated by a novel approach using fluorescent TaqMan methodology and a new instrument (ABI Prism 7700 Sequence Detection System) capable of measuring fluorescence in real time (Gibson *et al.,* 1996; Heid *et al.,* 1996). The TaqMan reaction is based on the 5' nuclease assay first described by Holland *et al.* (1991). The latter uses the 5' nuclease activity of Taq polymerase to cleave a specific fluorogenic oligonucleotide probe during the extension phase of PCR. The approach uses dual-labeled fluorogenic hybridization probes (Lee *et al.,* 1993). One fluorescent dye, co-valently linked to the 5' end of the oligonucleotide, serves as a reporter [FAM (*i.e.,* 6-carboxy-fluorescein)] and its emission spectrum is quenched by a second fluorescent dye, TAMRA (*i.e.,* 6-carboxy-tetramethyl-rhodamine) attached to the 3' end. During the extension phase of the PCR

*Correspondence to: Laboratoire de Génétique Moléculaire, Faculté des Sciences Pharmaceutiques et Biologiques de Paris, 4 Avenue de l'Observatoire, F-75006 Paris, France. Fax: (33)1-4407-1754. E-mail: mvidaud@teaser.fr

cycle, the fluorescent hybridization probe is hydrolyzed by the 5'-3' nucleolytic activity of DNA polymerase. Nuclease degradation of the probe releases the quenching of FAM fluorescence emission, resulting in an increase in peak fluorescence emission. The fluorescence signal is normalized by dividing the emission intensity of the reporter dye (FAM) by the emission intensity of a reference dye (i.e., ROX, 6-carboxy-X-rhodamine) included in TaqMan buffer, to obtain a ratio defined as the Rn (normalized reporter) for a given reaction tube. The use of a sequence detector enables the fluorescence spectra of all 96 wells of the thermal cycler to be measured continuously during PCR amplification.

The real-time PCR method offers several advantages over other current quantitative PCR methods (Celi et al., 1994): (i) the probe-based homogeneous assay provides a real-time method for detecting only specific amplification products, since specific hybridation of both the primers and the probe is necessary to generate a signal; (ii) the C_t (threshold cycle) value used for quantification is measured when PCR amplification is still in the log phase of PCR product accumulation. This is the main reason why C_t is a more reliable measure of the starting copy number than are end-point measurements, in which a slight difference in a limiting component can have a drastic effect on the amount of product; (iii) use of C_t values gives a wider dynamic range (at least 5 orders of magnitude), reducing the need for serial dilution; (iv) The real-time PCR method is run in a closed-tube system and requires no post-PCR sample handling, thus avoiding potential contamination; (v) the system is highly automated, since the instrument continuously measures fluorescence in all 96 wells of the thermal cycler during PCR amplification and the corresponding software processes, and analyzes the fluorescence data; (vi) the assay is rapid, as results are available just one minute after thermal cycling is complete; (vii) the sample throughput of the method is high, since 96 reactions can be analyzed in 2 hr.

Here, we applied this semi-automated procedure to determine the copy numbers of the 3 most frequently amplified genes in breast tumors (myc, ccnd1 and erbB2), as well as 2 genes (alb and app) located in a chromosome region in which no genetic changes have been observed in breast tumors. The results for 108 breast tumors were compared with previous Southern-blot data for the same samples.

MATERIAL AND METHODS

Tumor and blood samples

Samples were obtained from 108 primary breast tumors removed surgically from patients at the Centre René Huguenin; none of the patients had undergone radiotherapy or chemotherapy. Immediately after surgery, the tumor samples were placed in liquid nitrogen until extraction of high-molecular-weight DNA. Patients were included in this study if the tumor sample used for DNA preparation contained more than 60% of tumor cells (histological analysis). A blood sample was also taken from 18 of the same patients.

DNA was extracted from tumor tissue and blood leukocytes according to standard methods.

Real-time PCR

Theoretical basis. Reactions are characterized by the point during cycling when amplification of the PCR product is first detected, rather than by the amount of PCR product accumulated after a fixed number of cycles. The higher the starting copy number of the genomic DNA target, the earlier a significant increase in fluorescence is observed. The parameter C_t (threshold cycle) is defined as the fractional cycle number at which the fluorescence generated by cleavage of the probe passes a fixed threshold above baseline. The target gene copy number in unknown samples is quantified by measuring C_t and by using a standard curve to determine the starting copy number. The precise amount of genomic DNA (based on optical density) and its quality (i.e., lack

of extensive degradation) are both difficult to assess. We therefore also quantified a control gene (alb) mapping to chromosome region 4q11-q13, in which no genetic alterations have been found in breast-tumor DNA by means of CGH (Kallioniemi et al., 1994).

Thus, the ratio of the copy number of the target gene to the copy number of the alb gene normalizes the amount and quality of genomic DNA. The ratio defining the level of amplification is termed "N", and is determined as follows:

$$N = \frac{\text{copy number of target gene } (app, myc, ccnd1, erbB2)}{\text{copy number of reference gene } (alb)}.$$

Primers, probes, reference human genomic DNA and PCR consumables. Primers and probes were chosen with the assistance of the computer programs Oligo 4.0 (National Biosciences, Plymouth, MN), EuGene (Daniben Systems, Cincinnati, OH) and Primer Express (Perkin-Elmer Applied Biosystems, Foster City, CA).

Primers were purchased from DNAgency (Malvem, PA) and probes from Perkin-Elmer Applied Biosystems.

Nucleotide sequences for the oligonucleotide hybridization probes and primers are available on request.

The TaqMan PCR Core reagent kit, MicroAmp optical tubes, and MicroAmp caps were from Perkin-Elmer Applied Biosystems.

Standard-curve construction. The kinetic method requires a standard curve. The latter was constructed with serial dilutions of specific PCR products, according to Piatak et al. (1993). In practice, each specific PCR product was obtained by amplifying 20 ng of a standard human genomic DNA (Boehringer, Mannheim, Germany) with the same primer pairs as those used later for real-time quantitative PCR. The 5 PCR products were purified using MicroSpin S-400 HR columns (Pharmacia, Uppsala, Sweden) electrophorezed through an acrylamide gel and stained with ethidium bromide to check their quality. The PCR products were then quantified spectrophotometrically and pooled, and serially diluted 10-fold in mouse genomic DNA (Clontech, Palo Alto, CA) at a constant concentration of 2 ng/μl. The standard curve used for real-time quantitative PCR was based on serial dilutions of the pool of PCR products ranging from 10^{-7} (10^5 copies of each gene) to 10^{-10} (10^2 copies). This series of diluted PCR products was aliquoted and stored at $-80°C$ until use.

The standard curve was validated by analyzing 2 known quantities of calibrator human genomic DNA (20 ng and 50 ng).

PCR amplification. Amplification mixes (50 μl) contained the sample DNA (around 20 ng, around 6600 copies of disomic genes), 10× TaqMan buffer (5 μl), 200 μM dATP, dCTP, dGTP, and 400 μM dUTP, 5 mM MgCl₂, 1.25 units of AmpliTaq Gold, 0.5 units of AmpErase uracil N-glycosylase (UNG), 200 nM each primer and 100 nM probe. The thermal cycling conditions comprised 2 min at 50°C and 10 min at 95°C. Thermal cycling consisted of 40 cycles at 95°C for 15 s and 65°C for 1 min. Each assay included: a standard curve (from 10^5 to 10^2 copies) in duplicate, a no-template control, 20 ng and 50 ng of calibrator human genomic DNA (Boehringer) in triplicate, and about 20 ng of unknown genomic DNA in triplicate (26 samples can thus be analyzed on a 96-well microplate). All samples with a coefficient of variation (CV) higher than 10% were retested.

All reactions were performed in the ABI Prism 7700 Sequence Detection System (Perkin-Elmer Applied Biosystems), which detects the signal from the fluorogenic probe during PCR.

Equipment for real-time detection. The 7700 system has a built-in thermal cycler and a laser directed via fiber optical cables to each of the 96 sample wells. A charge-coupled-device (CDD) camera collects the emission from each sample and the data are analyzed automatically. The software accompanying the 7700 system calculates C_t and determines the starting copy number in the samples.

Determination of gene amplification. Gene amplification was calculated as described above. Only samples with an N value higher than 2 were considered to be amplified.

RESULTS

To validate the method, real-time PCR was performed on genomic DNA extracted from 108 primary breast tumors, and 18 normal leukocyte DNA samples from some of the same patients. The target genes were the *myc, ccnd1* and *erb*B2 proto-oncogenes, and the β-amyloid precursor protein gene (*app*), which maps to a chromosome region (21q21.2) in which no genetic alterations have been found in breast tumors (Kallioniemi *et al.*, 1994). The reference disomic gene was the albumin gene (*alb,* chromosome 4q11-q13).

Validation of the standard curve and dynamic range of real-time PCR

The standard curve was constructed from PCR products serially diluted in genomic mouse DNA at a constant concentration of 2 ng/µl. It should be noted that the 5 primer pairs chosen to analyze the 5 target genes do not amplify genomic mouse DNA (data not shown). Figure 1 shows the real-time PCR standard curve for the *alb* gene. The dynamic range was wide (at least 4 orders of magnitude), with samples containing as few as 10^2 copies or as many as 10^5 copies.

Copy-number ratio of the 2 reference genes (app and alb)

The *app* to *alb* copy-number ratio was determined in 18 normal leukocyte DNA samples and all 108 primary breast-tumor DNA
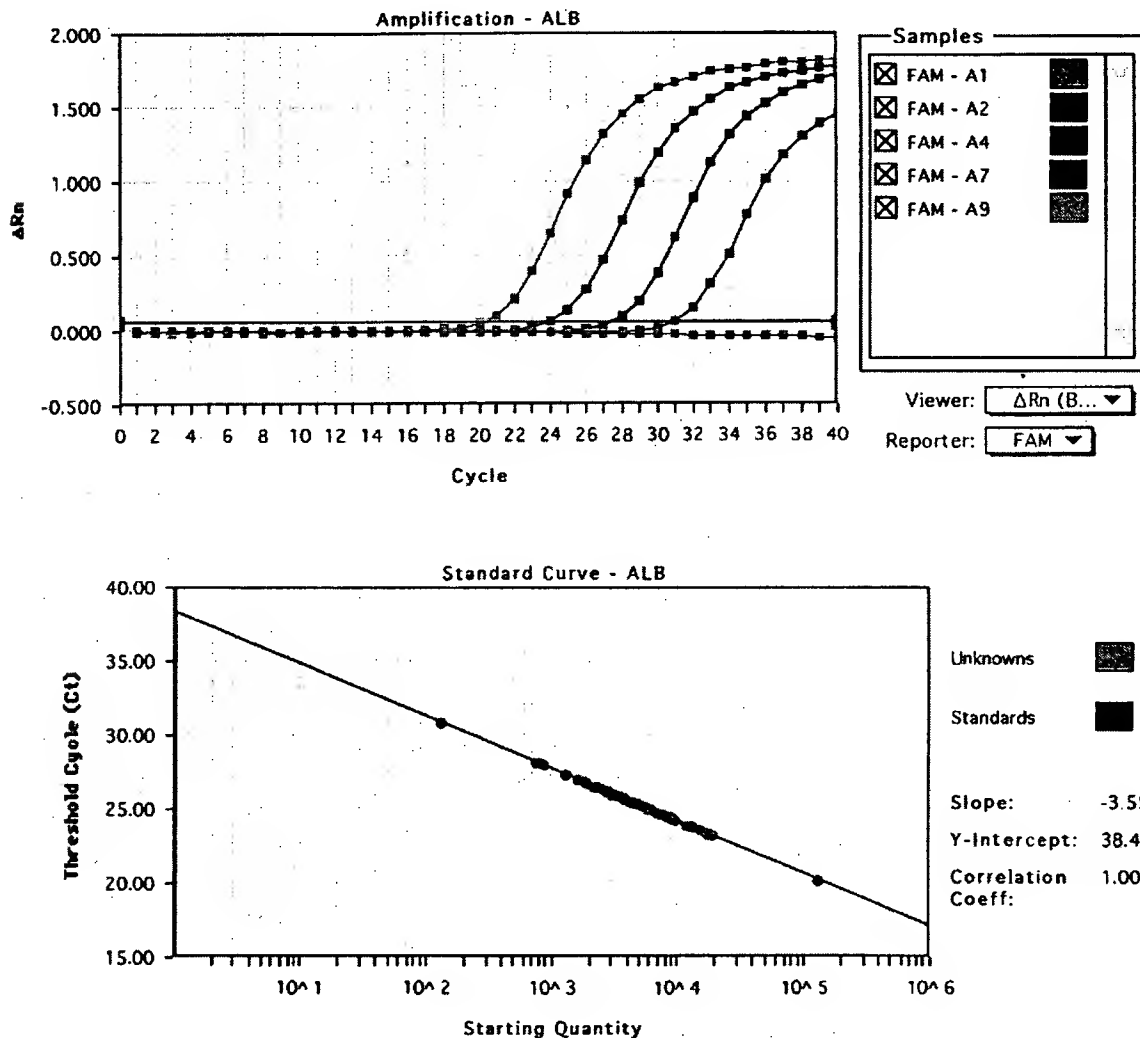

FIGURE 1 – Albumin (*alb*) gene dosage by real-time PCR. Top: Amplification plots for reactions with starting *alb* gene copy number ranging from 10^5 (A9), 10^4 (A7), 10^3 (A4) to 10^2 (A2) and a no-template control (A1). Cycle number is plotted *vs.* change in normalized reporter signal (ΔRn). For each reaction tube, the fluorescence signal of the reporter dye (FAM) is divided by the fluorescence signal of the passive reference dye (ROX), to obtain a ratio defined as the normalized reporter signal (Rn). ΔRn represents the normalized reporter signal (Rn) minus the baseline signal established in the first 15 PCR cycles. ΔRn increases during PCR as *alb* PCR product copy number increases until the reaction reaches a plateau. C_t (threshold cycle) represents the fractional cycle number at which a significant increase in Rn above a baseline signal (horizontal black line) can first be detected. Two replicate plots were performed for each standard sample, but the data for only one are shown here. Bottom: Standard curve plotting log starting copy number *vs.* C_t (threshold cycle). The black dots represent the data for standard samples plotted in duplicate and the red dots the data for unknown genomic DNA samples plotted in triplicate. The standard curve shows 4 orders of linear dynamic range.

samples. We selected these 2 genes because they are located in 2 chromosome regions (*app*, 21q21.2; *alb*, 4q11-q13) in which no obvious genetic changes (including gains or losses) have been observed in breast cancers (Kallioniemi *et al.*, 1994). The ratio for the 18 normal leukocyte DNA samples fell between 0.7 and 1.3 (mean 1.02 ± 0.21), and was similar for the 108 primary breast-tumor DNA samples (0.6 to 1.6, mean 1.06 ± 0.25), confirming that *alb* and *app* are appropriate reference disomic genes for breast-tumor DNA. The low range of the ratios also confirmed that the nucleotide sequences chosen for the primers and probes were not polymorphic, as mismatches of their primers or probes with the subject's DNA would have resulted in differential amplification.

myc, ccnd1 *and* erbB2 *gene dose in normal leukocyte DNA*

To determine the cut-off point for gene amplification in breast-cancer tissue, 18 normal leukocyte DNA samples were tested for the gene dose (N), calculated as described in "Material and Methods". The N value of these samples ranged from 0.5 to 1.3 (mean 0.84 ± 0.22) for *myc*; 0.7 to 1.6 (mean 1.06 ± 0.23) for *ccnd1* and 0.6 to 1.3 (mean 0.91 ± 0.19) for *erbB2*. Since N values for *myc*, *ccnd1* and *erbB2* in normal leukocyte DNA consistently fell between 0.5 and 1.6, values of 2 or more were considered to represent gene amplification in tumor DNA.

myc, ccnd1 *and* erbB2 *gene dose in breast-tumor DNA*

myc, *ccnd1* and *erbB2* gene copy numbers in the 108 primary breast tumors are reported in Table I. Extra copies of *ccnd1* were more frequent (23%, 25/108) than extra copies of *erbB2* (15%, 16/108) and *myc* (10%, 11/108), and ranged from 2 to 18.6 for *ccnd1*, 2 to 15.1 for *erbB2*, and only 2 to 4.6 for the *myc* gene. Figure 2 and Table II represent tumors in which the *ccnd1* gene was amplified 16-fold (T145), 6-fold (T133) and non-amplified (T118). The 3 genes were never found to be co-amplified in the same tumor. *erbB2* and *ccnd1* were co-amplified in only 3 cases, *myc* and *ccnd1* in 2 cases and *myc* and *erbB2* in 1 case. This favors the hypothesis that gene amplifications are independent events in breast cancer. Interestingly, 5 tumors showed a decrease of at least 50% in the *erbB2* copy number (N < 0.5), suggesting that they bore deletions of the 17q21 region (the site of *erbB2*). No such decrease in copy number was observed with the other 2 proto-oncogenes.

Comparison of gene dose determined by real-time quantitative PCR and Southern-blot analysis

Southern-blot analysis of *myc*, *ccnd1* and *erbB2* amplifications had previously been done on the same 108 primary breast tumors. A perfect correlation between the results of real-time PCR and Southern blot was obtained for tumors with high copy numbers (N ≥ 5). However, there were cases (1 *myc*, 6 *ccnd1* and 4 *erbB2*) in which real-time PCR showed gene amplification whereas Southern-blot did not, but these were mainly cases with low extra copy numbers (N from 2 to 2.9).

DISCUSSION

The clinical applications of gene amplification assays are currently limited, but would certainly increase if a simple, standardized and rapid method were perfected. Gene amplification status has been studied mainly by means of Southern blotting, but this method is not sensitive enough to detect low-level gene amplification nor accurate enough to quantify the full range of amplification values. Southern blotting is also time-consuming, uses radioactive

reagents and requires relatively large amounts of high-quality genomic DNA, which means it cannot be used routinely in many laboratories. An amplification step is therefore required to determine the copy number of a given target gene from minimal quantities of tumor DNA (small early-stage tumors, cytopuncture specimens or formalin-fixed, paraffin-embedded tissues).
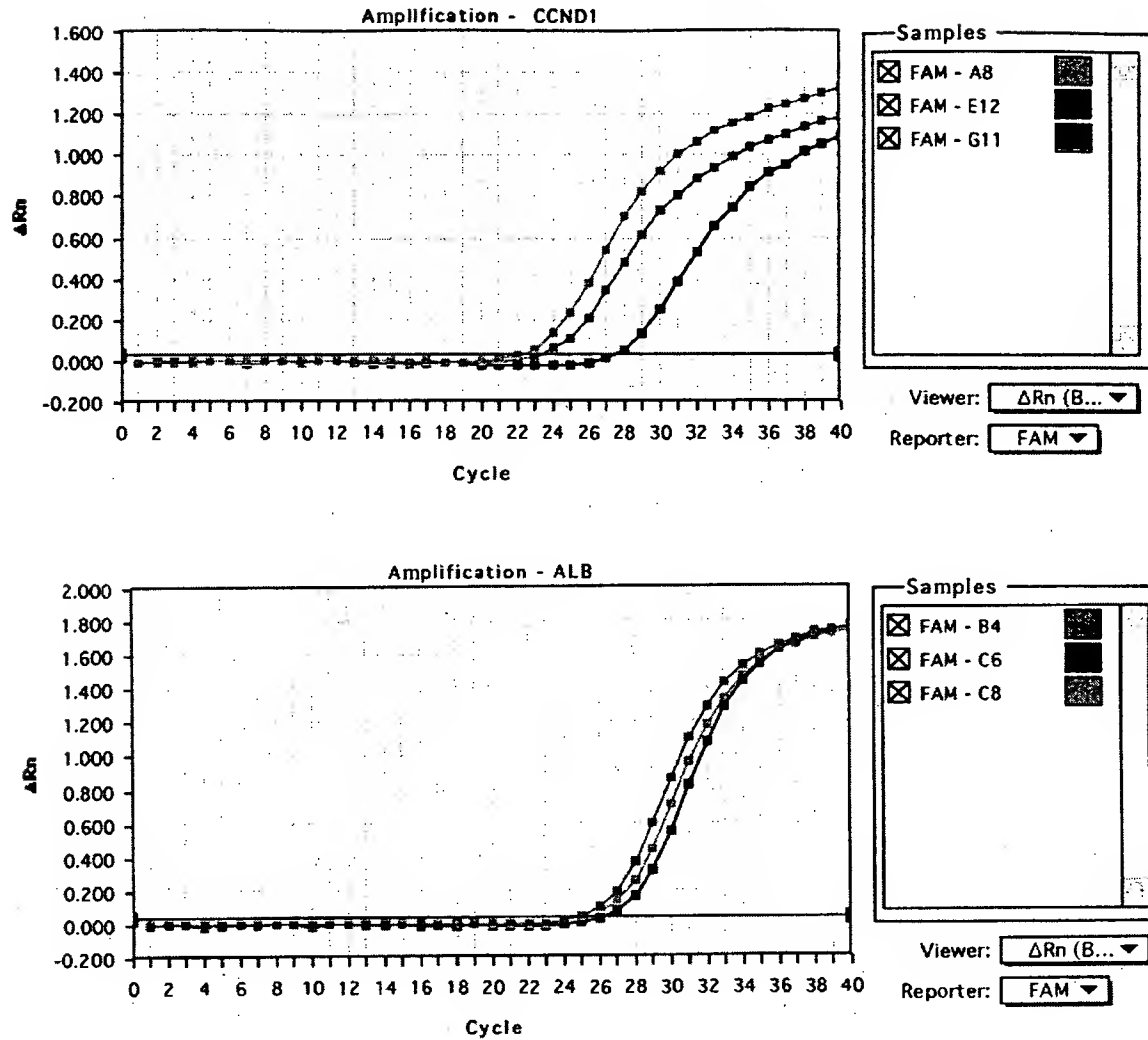
In this study, we validated a PCR method developed for the quantification of gene over-representation in tumors. The method, based on real-time analysis of PCR amplification, has several advantages over other PCR-based quantitative assays such as competitive quantitative PCR (Celi *et al.*, 1994). First, the real-time PCR method is performed in a closed-tube system, avoiding the risk of contamination by amplified products. Re-amplification of carryover PCR products in subsequent experiments can also be prevented by using the enzyme uracil N-glycosylase (UNG) (Longo *et al.*, 1990). The second advantage is the simplicity and rapidity of sample analysis, since no post-PCR manipulations are required. Our results show that the automated method is reliable. We found it possible to determine, in triplicate, the number of copies of a target gene in more than 100 tumors per day. Third, the system has a linear dynamic range of at least 4 orders of magnitude, meaning that samples do not have to contain equal starting amounts of DNA. This technique should therefore be suitable for analyzing formalin-fixed, paraffin-embedded tissues. Fourth, and above all, real-time PCR makes DNA quantification much more precise and reproducible, since it is based on C_t values rather than end-point measurement of the amount of accumulated PCR product. Indeed, the ABI Prism 7700 Sequence Detection System enables C_t to be calculated when PCR amplification is still in the exponential phase and when none of the reaction components is rate-limiting. The within-run CV of the C_t value for calibrator human DNA (5 replicates) was always below 5%, and the between-assay precision in 5 different runs was always below 10% (data not shown). In addition, the use of a standard curve is not absolutely necessary, since the copy number can be determined simply by comparing the C_t ratio of the target gene with that of reference genes. The results obtained by the 2 methods (with and without a standard curve) are similar in our experiments (data not shown). Moreover, unlike competitive quantitative PCR, real-time PCR does not require an internal control (the design and storage of internal controls and the validation of their amplification efficiency is laborious).

The only potential disavantage of real-time PCR, like all other PCR-based methods and solid-matrix blotting techniques (Southern blots and dot blots) is that is cannot avoid dilution artifacts inherent in the extraction of DNA from tumor cells contained in heterogeneous tissue specimens. Only FISH and immunohistochemistry can measure alterations on a cell-by-cell basis (Pauletti *et al.*, 1996; Slamon *et al.*, 1989). However, FISH requires expensive equipment and trained personnel and is also time-consuming. Moreover, FISH does not assess gene expression and therefore cannot detect cases in which the gene product is over-expressed in the absence of gene amplification, which will be possible in the future by real-time quantitative RT-PCR. Immunohistochemistry is subject to considerable variations in the hands of different teams, owing to alterations of target proteins during the procedure, the different primary antibodies and fixation methods used and the criteria used to define positive staining.

The results of this study are in agreement with those reported in the literature. (*i*) Chromosome regions 4q11-q13 and 21q21.2 (which bear *alb* and *app*, respectively) showed no genetic alterations in the breast-cancer samples studied here, in keeping with the results of CGH (Kallioniemi *et al.*, 1994). (*ii*) We found that amplifications of these 3 oncogenes were independent events, as reported by other teams (Berns *et al.*, 1992; Borg *et al.*, 1992). (*iii*) The frequency and degree of *myc* amplification in our breast tumor DNA series were lower than those of *ccnd1* and *erbB2* amplification, confirming the findings of Borg *et al.* (1992) and Courjal *et al.* (1997). (*iv*) The maxima of *ccnd1* and *erbB2* over-representation were 18-fold and 15-fold, also in keeping with earlier results (about

TABLE I – DISTRIBUTION OF AMPLIFICATION LEVEL (N) FOR *myc*, *ccnd1* AND *erbB2* GENES IN 108 HUMAN BREAST TUMORS

Gene	Amplification level (N)			
	<0.5	0.5–1.9	2–4.9	≥5
myc	0	97 (89.8%)	11 (10.2%)	0
ccnd1	0	83 (76.9%)	17 (15.7%)	8 (7.4%)
erbB2	5 (4.6%)	87 (80.6%)	8 (7.4%)	8 (7.4%)

Amplification - CCND1

Samples
- ☒ FAM - A8
- ☒ FAM - E12
- ☒ FAM - G11

Viewer: ΔRn (B... ▼)
Reporter: FAM ▼

Amplification - ALB

Samples
- ☒ FAM - B4
- ☒ FAM - C6
- ☒ FAM - C8

Viewer: ΔRn (B... ▼)
Reporter: FAM ▼

Tumor	CCND1		ALB	
	C_t	Copy number	C_t	Copy number
■ T118	27.3	4605	26.5	4365
▨ T133	23.2	61659	25.2	10092
▨ T145	22.1	125892	25.6	7762

FIGURE 2 – *ccnd1* and alb gene dosage by real-time PCR in 3 breast tumor samples: T118 (E12, C6, black squares), T133 (G11, B4, red squares) and T145 (A8, C8, blue squares). Given the C_t of each sample, the initial copy number is inferred from the standard curve obtained during the same experiment. Triplicate plots were performed for each tumor sample, but the data for only one are shown here. The results are shown in Table II.

30-fold maximum) (Berns *et al.*, 1992; Borg *et al.*, 1992; Courjal *et al.*, 1997). (*v*) The *erb*B2 copy numbers obtained with real-time PCR were in good agreement with data obtained with other quantitative PCR-based assays in terms of the frequency and degree of amplification (An *et al.*, 1995; Deng *et al.*, 1996; Valeron

et al., 1996). Our results also correlate well with those recently published by Gelmini *et al.* (1997), who used the TaqMan system to measure *erb*B2 amplification in a small series of breast tumors (n = 25), but with an instrument (LS-50B luminescence spectrometer, Perkin-Elmer Applied Biosystems) which only allows end-

BIECHE ET AL.

TABLE II – EXAMPLES OF *ccnd1* GENE OOSAGE RESULTS FROM 3 BREAST TUMORS[1]

Tumor	ccnd1			alb			Nccnd1/alb
	Copy number	Mean	SO	Copy number	Mean	SO	
T118	4525			4223			
	4605	4603	77	4365	4325	89	1.06
	4678			4387			
T133	59821			9787			
	61659	61100	1111	10092	10137	375	6.03
	61821			10533			
T145	128563			7321			
	125892	125392	3448	7762	7672	316	16.34
	121722			7933			

[1]For each sample, 3 replicate experiments were performed and the mean and the standard deviation (SD) was determined. The level of *ccnd1* gene amplification (N*ccnd1*/*alb*) is determined by dividing the average *ccnd1* copy number value by the average *alb* copy number value.

point measurement of fluorescence intensity. Here we report *myc* and *ccnd1* gene dosage in breast cancer by means of quantitative PCR. (vi) We found a high degree of concordance between real-time quantitative PCR and Southern blot analysis in terms of gene amplification, especially for samples with high copy numbers (≥5-fold). The slightly higher frequency of gene amplification (especially *ccnd1* and *erb*B2) observed by means of real-time quantitative PCR as compared with Southern-blot analysis may be explained by the higher sensitivity of the former method. However, we cannot rule out the possibility that some tumors with a few extra

gene copies observed in real-time PCR had additional copies of an arm or a whole chromosome (trisomy, tetrasomy or polysomy) rather than true gene amplification. These 2 types of genetic alteration (polysomy and gene amplification) could be easily distinguished in the future by using an additional probe located on the same chromosome arm, but some distance from the target gene. It is noteworthy that high gene copy numbers have the greatest prognostic significance in breast carcinoma (Borg *et al.*, 1992; Slamon *et al.*, 1987).

Finally, this technique can be applied to the detection of gene deletion as well as gene amplification. Indeed, we found a decreased copy number of *erb*B2 (but not of the other 2 proto-oncogenes) in several tumors; *erb*B2 is located in a chromosome region (17q21) reported to contain both deletions and amplifications in breast cancer (Bièche and Lidereau, 1995).

In conclusion, gene amplification in various cancers can be used as a marker of pre-neoplasia, also for early diagnosis of cancer, staging, prognostication and choice of treatment. Southern blotting is not sufficiently sensitive, and FISH is lengthy and complex. Real-time quantitative PCR overcomes both these limitations, and is a sensitive and accurate method of analyzing large numbers of samples in a short time. It should find a place in routine clinical gene dosage.

ACKNOWLEDGEMENTS

REFERENCES

AN, H.X., NIEOERACHER, D., BECKMANN, M.W., GÖHRING, U.J., SCHARL, A., PICARO, F., VAN ROEYEN, C., SCHNÜRCH, H.G. and BENOER, H.G., *erb*B2 gene amplification detected by fluorescent differential polymerase chain reaction in paraffin-embedded breast carcinoma tissues. *Int. J. Cancer (Pred. Oncol.)*, **64**, 291–297 (1995).

BERNES, E.M.J.J., KLIJN, J.G.M., VAN PUTTEN, W.L.J., VAN STAVEREN, I.L., PORTENGEN, H. and FOEKENS, J.A., c-*myc* amplification is a better prognostic factor than HER2/*neu* amplification in primary breast cancer. *Cancer Res.*, **52**, 1107–1113 (1992).

BIÈCHE, I. and LIOEREAU, R., Genetic alterations in breast cancer. *Genes Chrom. Cancer*, **14**, 227–251 (1995).

BORG, A., BALOETORP, B., FERNO, M., OLSSON, H. and SIGURDSSON, H., c-*myc* amplification is an independent prognostic factor in post-menopausal breast cancer. *Int. J. Cancer*, **51**, 687–691 (1992).

CELI, F.S., COHEN, M.M., ANTONARAKIS, S.E., WERTHEIMER, E., ROTH, J. and SHULOINER, A.R., Determination of gene dosage by a quantitative adaptation of the polymerase chain reaction (gd-PCR): rapid detection of deletions and duplications of gene sequences. *Genomics*, **21**, 304–310 (1994).

COURJAL, F., CUNY, M., SIMONY-LAFONTAINE, J., LOUASSON, G., SPEISER, P., ZEILLINGER, R., ROORIGUEZ, C. and THEILLET, C., Mapping of DNA amplifications at 15 chromosomal localizations in 1875 breast tumors: definition of phenotypic groups. *Cancer Res.*, **57**, 4360–4367 (1997).

DENG, G., YU, M., CHEN, L.C., MDORE, D., KURISU, W., KALLIONIEMI, A., WALOMAN, F.M., COLLINS, C. and SMITH, H.S., Amplifications of oncogene *erb*B-2 and chromosome 20q in breast cancer determined by differentially competitive polymerase chain reaction. *Breast Cancer Res. Treat.*, **40**, 271–281 (1996).

GELMINI, S., ORIANDO, C., SESTINI, R., VONA, G., PINZANI, P., RUOCCO, L. and PAZZAGLI, M., Quantitative polymerase chain reaction-based homogeneous assay with fluorogenic probes to measure c-*erB*-2 oncogene amplification. *Clin. Chem.*, **43**, 752–758 (1997).

GIBSON, U.E.M., HEIO, C.A. and WILLIAMS, P.M., A novel method for real-time quantitative RT-PCR. *Genome Res.*, **6**, 995–1001 (1996).

HEIO, C.A., STEVENS, J., LIVAK, K.J. and WILLIAMS, P.M., Real-time quantitative PCR. *Genome Res.*, **6**, 986–994 (1996).

HOLLANO, P.M., ABRAMSON, R.D., WATSON, R. and GELFANO, D.H., Detection of specific polymerase chain reaction product by utilizing the 5′ to 3′ exonuclease activity of *Thermus aquaticus* DNA polymerase. *Proc. nat. Acad. Sci. (Wash.)*, **88**, 7276–7280 (1991).

KALLIONIEMI, A., KALLIONIEMI, O.P., PIPER, J., TANNER, M., STOKKES, T., CHEN, L., SMITH, H.S., PINKEL, D., GRAY, J.W. and WALOMAN, F.M., Detection and mapping of amplified DNA sequences in breast cancer by comparative genomic hybridization. *Proc. nat. Acad. Sci. (Wash.)*, **91**, 2156–2160 (1994).

LEE, L.G., CONNELL, C.R. and BIOCH, W., Allelic discrimination by nick-translation PCR with fluorogenic probe. *Nucleic Acids Res.*, **21**, 3761–3766 (1993).

LONGO, N., BERNINGER, N.S. and HARTLEY, J.L., Use of uracil DNA glycosylase to control carry-over contamination in polymerase chain reactions. *Gene*, **93**, 125–128 (1990).

MUSS, H.B., THOR, A.D., BERRY, D.A., KUTE, T., LIU, E.T., KOERNER, F., CIRRINCIONE, C.T., BUOMAN, D.R., WOOO, W.C., BARCOS, M. and HENDERSON, I.C., c-*erb*B-2 expression and response to adjuvant therapy in women with node-positive early breast cancer. *New Engl. J. Med.*, **330**, 1260–1266 (1994).

PAULETTI, G., GOOOLPHIN, W., PRESS, M.F. and SALMON, D.J., Detection and quantification of HER-2/*neu* gene amplification in human breast cancer archival material using fluorescence *in situ* hybridization. *Oncogene*, **13**, 63–72 (1996).

PIATAK, M., LUK, K.C., WILLIAMS, B. and LIFSON, J.D., Quantitative competitive polymerase chain reaction for accurate quantitation of HIV DNA and RNA species. *Biotechniques*, **14**, 70–80 (1993).

SCHUURING, E., VERHOEVEN, E., VAN TINTEREN, H., PETERSE, J.L., NUNNIK, B., THUNNISSEN, F.B.J.M., DEVILEE, P., CORNELISSE, C.J., VAN OE VIJVER, M.J., MOOI, W.J. and MICHALIOES, R.J.A.M., Amplification of genes within the chromosome 11q13 region is indicative of poor prognosis in patients with operable breast cancer. *Cancer Res.*, **52**, 5229–5234 (1992).

SLAMON, D.J., CLARK, G.M., WONG, S.G., LEVIN, W.S., ULLRICH, A. and McGUIRE, W.L., Human breast cancer: correlation of relapse and survival with amplification of the HER-2/*neu* oncogene. *Science*, **235**, 177–182 (1987).

SLAMON, D.J., GODOLPHIN, W., JONES, L.A., HOLT, J.A., WONG, S.G., KEITH, D.E., LEVIN, W.J., STUART, S.G., UDOVE, J., ULLRICH, A. and PRESS, M.F., Studies of the HER-2/*neu* proto-oncogene in human breast and ovarian cancer. *Science*, **244**, 707–712 (1989).

VALERON, P.F., CHIRINO, R., FERNANOEZ, L., TORRES, S., NAVARRO, D., AGUIAR, J., CABRERA, J.J., DIAZ-CHICO, B.N. and DIAZ-CHICO, J.C., Validation of a differential PCR and an ELISA procedure in studying HER-2/*neu* status in breast cancer. *Int. J. Cancer*, **65**, 129–133 (1996).